National Library
of Canada

Acquisitions and
Bibliographic Services Branch

395 Wellington Street
Ottawa, Ontario
K1A 0N4

Bibliothèque nationale
du Canada

Direction des acquisitions et
des services bibliographiques

395, rue Wellington
Ottawa (Ontario)
K1A 0N4

Your file Votre référence

Our file Notre référence

NOTICE

The quality of this microform is heavily dependent upon the quality of the original thesis submitted for microfilming. Every effort has been made to ensure the highest quality of reproduction possible.

If pages are missing, contact the university which granted the degree.

Some pages may have indistinct print especially if the original pages were typed with a poor typewriter ribbon or if the university sent us an inferior photocopy.

AVIS

La qualité de cette microforme dépend grandement de la qualité de la thèse soumise au microfilmage. Nous avons tout fait pour assurer une qualité supérieure de reproduction.

S'il manque des pages, veuillez communiquer avec l'université qui a conféré le grade.

La qualité d'impression de certaines pages peut laisser à désirer, surtout si les pages originales ont été dactylographiées à l'aide d'un ruban usé ou si l'université nous a fait parvenir une photocopie de qualité inférieure.

Canada

GLYCOLIPID CONFORMATION AND DYNAMICS

IN

MODEL AND BIOLOGICAL MEMBRANES

by

BeAtrice G. Winsborrow, B.Sc., M.Sc.

ISBN 0-315-82535-9

Canada

UNIVERSITÉ D'OTTAWA
UNIVERSITY OF OTTAWA

when i am

an old woman

I shall wear purple
With a red hat which doesn't go, and doesn't suit me.
And I shall spend my pension on brandy and summer gloves
And satin sandals, and say we've no money for butter.
I shall sit down on the pavement when I'm tired
And gobble up samples in shops and press alarm bells
And run my stick along the public railings
And make up for the sobriety of my youth.
I shall go out in my slippers in the rain
And pick the flowers in other people's gardens
And learn to spit.
You can wear terrible shirts and grow more fat
And eat three pounds of sausages at a go
Or only bread and a pickle for a week.
And hoard pens and pencils and beermats and things in boxes.
But now we must have clothes that keep us dry
And pay our rent and not swear in the street
And set a good example for the children.
We will have friends to dinner and read the papers.
But maybe I ought to practise a little now?
So people who know me are not too shocked and surprised
When suddenly I am old and start to wear purple.

From Warning - by Jenny Joseph

ABSTRACT

Glycolipids constitute an important class of molecules which are involved in biomolecular recognition; the significance of head group conformation in such processes is well documented. Glycolipids also occur as major components of the complex heterogeneous membrane matrices of plants and photosynthetic bacteria. As a result, the glycolipid-rich membranes serve as a spatial frame in which proteins may function.

The focus of this dissertation has been the biophysical analysis of two related research subjects: a model membrane glycolipid system and glycolipid-rich biomembranes. The objective of the model system study was to provide a biological understanding of the molecular conformation and dynamics at the membrane surface. The biomembrane project is in the first stages of development where the immediate goal is to observe the structure and phase behaviour of cyanobacterial thylakoid membranes.

It has been possible to apply a motional model deduced for the glycerol C3' position of 1,2-di-*O*-tetradecyl-3-*O*-(β-D-glucopyranosyl)-*sn*-glycerol (β-DTGL) in the gel state not only to the more fluid liquid crystalline state, but also to the analysis of the glucose head group ($\{1\text{-}^2H_1\}$) motions. The transference of modelled motion from the glycerol backbone to the head group was intended to describe the basic head group motions. The techniques and approach used to test the motional model (two frequencies, oriented multibilayers, powder spectra lineshapes, and both T_{1Z} and T_{1Q} experiments) have outlined the complex motions of β-DTGL in its biologically relevant liquid crystalline state.

The above model, however, did not completely simulate the relaxation data of the β-DTGL glucose head group. Therefore, conformational energy calculations have been used to assess the flexibility of the head group about its glycosidic bond, in a liquid-crystalline membrane matrix. ^2H NMR and neutron diffraction parameters

calculated in this study agree well with experiment, demonstrating the importance of including surface interactions when considering the conformational space accessible to cell surface carbohydrates.

Algal thylakoid membranes are known for their ability to undergo conformational changes during periods of photosynthetic activity. The ultimate goal of the biomembrane project was to use ^{2}H NMR to study such conformational changes in thylakoid membranes. However, this project is in the first stages of development; the more modest but attainable short term goal was to observe directly the structure and phase behaviour of two strains of cyanobacterial thylakoid membranes, *Anacystis nidulans* and *A.nidulans R2*.

Two basic criteria have been used to relate the physical properties measured by ^{2}H NMR to the heterogeneous thylakoid membrane structure: acyl chain unsaturation and lipid head group class. *A.nidulans* cells were harvested after 48 hours and *A.nidulans R2* cells after both 48 and 96 hours of growth in medium supplemented with perdeuterated palmitic acid. *A.nidulans* was also grown, for 48 hours, in medium supplemented with specifically deuterated oleic acid.

The ^{2}H NMR spectra are very similar to those of membranes of *A.laidlawii* grown in media containing myristic acid (Smith et al., 1979; Jarrell et al., 1982) and oleic acid (Rance et al., 1980). In both the previous studies and this study, it was found that the heterogeneous systems undergo broad phase transitions and that acyl chain unsaturation lowers the phase transition temperature of the membranes.

Although pure digalactosyldiacyglycerol is known to stabilize lamellar membrane phases, it appears as though phosphatidylglycerol (PG) is more influential in stabilizing the lamellar membrane structure of the cyanobacterial thylakoid membranes. This effect was more noticeable for the spectra of extracted lipids; in the absence of protein and with low PG levels, the lipids formed non-lamellar phases at lower temperatures.

ACKNOWLEDGEMENTS

As a graduate student at the University of Ottawa, I was given the opportunity to do the research necessary for this dissertation at the National Research Council of Canada (NRC). This has been a very positive and rewarding experience. The research group in which I have been working has an atmosphere of excellence and co-operativity. During my tenure at NRC I was able to work with many world-class scientists, two of which are my co-supervisors Ian C. P. Smith and Harold C. Jarrell.

Ian C. P. Smith has provided me with the freedom to explore, ask questions, and learn. Ian has always been enthusiastic and honest about my ideas; through his honesty I gained insight and perspective. Above all, I am most thankful for his unwavering support, even when I was not sure in which directions I was heading.

Harold C. Jarrell has helped me to mature as a scientist. Harold taught me how to recognize when a challenging project should be developed into fruition and when it should be let go. I particularly appreciate the manner in which Harold guided my decision making processes; he treated me as a co-worker.

Over my five year stay at NRC I have come to appreciate the scientific community in which I worked. There are a number of people whom I would like to acknowledge for their helpful discussions, input, and friendship. These people are John Baenziger, Leo Turner, Dave Siminovitch, Francesco Zerbetto, Anne Daley, Jean-Robert Brisson, John Rendell, François André, Ron Curtis, Danielle Carrier, Michèle Auger, Dave Fenske, and Allison Rutter.

Within this community I have also developed a small circle of very close friends who have come to mean a lot to me through their steadfast friendship and our many memorable times together. These very special friends are Tanya Dahms, Heather Gordon, Ranjana Ghosh, Annette Kuesel, Karol Mikulash, and Eneida de Paula.

Sport climbing is an integral part of my lifestyle and I would be remiss if I did not mention my climbing partners, Karol Mikulash and Peter Slivka. These two friends have taught me about inner focus and striving for excellence through commitment. My happiest times have stemmed from climbing.

Finally, my family has been very supportive of my many endeavours. I would like to acknowledge my family's contribution to this stage of my life. My parents, Viola and Robert; my brothers and their families: Ken and Maria; Kevin, Anne and their children, Kerry, Amanda and Robert Alexander; Eric; my sister, Jo'Anna and her sons, Jason, Jonathan, and Jeremy; and my cousins, Jim, Lee and Dustin. With such a large group of people sending me love and encouragement every day, I was assured of success.

TABLE OF CONTENTS

Part I: Introductory Details

Chapter 1 -- Introduction

Chapter 2 -- NMR Background

Chapter 3 -- Methods

Part II: Model Membranes

Chapter 4 -- Glycolipid Dynamics in The Liquid Crystalline State. A ^{2}H NMR Relaxation Study With Lineshape Analysis.

Part III: Biomembranes

Chapter 6 -- ^{2}H NMR and Cyanobacterial Membranes.
Preliminary Physical Studies.

Chapter 7 -- More on Cyanobacteria. A Tale of Two Strains.

Part IV: Conclusions

Chapter 8 -- Concluding Remarks

List of Figures

List of Tables

Abbreviations

β-DTGL	1,2-di-*O*-tetradecyl-3-*O*-(β-D-glucopyranosyl-*sn*-glycerol
CHAPSO	3-(cholamidopropyl)dimethylammonio-2-hydroxy-1-propanesulfonate
Chl	chlorophyll a
DGDG	digalactosyldiacylglycerol
DMPC	1,2-dimyristoyl-*sn*-glycero-3-phosphocholine
D_2O	deuterated water
DPPC	1,2-dipalmitoyl-*sn*-glycero-3-phosphocholine
eq	electric field gradient along principal axis (Cartesian coordinates)
eQ	electric quadrupole moment
e^2qQ/h	quadrupolar coupling constant
E_m	quantized energy of interaction
ESR	electron spin resonance
FID	free induction decay
g^+	gauche plus conformation, +60°
g^-	gauche minus conformation, -60°
Glc	glucose
Gal	galactose
h	Planck's constant
ħ	Planck's constant divided by 2π
$\mathcal{H}$	Hamiltonian operator
^2H	deuterium
$\mathbf{H}_0$	external magnetic field
$\mathbf{H}_1$	local magnetic field
H_2^1O	deuterium depleted water
I	spin angular momentum operator
J	angular momentum
J(mω)	spectral density function

k	Boltzmann's constant
$L_{\beta'}$	gel state in the lamellar phase
L_α	liquid crystalline state in the lamellar phase
ms	milliseconds
M_o	magnetization at equilibrium
M_z	macroscopic longitudinal magnetization
MGDG	monogalactosyldiacylglycerol
NL	neutral lipids
NMR	nuclear magnetic resonance
PFOS	Potential Functions of OligoSaccharides
PG	phosphatidylglycerol
r_{ij}	internuclear distance
RF	radio frequency
S	molecular order parameter
SL	sulfoquinovosydiacylglycerol
t	trans conformation, 180°
T	temperature (Kelvin scale)
T_{1Z}	longitudinal relaxation time, Zeeman order
T_{1Q}	longitudinal relaxation time, quadrupolar order
$T_1(\beta)$	orientation-dependent longitudinal relaxation time
TES	(N-tris[Hydroxymethyl-2-aminoethanesulfonic acid; 2-([Hydroxy-1,1-bis(hyroxymethyl)ethyl]amino)ethanesulfonic acid)
Tris	(tris[Hydroxymethyl]aminomethane)
VD	variable delay between pulses in an NMR experiment
γ	gyromagnetic ratio
η	asymmetry parameter
μ	dipole moment
μs	microseconds
$\Delta\upsilon_D$	dipolar coupling
$\Delta\upsilon_Q$	quadrupolar coupling

τ	tau, delay between pulses in an NMR experiment
τ_c	correlation time
ω_o	nuclear Larmor frequency
Ψ	stationary state wave function
2D	two-dimensional
14:0	myristic acid
14:1	myristoleic acid
16:0	palmitic acid
16:1	palmitoleic acid
18:0	stearic acid
18:1	oleic acid

Part I

Introductory Details

Chapter 1

Introduction

1.1 BIOMEMBRANE DIVERSITY

If not for the presence of boundaries there would be no life; in biological systems these boundaries are membranes. All living organisms not only need membranes for cell, tissue, and organ differentiation, but also as a site of biochemical activity. The level of membrane diversity within a single cell is incredible, as is demonstrated by the depiction of an animal cell in Figure 1.1. The outer membrane (plasma membrane) is not smooth, which is a common misconception envisioned by most people. Rather, it is a rough surface with a large number of invaginations suitable for inter-cellular interactions. The organelles within the cell are separate entities. In Figure 1.1, the blue structure represents the nucleus, the pink ellipses correspond to mitochondria, green shapes signify Golgi vesicles, the endoplasmic reticulum is depicted by the narrow orange ribbons, and the orange spheres portray lysosomes and perioxisomes. The organelles all provide different cellular functions and are separated by their own specialized membranes.

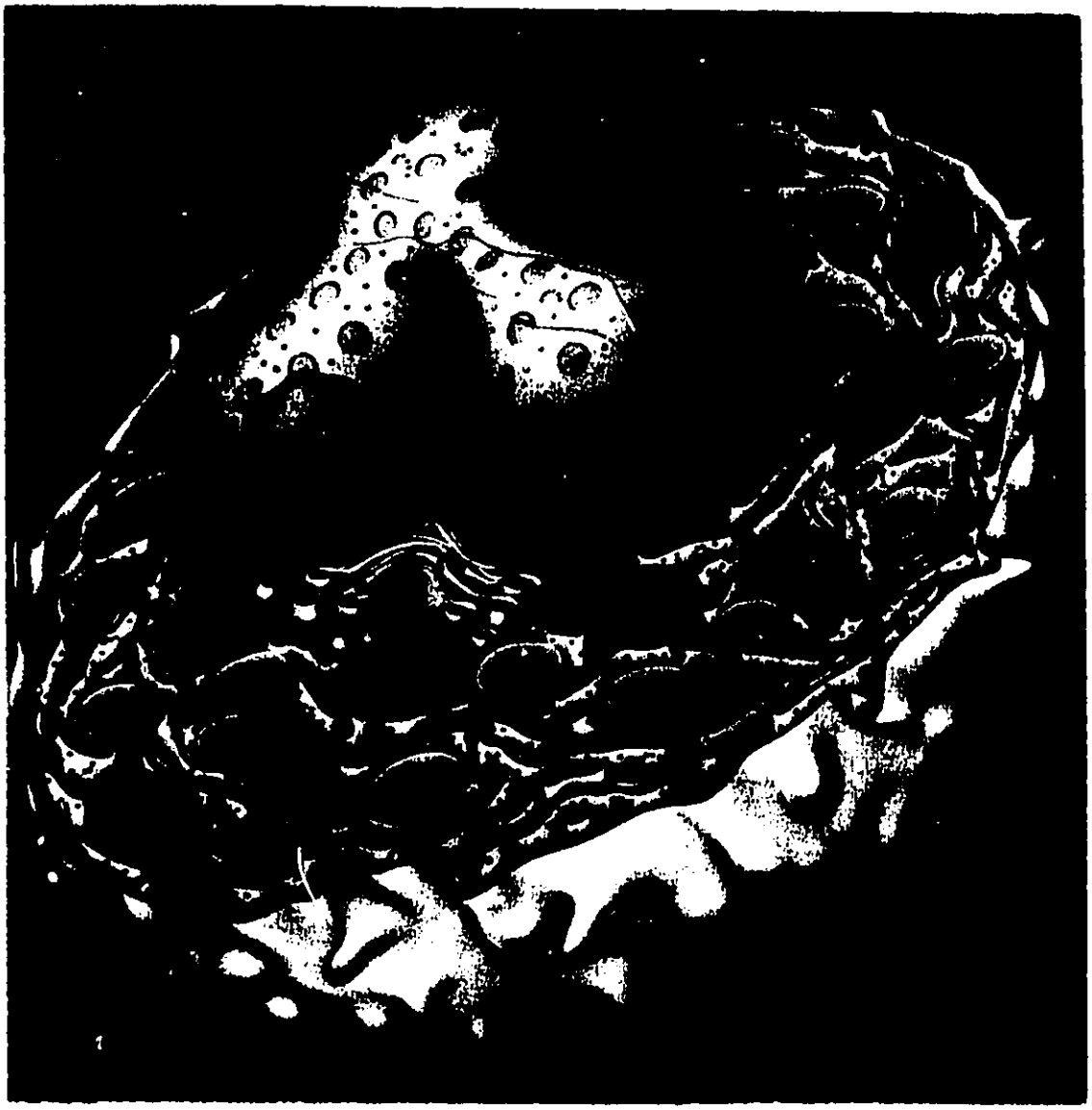

Figure 1.1. Diagram of an animal cell (from Darnell et al., 1990).

1.1.1 Membrane Composition

The membrane has been long accepted as a heterogeneous asymmetric bilayer composed of many different components (Figure 1.2). As early as 1895 the lipid nature of the membrane has been known (Overton, 1895). Since then a number of membrane structures have been postulated concerning the bilayer nature of the membrane (Gorter and Grendel, 1925), its protein content (Danielli and Davson, 1935), its membrane structure (Branton, 1966), and its "fluidity" (Frye and Edidin, 1966). Singer and Nicholson (1972) amalgamated these ideas into the Fluid Mosaic Model, which basically pictures the membrane as a fluid-like phospholipid bilayer into which freely diffusing globular proteins are embedded to varying degrees. Although it is now clear that the membrane proteins do not all diffuse freely in the lipid bilayer (Jacobson, 1983), the following generalized picture of a bilayer is widely used.

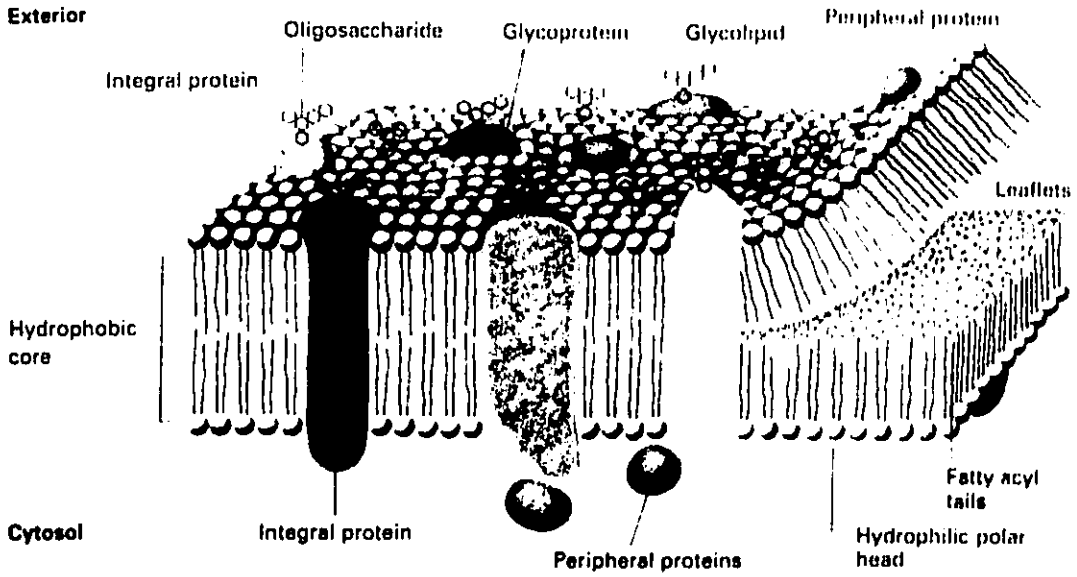

Figure 1.2. The membrane Fluid Mosaic Model (from Darnell et al., 1990).

Hydrophobic interactions between the lipid hydrocarbon region and an aqueous medium are the driving forces in the formation and maintenance of the membrane bilayer. All lipids are amphipathic with hydrophobic and hydrophilic portions. The hydrophilic region is in direct contact with the aqueous media (i.e. interstitial fluid, blood, cytosol) on both sides of the membrane. The lipid hydrophobic fragment is repelled by the polar medium and forms the interior of the membrane bilayer. The lipid composition and lipid-protein ratios vary enormously with different membranes.

There are three major classes of membrane lipids: sterol, sphingolipid and glycerolipid (Figure 1.3). Cholesterol, a sterol, is found in many membranes; it is especially abundant in mammalian cells and is absent from prokaryotic cells (bacteria). Other sterols are also very common in plant plasma membranes. Unlike the fused hydrocarbon rings of sterols, sphingolipids and glycerolipids have two hydrocarbon chains with varying degrees of length, unsaturation, and oxidation. The polar head groups of sphingolipids and glycerolipids are very diverse, they may be polar, zwitterionic, or charged: carbohydrates, substituted phosphates, and sialic acid. There are two essential differences between sphingo- and glycerolipids. First, the possible combinations of head groups and hydrophobic groups vary. Second, the glycerolipid backbone is glycerol and that of sphingolipid is ceramide, an amino alcohol. These differences and the corresponding variations in membrane function and structure in living cells have often been the source of many teleological discussions.

Glycoconjugates are an interesting and important membrane constituent sub-class; carbohydrates are covalently bound to proteins (glycoproteins) or lipids (glycolipids). For example, fibrinogen is a glycoprotein which has been implicated in the process of platelet aggregation (Woods et al. 1986). Whereas the glyceroglycolipids, mono- and digalactosyldiacylglycerol (MGDG and DGDG, respectively), are the principal lipids in the thylakoid membranes found in plants, algae, and photosynthetic bacteria. In addition, gangliosides are the most complex sphingolipids; they are carbohydrate-rich with at least one sialic acid sugar residue.

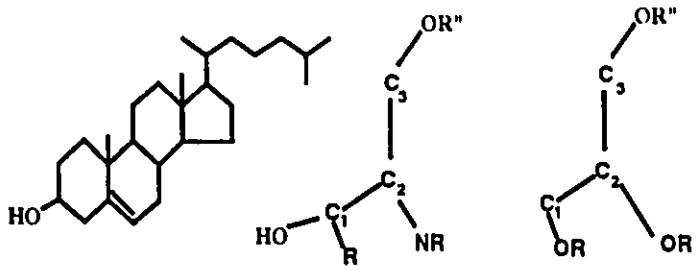

A B C

Glycolipid

R"		Polarity
- Glc	Glucose	Polar
- Glc-Gal-GalNAc-Gal | NAN	Ganglioside G_{M1} (sphingolipid only)	Charged (-)

Phospholipid

R"		Polarity
$-P(\bar{O})_2OH$	Phosphatidic acid	Charged (-)
$-P(\bar{O})_2O-CH_2-CH_2-\overset{+}{N}(CH_3)_3$	Phosphatidyl choline	Zwitterionic

Figure 1.3 Some membrane lipids. A) Cholesterol, B) sphingolipid with a ceramide group, C) glycerolipid with a glycerol group. R represents hydrocarbon chains. R" represents some hydrophillic head groups. Abbreviations used: Glc, glucose; Gal, galactose; GalNAc, N-acetylgalactosamine; NAN, N-acetylneuraminate (sialate).

1.1.2 Lipid Function

The primary role of lipids is to form a membrane, which differentiates cells and provides a matrix wherein the proteins interact. However, lipids are increasingly being recognized as active participants in membrane-associated processes. Many examples of lipid activity have been cited in the literature (Cull et al., 1983, Hakomori, 1984, Hanahan, 1986). A few examples are listed here because they relate to the research

reported in this dissertation. Gangliosides have been implicated in playing a role in the regulation of cell growth (Spiegel and Fishman, 1987), in binding to specific receptors in the plasma membrane (Cheresh et al., 1987) and in cell adhesion (Laitinen et al., 1987). A minor membrane component, diacylglyceride, is not only a precursor to membrane lipids, it also serves an important function as a second messenger in signal transduction to increase intracellular Ca^{2+} (Piomelli et al., 1987). Some lipids may be required in the membrane because their molecular shapes may be necessary to stabilize regions of high curvature and membrane junctions, or to optimize interaction with specific proteins (Curatolo, 1987; de Kruijff, 1987).

1.2 MODEL MEMBRANE SYSTEMS

Biological membranes are complex in their level of organization, structure, and function. Since the postulation of the Fluid Mosaic Model, much of the focus in membrane research has been directed towards the structure and dynamics of the membrane and their relationship with membrane function. Membrane spectroscopy is greatly simplified when the number of components in a system is limited to three or less, and when these systems can be physically manipulated (§1.2.2), therefore, model membrane systems are studied.

1.2.1 Lipid Polymorphism

Lipid-water mixtures are polymorphic (more than one structure), even for single purified lipids. The particular polymorph which predominates depends on a number of thermodynamic factors such as concentration, temperature, pressure, ionic strength, and pH. The major organized aggregate structures formed by lipid-water systems are depicted schematically in Figures 1.4.a-d (from Lindblom and Rilfors, 1988).

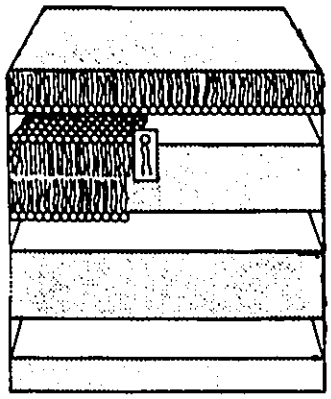

Figure 1.4.a Lamellar phase.

The lamellar phase can be in one of the following three states:

Gel state ($L_{\beta'}$): Lipids form a tightly packed bilayer at low temperatures where the acyl chains are highly ordered, corresponding to the all-trans configuration.

Liquid crystalline state (L_{α}): The bulk of biomembrane lipids are in this higher temperature state. There is two-dimensional order but the acyl chains are more disordered than in the $L_{\beta'}$ phase. When in these states the molecules are packed into a cylindrical space.

Ripple state ($P_{\beta'}$): This state (not shown) is intermediate between the above lamellar phases and the following non-lamellar phases.

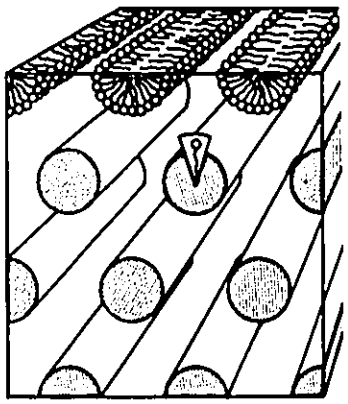

Figure 1.4.b Hexagonal I phase (H_I or H_{α}). At higher temperatures, lipids form hexagonally packed parallel cylinders with the polar groups on the outside. The molecules fit into an inverted cone-shaped space.

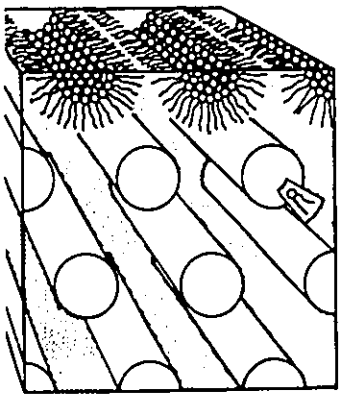

Figure 1.4.c Hexagonal II phase (H_{II} or H_β). This polymorph is similar to H_I except the polar groups face inwards, effectively surrounding a column of water. The molecules most easily conform to a cone-shaped space.

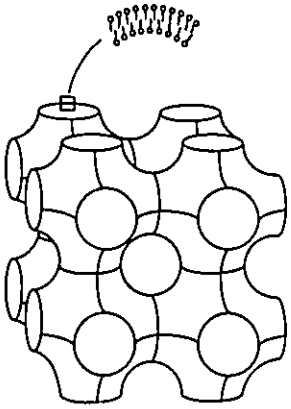

Figure 1.4.d Cubic Phase (Q_α). This high temperature phase forms columns, with the polar groups facing in. The columns are continuous in three dimensions, therefore the symmetry is isotropic. The molecules fill a cone-shaped area.

Three lipids that are considered in this dissertation have very different lipid-water phase diagrams (Figure 1.5): MGDG, DGDG, and 1,2-dipalmitoyl-*sn*-glycero-3-phosphocholine (DPPC). Both MGDG and DGDG exist in one predominant type of phase. DGDG forms stable bilayers, typical of many biomembrane lipids. However, MGDG forms the non-lamellar H_{II} phase, presumably, because of the small amount of space occupied by the head group. The phase behaviour of DPPC is considerably more complicated; at some conditions two different types of phase coexist.

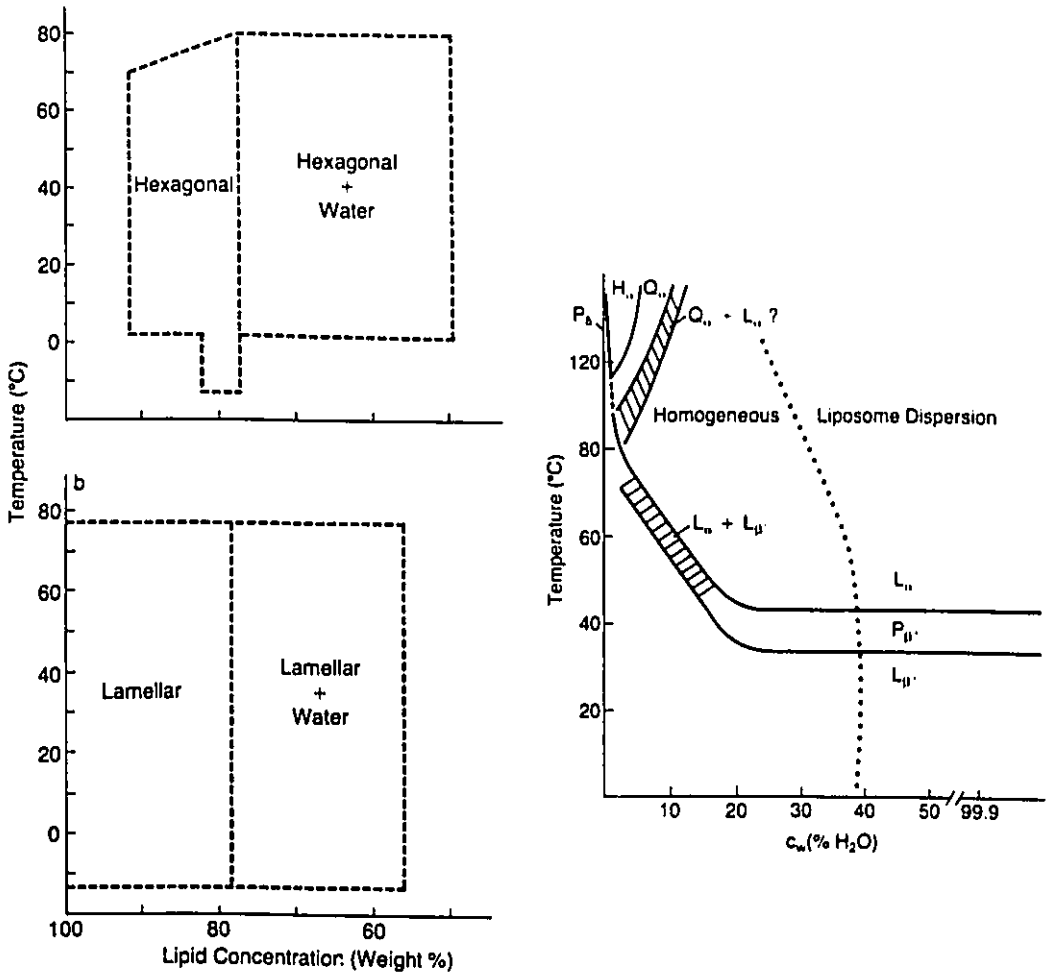

Figure 1.5 Pure lipid/water phase diagrams. Monogalactosyldiacylglyceride (MGDG), **top left,** digalactosyldiacylglyceride (DGDG), **bottom left,** and dipalmitoylphosphatidylcholine (DPPC), **above right** (from Gennis, 1989). The galactolipids were extracted from plant leaves, the acyl chains are predominantly unsaturated.

Another lipid studied is 1,2-di-*O*-tetradecyl-3-*O*-(β-D-glucopyranosyl-*sn*-glycerol (β-DTGL). Under the conditions at which β-DTGL is studied it forms the L_α phase (55°C, Hinz et al., 1985). The above mentioned lipids have been single-component systems, in this dissertaion they will be studied as lipid mixtures and as biomembranes; their phase behaviour will be more complex.

1.2.2 Oriented Systems

Most model systems employed are liquid crystalline, some of which are orientable in a magnetic field. This property is very useful in spectroscopic studies, and particularly convenient in nuclear magnetic resonance (NMR) studies. The orientation of membrane systems results in remarkable spectral simplification and a significant improvement in sensitivity (Winsborrow et al., 1991). The details of the effect on NMR spectra are discussed in Chapter 2.

Many orientable systems described in the literature are based on fatty acid salts (Biodart et al., 1988). There are at least two drawbacks to these systems. First the major components are not found in biological membranes, and second, some are protein denaturants. If biological applications of model systems are to be considered, phospholipid-based orientable systems are necessary because these lipids are the single most common animal cell membrane component. A phospholipid based system has been reported (Sanders and Prestegard, 1991) which has the benefits of providing a biologically relevant bilayer matrix that is magnetically orientable. The major components are 1,2-dimyristoyl-*sn*-glycero-3-phosphocholine (DMPC) and 3-(cholamidopropyl)dimethylammonio-2-hydroxy-1-propanesulfonate (CHAPSO).

Systems which do not orient spontaneously can also be ordered by stacking multibilayers on glass plates (Jarrell et al., 1987*a*). This method is especially advantageous because the sample can be treated as a single crystal and mechanically rotated over a range of angles (0°-90°, § Chapter 3).

1.3 DYNAMICS OF MEMBRANE EMBEDDED LIPIDS

1.3.1 Introduction

Cell surface carbohydrates play a crucial role in cellular biology. For example, gangliosides, a class of sphingolipids, have been implicated in important cellular events (§ 1.1.2). The accessibility of glycolipids to such interactions is governed, in part, by two properties: head group conformation/orientation at the membrane surface, and lipid

dynamics. That is, in order for an event to occur at a membrane surface the orientation of the lipid head group, with respect to the membrane surface, and the motion that the lipid is undergoing may be significant. Conformation/orientation studies probe the spatial organization of these molecules, and will be discussed in the next section (§ 1.4). The analysis of lipid dynamics involves the investigation of the types and rates of lipid motion and is considered below.

1.3.2 Physical Studies

A number of physical techniques are used for dynamical analysis: Raman, infrared (IR), electron spin resonance (ESR), fluorescence depolarization, phosphorescence depolarization, and nuclear magnetic resonance (NMR). Raman, IR, and NMR studies investigate the dynamics of both isotopically labelled and unmodified membrane lipids. ESR, fluorescence, and phosphorescence studies, on the other hand, are less direct, wherein they employ membrane embedded lipid analogue probes. The advantage of using probes is that small concentrations of probes can be used because the spectroscopic techniques are very sensitive. However, these probes are perturbing and may actually disrupt the membrane under consideration.

Three quantifiable parameters of lipids and analogue probes that can be obtained from the above physical studies are: rotational correlation times, lateral diffusion constants, and order parameters. Rotational correlation times indicate the rate at which a lipid molecule or probe rotates about a given molecular axis. Diffusion constants specify the rate at which the detected molecules diffuse (move) laterally across a membrane. Order parameters generally indicate the degree of motional averaging (disorder) that a molecular segment undergoes within the time frame of the experiment. These parameters are used to characterize aspects of lipid dynamics; some will be discussed in greater detail in Chapter 2.

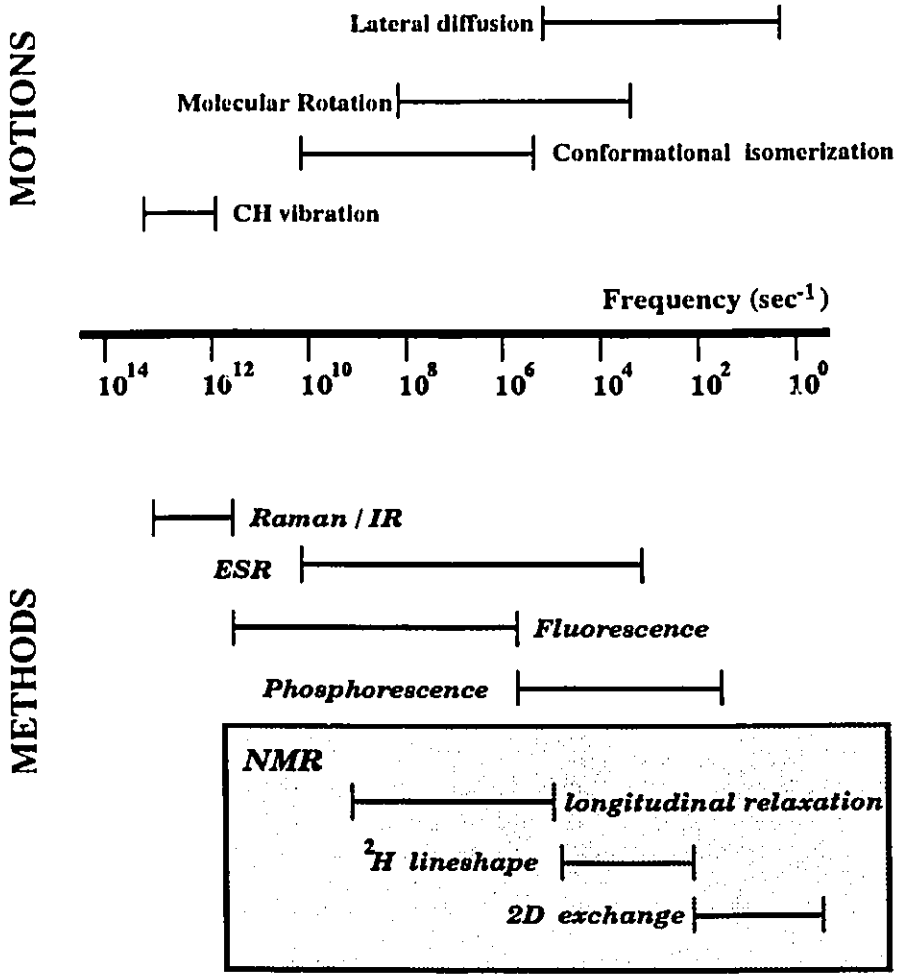

Figure 1.6 Methods and Motions. Some characteristic frequencies of membrane lipid molecular motions compared with the frequency ranges in which various spectroscopic techniques are sensitive to molecular motion. Boundaries are very approximate.

Deuterium NMR (^{2}H NMR) has proven to be an extremely valuable tool in studying the dynamics of ordered environments, such as model membrane systems (Seelig, 1977; Seelig and Seelig, 1980; Smith, 1989; Davis, 1991). As indicated in Figure 1.6, the time frame of many lipid motions (1 - 10^{10} sec^{-1}) can be accessed by a number of ^{2}H NMR techniques, each with a different spectral window. Transverse relaxation times, T_{2e} (Jeffrey, 1981), and the two-dimensional exchange technique (Schmidt et al., 1988; Wefing and Speiss, 1988) probe the slow motions of deuterium

labelled lipids (1 - 10^3 sec^{-1}). Intermediate frequency motions (10^4 - 10^6 sec^{-1}) are elucidated with the use of ^2H NMR lineshape studies (Wittebort et al., 1987, Dufourc et al., 1984b). Finally, the faster lipid motions (10^7 - 10^{10} sec^{-1}) are investigated with ^2H NMR longitudinal relaxation studies (T_{1Z} and T_{1Q}). Anisotropic longitudinal relaxation measurements are particularly useful for obtaining unambiguous motional information (Siminovitch et al., 1988; Jarrell et al., 1988; Winsborrow et al., 1991).

1.3.3 Physical Interpretation

Once the experimental parameters are measured, it is important to relate them to a physical understanding of the molecular motions. One might wonder, for example, how it is possible to attach a time frame to a particular motion (Figure 1.6). To this end theoretical models are created to describe the molecular motions. The models are tested by comparing the predicted results with the observable physical parameters. A variety of motional models have been devised which range from discrete intramolecular jumps to collective motions for an ensemble of molecules (Torchia and Szabo, 1982; Meier et al., 1986; Vold and Vold, 1988; Van Den Ven and Levine, 1984). The basis of these models are discussed in Chapter 2.

1.3.3 Research Direction

As discussed above, cell surface glycolipids play very important roles in intercellular interactions (§ 1.1.2). Figure 1.7 is a depiction of the type of interaction that may occur at the cell surface between a ganglioside antigen and an antibody as suggested by Hakomori (1986). In order to appreciate the possible sensitivity of these interactions to glycolipid conformation and dynamics, we have devoted much attention to the glycolipid 1,2-di-*O*-tetradecyl-3-*O*-(β-D-glucopyranosyl-*sn*-glycerol (β-DTGL) (Jarrell et al., 1986, 1987a, 1987b; Winsborrow et al., 1992). β-DTGL is a mono-glucoside; it is a reasonable analogue of many gangliosides where the first sugar in the head group is usually glucose (§ 1.1.1). Our ultimate goal has been to define the conformation and dynamics of the glucose head group at the membrane surface.

The glucose head group of β-DTGL is exposed to the aqueous medium and both the glycerol backbone and hydrocarbon chains reside in the motionally restrictive membrane. A consistent trend has been observed in our ^{2}H NMR studies of partially ordered systems: the head group order parameter (S) is smaller than that of the entire lipid molecule portion (Carrier et al., 1989; Renou et al., 1989; Jarrell et al., 1987a, 1987b). ^{2}H NMR studies have also shown that there is a flexibility gradient along the hydrocarbon chain: the resistance to motion diminishes deeper into the membrane bilayer (Seelig and Seelig, 1974, 1975). It is expected, therefore, that the motions of the glycerol backbone will be less complex than that of the carbohydrate head group (Strenk et al., 1985). With this in mind we have undertaken the task of elucidating the hierarchy of membrane associated glycolipid dynamics.

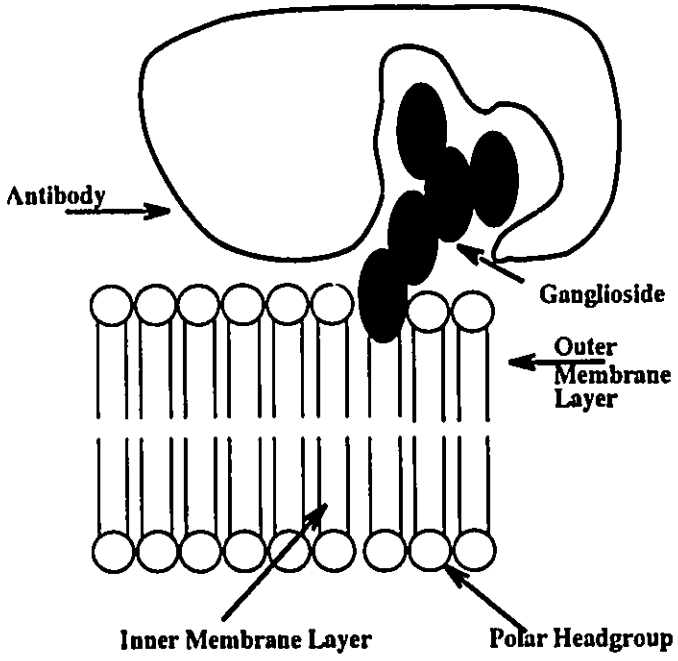

Figure 1.7 Intercellular Interaction. Depiction of an antibody interacting with the carbohydrate head group of a ganglioside antigen, indicating the possible significance of glycolipid motions and conformation at the membrane surface.

Previous work from this laboratory concluded that, for β-DTGL in the gel (L_β) phase, two motions were manifest at the glycerol *sn*-3 position (Auger et al., 1990). When we consider the dynamics of the less ordered liquid crystalline (L_α) phase, we

anticipate that there will be a stepwise progression in motional complexity: motions at the glycerol backbone are more restricted than in the carbohydrate region. Moreover, carbohydrate motions are superimposed upon the already established glycerol motions.

These studies rigorously test the ability of the model used previously for the gel phase to describe dynamics in the liquid crystalline phase of β-DTGL by using two ^2H NMR observation frequencies, oriented multibilayers, and two relaxation experiments (T_{1Z} and T_{1Q}). Frequency-dependent studies are a valuable approach to testing motional models in lipid systems (Dufourc et al., 1986; Brown, 1984). The importance of utilizing oriented samples and the T_{1Q} experiment to obtain unambiguous information on the system of interest will be further established.

1.4 CONFORMATIONAL ANALYSIS

1.4.1 Introduction

Biological, chemical , or physical properties of cell surface glycoconjugates are determined by their carbohydrate head groups which protrude from the membrane matrix. Before evaluating the dynamics of the carbohydrate head group, there must be an appreciation of its available three-dimensional space. The importance of describing the conformation of the carbohydrate region towards an understanding of the biological function is now widely accepted (Hakomori, 1986; Blackburn et al., 1986; Olden et al. 1985; Lemieux and Bock, 1983).

1.4.2 Physical Studies

There have been several approaches to obtaining a conformational description of the carbohydrate region of cell surface glycoconjugates. X-ray and NMR structural determinations are the two most common techniques employed.

X-ray analysis gives the most precise data for oligosaccharide conformation (Deisenhofer, 1981; Huber, 1980). However, the crystal environment is not the same

as in biological systems. Furthermore, larger oligosaccharides do not tend to crystallize, limiting the number of structures that may be studied by this technique. High field NMR methods applied to solution samples have also identified many carbohydrate head group structures (Meyer, 1990). In solution, however, there may be more than one preferred conformation; the head groups usually undergo rapid interconversion and most experimental techniques, like NMR, yield only the time-averaged conformation. In biological systems, head group motions may be dampened because the membrane surface may act as a barrier to full head group motion. With restricted motional averaging at the carbohydrate head group region of membrane glycolipids, the head group is very likely more ordered than in solution.

Solid state NMR is a technique which can investigate the head group conformations in a biologically relevant membrane environment, which is motionally limiting. This approach is technically difficult and is largely unexplored. However, several magnetic nuclei have been used (^{1}H, ^{2}H, ^{13}C, and ^{31}P) to measure a number of physical parameters: chemical shifts, coupling constants, relaxation rates, and order parameters (Jarrell et al. 1986, 1987a, and 1987b; Seelig and Macdonald, 1987; Renou et al., 1989; Carrier et al., 1989; Ram and Prestegard, 1988; Sanders and Prestegard, 1991).

Usually NMR spectroscopy alone does not give an unambiguous assignment of specific conformations, but rather supplies limits for the conformations. Calculations of the preferred carbohydrate conformations are very important as they allow a complementary assignment and an interpretation of the experimental parameters which makes dynamical analysis possible.

1.4.3 Theoretical Calculations

Insight into the conformational equilibrium that may exist about the glycosidic bond can be gained by means of conformational energy calculations which define the available conformational space of the carbohydrate moiety. The conformational energies

are calculable, in principle, from either classical (empirical) or quantum mechanical (non-empirical) procedures, or an amalgamation of the two (semi-empirical) (Thørgersen et al, 1982; Péréz et al. 1985).

There are a variety of classical methods which use a combination of energy contributions such as van der Waals interactions, bond torsion around the glycosidic C-O bond, and the exo-anomeric effect (Tvaroška, 1989). The monosaccharide units are treated as rigid units and a grid search over the glycosidic angles is performed. The classical energy functions rely mostly upon van der Waals interactions which have a dominant influence on the conformations of many oligosaccharides. It is also relatively easy to rank conformations in order of increasing or decreasing van der Waals repulsions. The exo-anomeric effect is another important parameter, it is responsible for preferred conformations and stabilities of α and β-pyranosides (Lemieux et al., 1980).

Force field or molecular mechanics (MM) methods have an approach similar to that above, except that the molecule is considered to be non-rigid; it is treated as a collection of atoms held together by harmonic forces (Tvaroška and Václavik, 1987). These forces can be described by the potential functions of structural features such as bond lengths and bond angles: the combination of these potential functions is the force field. In addition, Monte Carlo and molecular dynamics programs (Brady, 1987) provide other semi-empirical approaches to macromolecular structure determination.

Finally, non-empirical *ab initio* calculations are concerned with the three dimensional distribution of electrons around the nuclei. Therefore, they are the most rigorous of the computational methods. However, because these calculations make such heavy demands on computer time, only the structures of molecular fragments have been determined (Perczel et al., 1991).

1.4.4 Research Direction

The average head group conformation of β-DTGL has been previously determined by ^{2}H NMR, which assess the average head group conformation (Jarrell et al., 1987b). However, it has been acknowledged that a conformational equilibrium most likely exists at the carbohydrate head group (Jarrell et al., 1987b; Meyer, 1990; Winsborrow et al., 1991). An attempt at describing the potentially non-rigid nature of the glycosidic bond has also been made by Scarsdale and co-workers (1986, 1988). They have described an equilibrium between two possible head group conformations of glycolipids in dilute solution. For the calculations they used NMR results to weight energy functions of the molecular mechanics program AMBER (Assisted Molecular Building with Energy Refinement; Weiner et al., 1986).

As the next step in defining the molecular details of the recognition processes involving carbohydrates at membrane surfaces, it is very important to appreciate the types, amplitudes, and rates of motion that the head groups may undergo in highly organized structures such as lamellae (Winsborrow et al., 1992). In the following body of work classical conformational energy calculations are used to assess the conformational space available to the glucose head group of β-DTGL in a modelled lipid membrane matrix. Calculated ^{2}H NMR quadrupolar splittings are compared with those observed experimentally (Jarrell et al, 1987b). The importance of including surface interactions when considering cell surface carbohydrate conformations is demonstrated.

1.5 BIOMEMBRANES

1.5.1 Introduction

One of the most active areas of biological research is in the effort to establish relationships between molecular structure and biological function. In the case of membrane systems these questions of function are often formulated in terms of membrane structure: lipid and protein content, conformation, and dynamics. An

example of such interest in membrane structure and function is that in photosynthetic membranes of green plants and photosynthetic bacteria, which transform the physical energy of the sunlight into chemical energy (Renger, 1983). The membranes of the photoautotrophic prokaryotes, cyanobacteria, are studied herein by ^{2}H NMR.

Cyanobacteria contain only two types of membranes: plasma and thylakoid membranes (Murata and Omata, 1988). The thylakoid membranes contain the structural and functional basis for the light-dependent reactions of photosynthesis. They are composed of approximately 60% (by weight) protein. The four major classes of polar lipids in these membranes are mono- and digalactosyl diacylglycerol (MGDG and DGDG, respectively), sulfoquinovosyl diacylglycerol (SQDG), and phosphatidylglycerol phosphate (PG). The galactolipids comprise up to 70% of the thylakoid membrane polar lipids with approximately 3:2 MGDG to DGDG. Small amounts of neutral lipids (di- and triglycerides) are also found in these membranes (Quinn and Williams, 1983). Extensive studies have shown that the composition of the thylakoid membranes of *Anacystis nidulans* (Synecoccochus sp 6301) is influenced by the environmental conditions: growth temperatures, exogenous fatty acids in the growth medium (Quinn and Williams, 1983; Sato and Murata, 1988; Williams et al., 1990; Nicholov et al., 1991). The thylakoid membranes of *Anacystis nidulans* are ideal biomembranes to study because of their abundance, accessibility, and adaptability.

1.5.2 Physical Studies

The role of the membrane structure in the photosynthetic process has been the focus of a number of physical spectroscopic studies: absorption (Biggins, 1983), electron spin resonance, ESR, (Mansfield et al., 1987; Hore et al., 1986; Khanna et al., 1981), fluorescence emission (Laskay and Lehoczki, 1986), infrared (Nabedryk et al., 1984), and nuclear magnetic resonance, NMR, (Coleman et al., 1987; Ekiel et al., 1981; Khanna et al., 1981, Wong et al., 1977).

^{2}H NMR of deuterated lipids is very sensitive to the motions of the C-^{2}H bond

and is therefore indicative of the detailed structure of membranes (Seelig, 1977). For the investigation of biological membranes by ^2H NMR, ^2H-labelled fatty acids have been added to the growth media of unicellular organisms, which were then incorporated into membrane lipids: *Acholeplasma laidlawii* (Stockton et al, 1977; Rance et al., 1980) and *Eschericha coli* (Davis et al., 1979; Gally et al., 1979). This modality of labelling is advantageous because the deuterated lipids are essentially non-perturbing probes. For this reason ^2H NMR has been the method of choice for studying the structure and dynamics of both model and biological membranes (Seelig, 1980; Smith 1989; Davis, 1983 and 1991).

1.5.3 Research Direction

Murata and Omata (1988) have identified two thylakoid membrane bands after sucrose density gradient centrifugation (SDGC) of fractionated *A.nidulans* cells: **top band** (30/39% sucrose layer interface) and **bottom band** (39/50% interface). For *Anacystis nidulans R2* (Synecoccochus sp. PCC 7942-R2), another strain of *A.nidulans*, the relative amount of thylakoid membranes in the two bands is markedly different than that found for *A.nidulans*. However, up to now, the differences in the composition or function of the two thylakoid membrane bands have not yet been investigated. To date the main functional difference between the two strains is that the *A.nidulans R2* cells readily incorporate exogenous DNA into their cells, and are used for modification/ adaptation studies (Wada et al., 1990). However, no further data are available concerning any structural or compositional differences between *A.nidulans* and *A.nidulans R2* thylakoid membranes.

We have used ^2H NMR for the first time to study the thylakoid membranes of *A.nidulans* and *A.nidulans R2*. The labelling of the membranes was achieved by cultivating both strains for 48 hours in medium supplemented with perdeuterated palmitic acid ($^2H_{31}$ 16:0). In order to obtain more information on the membrane metabolism, the thylakoid membranes of *A.nidulans R2* were investigated also after 96 hours of culture in medium containing perdeuterated palmitic acid. Additionally, a

profile of the temperature-dependent spectra of specifically labelled oleic acid ($18:1^{\Delta 9}$) incorporated into membranes has been obtained for the thylakoid membranes of *A.nidulans*. As a means to gain further insight into the factors that influence the phase behaviour of the thylakoid membranes, their lipids were extracted and lipid analysis as well as ^2H NMR studies were performed.

1.6 OUTLINE

This dissertation is divided into four parts. Part I presents an overview of the main concepts within this dissertation (Chapter 1), basic NMR theory relevant to the work carried out herein (Chapter 2), and a description of the materials and methods used (Chapter 3).

Part II discusses a variety of studies performed on model membrane systems. Particular attention has been devoted to the glycolipid β-DTGL. A ^2H NMR lineshape analysis defines its dynamics in the liquid crystalline state (Chapter 4). Conformational potential energy calculations demonstrate the significance of including surface interactions in assessing the conformational space of the β-DTGL head group (Chapter 5).

Part III evaluates the ^2H NMR spectra of biological membranes. A study of lipid-protein interactions and the effects of exogenous unsaturated fatty acids on the thylakoid membranes of the cyanobacterium *Anacystis nidulans* is presented (Chapter 6). A metabolic study compares the thylakoid membrane structure of *A.nidulans* and *A.nidulans R2* (Chapter 7).

Part IV closes this dissertation with concluding remarks and suggestions for future work (Chapter 8).

Chapter 2

NMR Background

As discussed in Chapter 1, membrane phenomena at the molecular level are complex. Semi-rigid membrane dynamics and the lack of long range order limit most spectroscopic techniques. Solid state nuclear magnetic resonance (NMR) has proven to be a very useful technique because it is sensitive to the incompletely averaged orientation-dependent tensorial interactions between the nuclear spin system and its environment. This chapter is intended to review the quantum mechanical descriptions of the energetics of such interactions and their significance in the NMR experiment. One of the more important points to be made is the recurring concept of the orientational dependence of the tensorial interactions and its utility in the elucidation of conformational and dynamical properties.

2.1 MAGNETIC RESONANCE

The nuclear spins which possess angular momentum, **J**, generate a magnetic dipole moment, μ. Both properties are vectors and are related by a scalar factor (Abragam, 1961):

$$\mu = \gamma \cdot \mathbf{J} \qquad 2.1$$

where γ is the gyromagnetic ratio. In an external magnetic field, $\mathbf{H}_o$, the angular momentum is quantized by the spin angular momentum operator **I** ($\mathbf{I} = \mathbf{I}_x + \mathbf{I}_y + \mathbf{I}_z$), along the magnetic field z-axis:

$$\mathbf{J} = \hbar \cdot \mathbf{I}_z \qquad 2.2$$

$\hbar$ is Planck's constant divided by 2π. Quantization of angular momentum implies a quantization of energy. Each energy state (E) of the nucleus is specified by the magnetic (m) and spin angular momentum (I) quantum numbers and has a stationary state wave function, Ψ, which satisfies the Schrodinger equation:

$$\mathcal{H}\,\Psi = E\,\Psi \qquad 2.3$$

$\mathcal{H}$ is a Hamiltonian operator, which defines particular energetic interactions operating on a given state. For the Zeeman interaction, described above:

$$\mathcal{H}_z = -\mu\,\mathbf{H}_o \qquad 2.4$$

$$= -\gamma\,\hbar\,\mathbf{I}_z\mathbf{H}_o \qquad 2.5$$

The resultant energy of interaction is:

$$E_m = -\gamma\,\hbar\,m\,\mathbf{H}_o \qquad (m = -I, -I+1,\ldots,I) \qquad 2.6$$

Therefore, there are (2I + 1) energy states, known as Zeeman energy levels.

The magnetic dipole moment precesses about the nuclear axis at the nuclear Larmor frequency, ω_o, in the radio frequency (RF) region, at typical field strengths:

$$\omega_o = \gamma \mathbf{H}_o \qquad 2.7$$

If a smaller magnetic field, $\mathbf{H}_1$, is applied perpendicular to $\mathbf{H}_o$, which matches the Larmor frequency, the system will absorb energy and a transition between the energy levels will be induced when $\Delta m = \pm 1$. This phenomenon is magnetic resonance and its detection is the basis of any NMR experiment.

2.2 DIFFERENT HAMILTONIANS FOR DIFFERENT INTERACTIONS

2.2.1 A Collection of Interactions

The magnitude of the Zeeman interaction is of the order of 10^7 - 10^8 Hz, as specified by the Larmor frequency. In addition, there are a number of lower energy interactions, $\mathcal{H}_{lc}$ (10^1 - 10^5 Hz), that can be detected by NMR spectroscopy:

$$\mathcal{H}_{total} = \mathcal{H}_z + \mathcal{H}_{lc} \qquad 2.8$$

Although the lower energy interactions are considered as first order perturbations of the Zeeman interaction, $\mathcal{H}_z$, their detection and analysis gives insight into molecular conformation and dynamics. All of the following interactions are orientation dependent second rank tensors (Mehring, 1983) and are described in frequency units:

$$\mathcal{H}_{lc} = \mathcal{H}_s + \mathcal{H}_J + \mathcal{H}_D + \mathcal{H}_Q. \qquad 2.9$$

Each of these lower energy interactions will be discussed in the following four sections.

2.2.2 High Resolution Hamiltonians

2.2.2.a The Shielding Hamiltonian

The nucleus is partially shielded from $\mathbf{H}_o$ by its electronic environment, this interaction is defined by $\mathcal{H}_s$ (the ~ above a symbol denotes a second rank tensor):

$$\mathcal{H}_s = \gamma \hbar \mathbf{I}_z \tilde{\sigma} \mathbf{H}_o \qquad 2.10$$

The shielding tensor, $\tilde{\sigma}$, is only slightly asymmetric, therefore, to a first order approximation it is considered to be symmetric. The maximum frequency of this interaction is about 10^3 Hz for protons (at 4.7 T field strength). In the solid state the directional anisotropy in the diagonalized tensor can be evaluated. In solution, the molecule undergoes rapid isotropic tumbling and the tensor is averaged to a single isotropic scalar value, equal to one third of its trace. Although this term may not always be significant in the solid state, it is the dominant perturbing interaction in high resolution NMR experiments.

2.2.2.b The Indirect Scalar Coupling Hamiltonian

Transverse or J coupling results from scalar through bond coupling between proximal spins:

$$\mathcal{H}_J = \sum_{i,j} \mathbf{I}_i \cdot \tilde{\mathbf{J}} \cdot \mathbf{I}_j \qquad 2.11$$

The magnitude of this low energy interaction is most often very small (10^0 - 10^2 Hz) and is usually of no consequence in solid state NMR experiments.

2.2.3 The Solid State Hamiltonians

The last two interactions, $\mathcal{H}_D$ and $\mathcal{H}_Q$, are defined by symmetric, traceless second rank tensors and are therefore completely averaged to zero in high resolution NMR experiments; their effect will remain indirectly manifest in longitudinal relaxation. However, in the case of a rigid solid, these tensors are not averaged. Hence, a wealth of structural information is available because the tensors are sensitive to the molecular orientation in the magnetic field. These Hamiltonians are described below in fairly general terms, for a more analytical description the reader is referred to Abragam (1961), Mehring (1983, Appendix), and Slichter (1990). Both Seelig (1977) and Davis (1983) present excellent descriptions and derivations of the quadrupolar Hamiltonian.

2.2.3.a The Direct Dipolar Coupling Hamiltonian

Dipolar coupling, $\mathcal{H}_D$, is the direct through-space interaction between magnetic dipole moments of two nuclei (i and j), in general:

$$\mathcal{H}_D = \sum_{i,j} \mathbf{I}_i \cdot \tilde{\mathbf{D}} \cdot \mathbf{I}_j \qquad 2.12$$

For a strong magnetic field it can be expressed by:

$$\mathcal{H}_D = \sum_{i,j} \frac{\gamma_i\gamma_j h}{4\pi^2 r_{ij}^3} \frac{(3\cos^2\theta - 1)}{2} (3\mathbf{I}_{iz} \cdot \mathbf{I}_{jz} - \mathbf{I}_i\mathbf{I}_j) \qquad 2.13$$

where γ, h, $\mathbf{I}_z$ and I have their usual meanings. r_{ij} is the internuclear distance and 0 is the angle that the internuclear vector makes with $\mathbf{H}_o$. The constants collectively define the dipolar coupling constant, $\gamma^2h/4\pi^2r^3$, which is in the order of 10^5 Hz for ^{13}C-^1H interactions.

2.2.3.b The Quadrupolar Hamiltonian

$\mathcal{H}_Q$ is the quadrupolar Hamiltonian, which only applies to quadrupolar nuclei ($I > ½$). In these cases there is a non-symmetrical charge distribution within the nucleus creating an electric quadrupole moment, eQ, which interacts with the electric field gradient (efg) at the nucleus.

$$\mathcal{H}_Q = \frac{eQ}{2I(2I-1)h} \mathbf{I} \cdot \tilde{\mathbf{V}} \cdot \mathbf{I} \qquad 2.14$$

$\tilde{\mathbf{V}}$ is the efg tensor; when diagonalized it is characterized by only two parameters, V_{zz} and $V_{xx} - V_{yy}$. In the molecular frame the efg is defined along the V_{zz} principal axis (in Cartesian coordinates):

$$V_{zz} = eq \qquad 2.15$$

and its asymmetry is defined by:

$$\frac{V_{xx} - V_{yy}}{V_{zz}} = \eta \qquad 2.16$$

After transformation of the efg tensor to the laboratory frame and all tensors into spherical polar coordinates, the quadrupolar Hamiltonian takes on the following form (Seelig, 1977; Davis, 1983; Mehring, 1983; Slichter, 1990):

$$\mathcal{H}_Q = \frac{eQ}{2I(2I-1)h} \cdot \sum_{q=-2}^{2}(-1)^q T^{2q} \sum_{q=-2}^{4} D^{(2)}_{pq}(\alpha,\beta,\gamma)\, V^{2p} \qquad 2.17$$

T^{2q} represents the symmetrical second rank elements of $\mathbf{I}$ in spherical polar coordinates. D_{pq} are the elements of the Wigner rotation matrices, which are used to transform the efg tensor from the molecular frame (principal axis system) to the laboratory frame by rotation about the Euler angles (α,β,γ) (Rose, 1957). NMR experiments use large magnetic fields, therefore only the $q = 0$ elements of the spin operator and the Wigner rotation matrix are significant ($\gamma = 0$). In addition the Euler angles (α,β) correspond to the spherical polar angles (θ,ϕ) (p 50 in Rose, 1957). $\mathcal{H}_Q$ can be simplified to:

$$\mathcal{H}_Q = \frac{e^2qQ}{4I(2I-1)h} \cdot (3I_z^2 - I(I+1)) \cdot \left[\frac{(3\cos^2\theta - 1)}{2} + \frac{\eta\sin^2\theta\cos 2\phi}{2}\right] \qquad 2.18$$

Like the dipolar Hamiltonian, this equation can be decomposed into two components: a constant and a geometric term. The quadrupolar coupling constant is the collection of constants, e^2qQ/h; in solid state NMR, at high fields, this is the single dominant interaction where the maximum value is approximately 250 kHz for deuterons. The geometric term, in square brackets, describes the orientation of the principal components of the efg tensor, with respect to $\mathbf{H}_o$, in spherical polar coordinates.

2.3 SOLID STATE ^2H NMR SPECTRA

Although membrane systems can be very complex, their analysis may be simplified considerably by isotopic labelling of specific sites in selected molecules. Deuterium (^2H) labelling has made solid state NMR of membranes more accessible. The following is a discussion of ^2H NMR spectra for a rigid system.

Table 2.1 Nuclear Parameters of ^2H nuclei.

Properties	^2H
Spin, I	1
Electric Quadrupole Moment (m^2)	2.87×10^{-31}
Gyromagnetic Ratio (rad s^{-1} T^{-1})	4.1×10^7
Natural Abundance (%)	0.015
Larmor Frequency at 7.1T (MHz)	46.1

Deuterium is a quadrupolar nucleus ($I > ½$, Table 2.1), therefore the solid state spectrum will usually be dominated by the quadrupolar interaction. The sum of the Zeeman (eq. 2.6) and quadrupolar (eq. 2.18) interactions is:

$$E_m = -\frac{\hbar\omega_o m}{2\pi} + \frac{e^2qQ}{4I(2I-1)h} \cdot (3I_z^2 - m(m+1)) \cdot \left[\frac{(3\cos^2\theta - 1)}{2} + \frac{\eta\sin^2\theta\cos 2\phi}{2}\right] \qquad 2.19$$

As shown in Figure 2.1, there are two $\Delta m = \pm 1$ transitions; the quadrupolar interaction removes the degeneracy of the transitions. Hence, two resonance lines separated by the quadrupolar splitting, $\Delta\upsilon_Q$, are observed in the NMR spectrum:

$$\Delta\upsilon_Q = \frac{3e^2qQ}{2h} \cdot \left[\frac{(3\cos^2\theta - 1)}{2} + \frac{\eta\sin^2\theta\cos 2\phi}{2}\right] \qquad 2.20$$

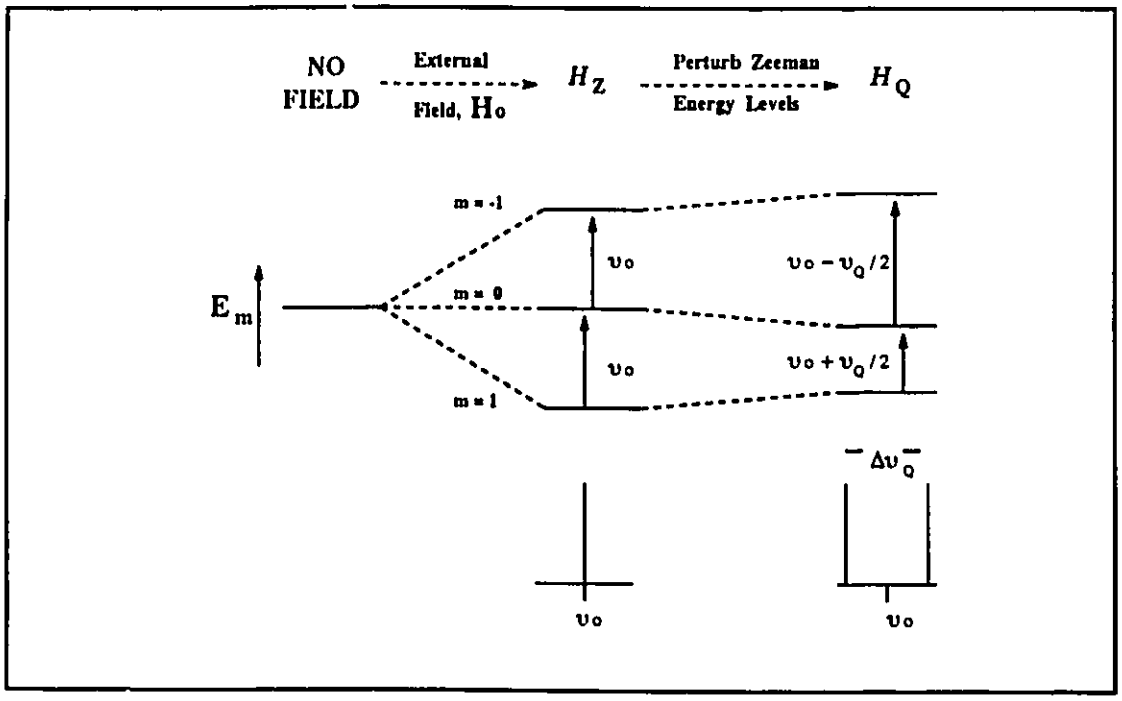

Figure 2.1 Depiction of the energy levels of a nucleus, spin I = 1. Outside a magnetic field (left), in a magnetic field with Zeeman interactions (centre), and then perturbation by the quadrupolar interaction (right). The observable NMR spectra for one nucleus are represented below the corresponding energy levels.

When the efg is axially symmetric the asymmetry parameter, η (eq. 2.16), is reduced to zero; the quadrupolar splitting is dependent upon one orientation angle, θ, which the V_{zz} makes with $\mathbf{H}_o$. In a polycrystalline sample the nuclear sites are randomly

oriented approximately in the zone of a sphere; the probability density of their orientation at an angle θ is $P(\theta) = \frac{1}{2} \sin\theta$ (Seelig, 1977). The signal intensities are proportional to $P(\theta)$, and their superposition results in a powder spectrum. Since the chemical shielding for deuterium is insignificant relative to the quadrupolar interaction (10^2 Hz vs. 10^5 Hz, respectively), the spectra will be a superimposed sum of signals centred about the Larmor frequency, separated by their respective quadrupolar splittings:

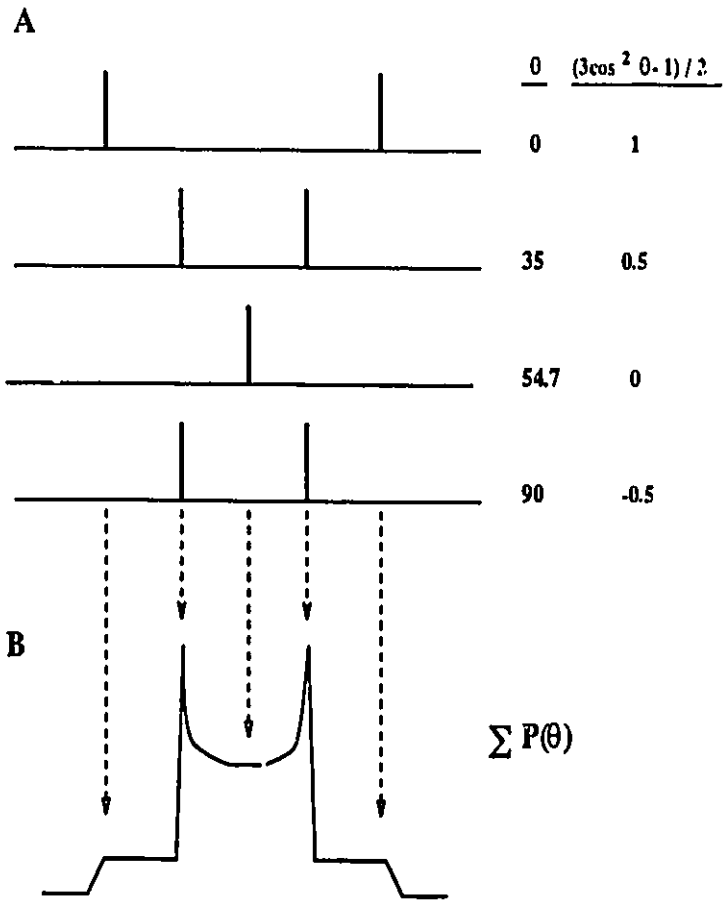

Figure 2.2 Angular dependence of the NMR spectrum when $\eta = 0$. A) deuterium spectra of a nucleus oriented at several angles with respect to H_o. B) a powder spectrum, which is the sum of all orientations; the intensities are dependent upon the probability densities $P(\theta) = \frac{1}{2} \sin\theta$.

If the nuclear environment is not symmetrical, the asymmetry parameter is not equal to zero and spectra are dependent upon both θ and ϕ. For comparison, Figure 2.3 depicts simulated ^2H NMR spectra when η = 0 and 0.5:

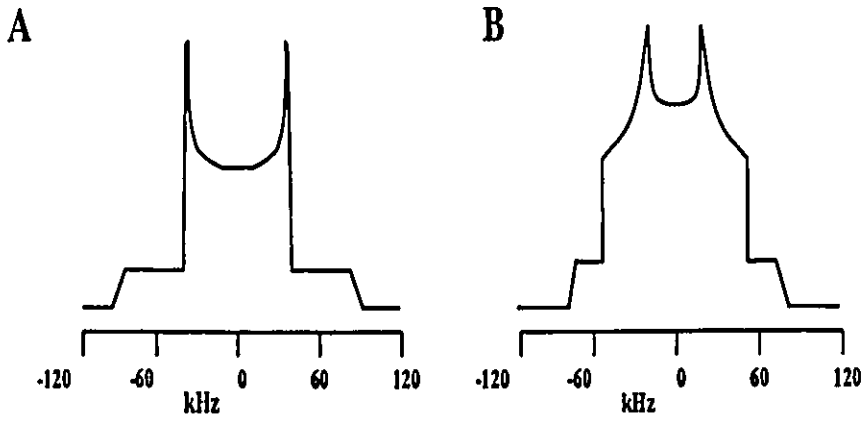

Figure 2.3 Simulated ^2H NMR spectra of a randomly oriented powder sample. A) η = 0, the spectrum is dependent upon θ. B) η = 0.5, the spectrum is dependent upon both θ and ϕ.

2.4 NMR LINESHAPES OF NON-RIGID SYSTEMS

2.4.1 Introduction

The Zeeman, dipolar, and quadrupolar interactions are the largest interactions that occur in the solid state. If the system under investigation is not rigid, the motion will be manifest in the NMR spectral line shape in a manner dependent upon the nature and frequency of motion. The motional rates can be broken down into three general regimes where the correlation time of a given motion, τ_c, is related to a transition frequency: slow limit, $\tau_c\omega >>> 1$; intermediate limit, $\tau_c\omega \approx 1$; fast limit, $\tau_c\omega <<< 1$. ω is a transition frequency ($\omega = 2\pi\upsilon$) which corresponds to one of the detectable interactions (i.e. Zeeman, υ_o; quadrupolar, $\Delta\upsilon_Q$; dipolar, $\Delta\upsilon_D$).

Motions that are slow enough may produce separate sets of observable signals. In a very simple case, a molecule undergoing a slow two site conformational jump may generate a separate set of observable signals for each conformation. When the rate of motion increases, the spectral line shape will change, ultimately resulting in a spectrum where the observable signals are averaged. As alluded to in the above example, the motional frequency is not the only factor affecting the line shape; the number of conformational sites, their respective populations, and the orientation with respect to $\mathbf{H}_0$ are also important parameters.

In biological systems this motional averaging is both common and complex. There have been a number of approaches in the analysis and description of the motions which give rise to the NMR spectral line shapes. The following is a brief discussion of ^{2}H NMR line shape analysis with regards to motional narrowing (order parameters), relaxation (spectral density treatment), and creating a physical picture of the motions (motional models).

2.4.2 Motional Narrowing of NMR Spectra (Order Parameters)

In the liquid crystalline phase, lipid molecules tend to fill cylindrical spaces and align with their molecular long axes parallel to each other (see Figure 1.4d). The molecular long axes are coincident with the normal to the membrane surface ($\vec{\mathbf{n}}$). These systems are not rigid; rotations around the long axes are symmetric and fast enough to average the asymmetry parameter, η, to zero in a ^{2}H NMR spectrum (Figure 2.4A). Although rotations perpendicular to the molecular long axes are restricted, angular excursions of small amplitude occur (Figure 2.4B). The time frame of these fluctuations (fast limit with respect to quadrupolar coupling; $\omega_Q^2\tau_c^2 <<< 1$) is such that an averaged (less broad) signal is observed.

Saupe (1964) first described these fluctuations in relation to an ordering of the system and introduced a second rank ordering tensor, $\tilde{\mathbf{S}}_{ij}$ (i,j = 1,2,3 or x,y,z). When used with diagonalized tensors, such as $\tilde{\mathbf{V}}$ (eq. 2.17), only the diagonal elements are

necessary to describe the ordering of the system. Furthermore, if a molecule has a rotation axis C_n, along the molecular z-axis with n > 2, then only the S_{zz} element needs to be specified (p 14, Emsley and Lindon, 1975). Therefore, for quadrupolar coupling in the laboratory frame (Seelig, 1977):

$$\Delta\upsilon_Q = \frac{3e^2qQ}{2h} \cdot \frac{(3\cos^2\beta - 1)}{2} \cdot S_{zz} \qquad 2.21$$

where β defines the orientation of the bilayer normal with respect $\mathbf{H}_o$, and:

$$S_{zz} = \frac{<3\cos^2\gamma - 1>}{2} \qquad 2.22$$

γ defines the angle between the fluctuating molecular axis (order director), $\vec{n}(t)$, and the bilayer normal; the angular brackets denote the time average of the angular fluctuations.

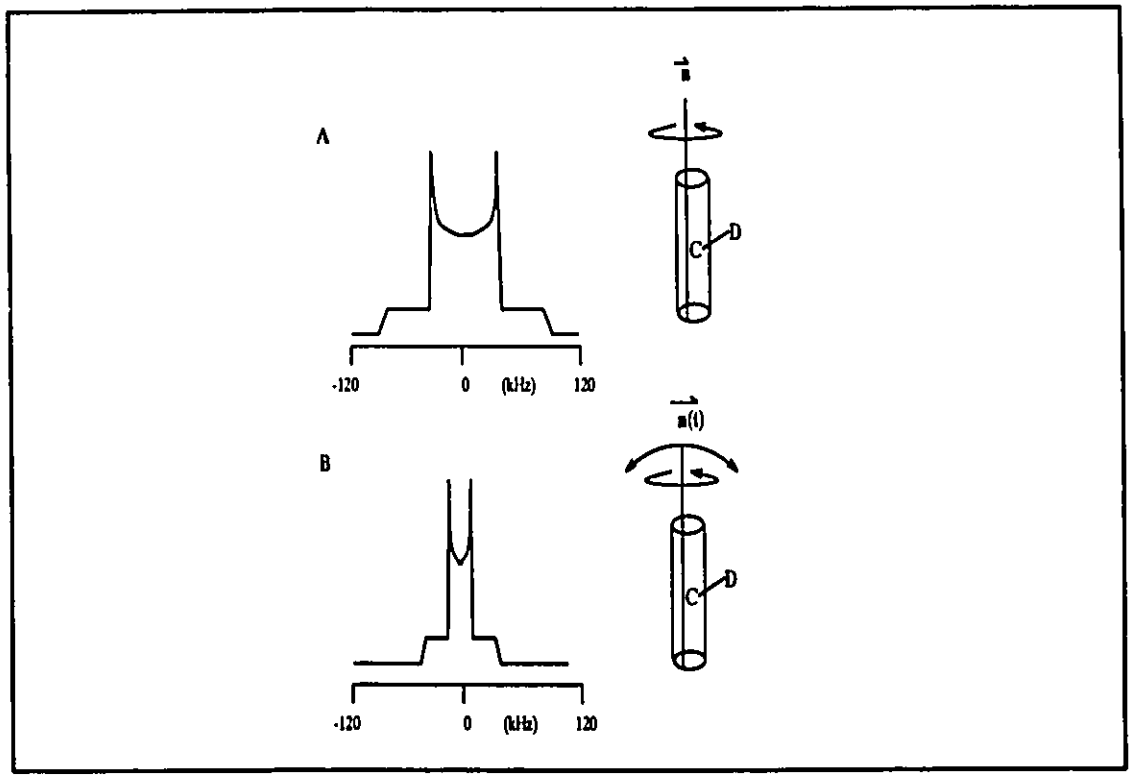

Figure 2.4 Motionally averaged ^{2}H NMR spectra. A) axially symmetric rotation around the molecular long axis averages η to zero. B) small angular excursions from $\vec{n}$ occur; the molecular long axis is now referred to as $\vec{n}(t)$ because its position is time dependent.

If the internal structure of the molecule is rigid, S_{zz} can be further decomposed into two angular terms (Petersen and Chan, 1977):

$$S_{zz} = \left\langle \frac{3\cos^2\gamma - 1}{2} \right\rangle \cdot \frac{(3\cos^2\theta - 1)}{2} \qquad 2.23$$

The molecular geometry is specified by the angle θ, which defines the angle between the C-^{2}H bond and the molecular long axis. The term in the angular brackets is the same as in eq. 2.22, and is also known as the segmental order parameter, *S*. $\Delta\upsilon_Q$ now takes the form:

$$\Delta\upsilon_Q = \frac{3e^2qQ}{2h} \cdot \frac{(3\cos^2\beta - 1)}{2} \cdot S \cdot \frac{(3\cos^2\theta - 1)}{2} \qquad 2.24$$

The three angular terms that are used to describe the orientation of the C-^{2}H bond with respect to the applied magnetic field are depicted below.

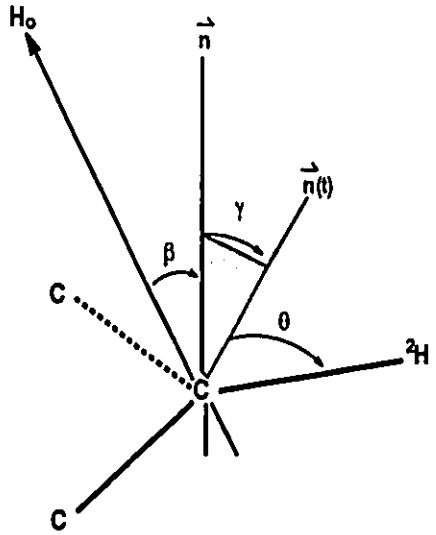

Figure 2.5 Angles relating C-^{2}H bond orientation to the applied magnetic field, H_o, direction. The angles are: θ, between the C-^{2}H bond and the molecular long axis; γ, between the molecular long axis and the bilayer normal; β, between the bilayer normal and H_o.

Although order parameters are quantitative, they do not necessarily lead to a description of the motional processes producing the averaged interactions. But it can be inferred from the line shapes (i.e. Figure 2.4) that the molecules are undergoing fast axially symmetric motions relative to the frequency of the quadrupolar splitting ($\Delta\upsilon_Q$).

2.4.3 Relaxation (Spectral Density Treatment)

The description of a particular molecular motion requires a geometric element and a temporal element; biological molecules usually undergo more than one type of motion. In an NMR experiment, motion has a very significant effect on the evolution (relaxation) of the spin system, and therefore, the resultant NMR spectrum. In general, it affects the spectral line width (T_2) and the time necessary to acquire a spectrum (T_{1Z}).

The time required by the system to rebuild Zeeman order after perturbation in an NMR experiment is defined by T_{1Z}, the longitudinal relaxation time, which is an exponential time constant (Abragam, 1961). The spectral line width is inversely proportional to the transverse relaxation time, T_2. This time constant is a measure of the relaxation which occurs via the energy exchange between nuclei. Relaxation occurs by a number of energy exchange interactions which involve the magnetic moment or the electric quadrupole moment of the nucleus (eq. 2.9). This discussion focuses on ^2H NMR relaxation. Since the quadrupolar interaction is the largest perturbation of the Zeeman interaction, the only significant relaxation process in solid state ^2H NMR experiments will be the quadrupolar interaction.

2.4.3.a Correlation Functions and Spectral Density Functions

An appreciation of the relaxation time dependence upon both geometric and temporal elements is gained from a discussion of the correlation function. Bloembergen et al. (1948) showed that the starting position of a molecule, G(0), and the position at time, τ, later, G(τ), are related in an exponential manner and expressed by the correlation function:

$$G(\tau) = G(0).\ \exp(-\tau/\tau_c) \qquad 2.25$$

τ_c is the correlation time of a motion, which essentially defines the time that a system remembers its starting point. In other words, as τ gets longer, the two positions are much more likely to be uncorrelated. According to the Weiner-Khintchine theorem, the relevant spectroscopic quantities, τ_c and ω_o, are obtained by Fourier transformation of

the correlation function (Weiner, 1930; Khintchine, 1934):

$$J(\omega) = \int G(\tau).\ \exp(-i\omega\tau).\ d\tau \qquad 2.26$$

$$= A \cdot \left[\frac{\tau_c}{1 + \tau_c^2\omega^2} \right] \qquad 2.27$$

where $J(\omega)$ is the spectral density function, in the frequency domain, which is an indication of the efficiency of energy transfer and serves to relate frequency and correlation time. A is a term denoting the angular dependence as described in 2.4.3.d.

2.4.3.b Spectral Densities and Relaxation Times

Theoretically, relaxation times can be written in terms of spectral density functions, after allowing time evolution of the density matrix in the NMR experiment (Jacobsen et. al, 1976; Jeffrey, 1981):

$$1/T_{1Z} = K[J_1(\omega_o) + 4J_2(2\omega_o)] \qquad 2.28$$

$$1/T_2 = K[\tfrac{3}{2} J_0(0) + \tfrac{5}{2} J_1(\omega_o) + J_2(2\omega_o)] \qquad 2.29$$

where $K = \{[3/80] \cdot [e^2qQ/hI(2I-1)]^2\}$, and eq, eQ, h, and I have their usual meanings.

Since quadrupolar nuclei have a non-vanishing electric quadrupole interaction, there is a second longitudinal relaxation time, T_{1Q} (Jacobsen and Schaumburg, 1976):

$$1/T_{1Q} = K[3J_1(\omega_o)] \qquad 2.30$$

T_{1Q} is the quadrupolar relaxation time, which defines the rate at which the quadrupolar order decays in an NMR experiment. This time constant is not manifest in a standard ^2H NMR spectrum, as T_{1Z} and T_2 are. However, it is very useful in unambiguously evaluating a system because there is only one spectral density function to evaluate.

T_2 is the only relaxation time dependent upon J(0) (slower motions); T_{1Z} and T_{1Q} relaxation times are sensitive to the faster motions, which occur in the biologically relevant liquid crystalline phase.

2.4.3.c Relaxation Times and Motional Regimes.

With regards to the temporal aspect of relaxation, T_{1Z} and T_2 are dependent upon both the rate of motion (inversely proportional to τ_c) and the Larmor frequency, ω_o, (Figure 2.6). In general, T_2 decreases with increasing correlation times; lines become broader with slower motions. The T_{1Z} dependence is somewhat more complicated; relaxation is most efficient in the intermediate motional regime ($\tau_c^2\omega_o^2 \approx 1$), and is least efficient in the fast ($\tau_c^2\omega_o^2 <<< 1$) and slow ($\tau_c^2\omega_o^2 >>> 1$) motional regimes.

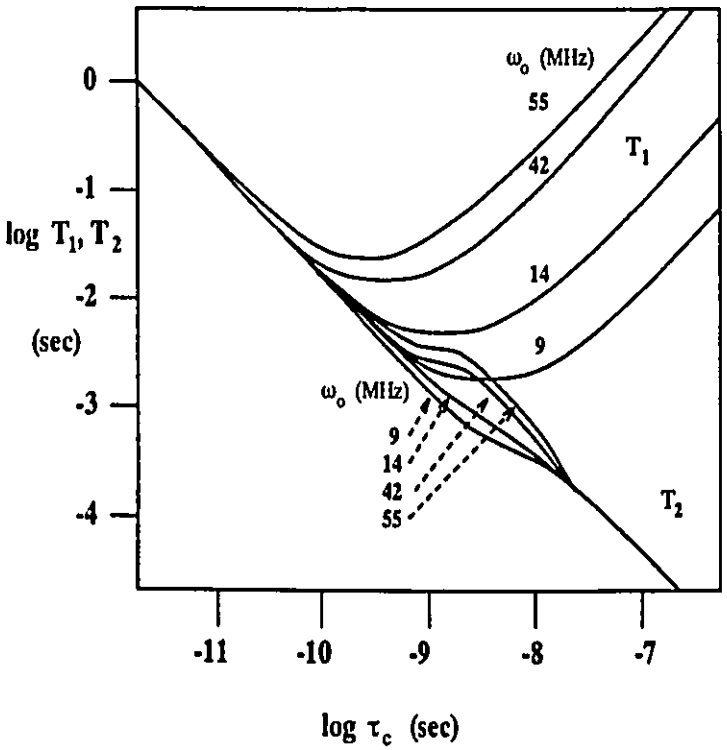

Figure 2.6 Relaxation time versus correlation time, τ_c. Schematic diagram of longitudinal, T_{1Z}, and transverse, T_2, relaxation times as a function of correlation time, at four ^2H Larmor frequencies, ω_o. Values are approximated for a quadrupolar relaxation mechanism.

2.4.3.d Angular Dependence of the Relaxation Times

A very general correlation function was presented in eq. 2.25, this function is actually dependent upon the orientation of the motional axis relative to $\mathbf{H}_o$. The precise nature of this angular dependence relies upon the details of the molecular reorientation (Jacobsen et al., 1976; Torchia and Szabo, 1982). Since $J_1(\omega_0)$ and $J_2(2\omega_0)$ may have partially opposing angular dependencies, T_{1Z}^{-1} (eq. 2.28) may exhibit a weaker orientational dependence than T_{1Q}^{-1}. This has been demonstrated by Jacobsen et al. (1976) in the general case of restricted anisotropic motion for a spin I = 1 nucleus:

$$J_1(\omega_0) = J_1(\omega_0)[\ 1 + (5/7)\langle D_{00}^{(2)}\rangle - (12/7)\langle D_{00}^{(4)}\rangle] \qquad 2.31$$

$$J_2(2\omega_0) = J_2(2\omega_0)[\ 1 - (5\sqrt{2}/7)\langle D_{00}^{(2)}\rangle + (3/7)\langle D_{00}^{(4)}\rangle] \qquad 2.32$$

where the description of both the orientational dependence and the molecular fluctuations is denoted by the Wigner rotation elements in the angular brackets. This behaviour has also been recognized by Wefing et al.(1984), who noted that the line shape changes of partially relaxed spectra observed in T_{1Z} experiments may only be minor compared to those observable in T_{1Q} experiments.

Relaxation experiments are necessary for unambiguously assessing the spectral density functions and elucidating the nature of the motion(s) (Winsborrow et al., 1991; Bonmatin et al., 1990). The following section describes the general approach adopted in assessing motional dynamics, with the focus being on longitudinal relaxation effects.

2.4.4 Motional Models

Biological systems generally undergo more than one type of motion and will therefore require a more complex motional description. It is often difficult to disentangle the information available from an NMR experiment. However, without an

appropriate interpretation of the molecular motions, any degree of experimentation is incomplete. Motional formalisms are used to relate a physical description of the motions to the experimental observations. The more popular formalisms use either the time evolution of the density matrix or order parameter analysis to describe such motions as: internal isomerization, molecular diffusion and rotation, and angular fluctuations.

The density matrix of a spin system evolves after perturbation in an NMR experiment. This evolution has been described by a large number of formalisms (Vilfan et al., 1987; Luz et al., 1981; Puopko et al., 1989; Pastor et al., 1988a; Torchia and Szabo, 1982; Wittebort et al., 1987; Ukleja et al., 1976). In general, a motion is related to an angular jump and a corresponding jump rate, which is used to calculate the experimental result via the spectral density function. The difference in all of the formalisms is the number and types of motions described, the way in which the correlation times are evaluated, and the importance that is placed on a particular motion relative to another.

Since the spectral density function is dependent upon the rate and nature of the motion (correlation time, and orientation angles), and the field strength, the motional description can be rigorously tested. In order for a model to be valid it would have to predict the spectral behaviour of the system under all experimental conditions; different motional regimes, and at specific well defined sample orientations with respect to $\mathbf{H}_o$.

An example of a formalism is the line shape analysis of anisotropic media by Griffin and coworkers (Griffin, 1981; Wittebort et al., 1981, 1987). This particular formalism is described in more detail here because it is used in this dissertation to evaluate the dynamics of the glycolipid β-DTGL. The formalism calculates spectral densities for a molecule undergoing discrete jumps, according to the density matrix treatment by Torchia and Szabo (1982). The dynamics are defined in a second rank jump matrix, $\mathbf{R}_{ij}$, which is included in the Zeeman spin operator for Larmor precession:

$$\mathcal{H}_z = (\mathbf{I}_z\omega_o + \mathbf{R}_{ij}) \qquad 2.33$$

The size of $\mathbf{R}_{ij}$ depends upon the number of jump sites, their respective populations and the jump rate. When the number of jump sites is sufficiently large, $\mathbf{R}_{ij}$ is considered to be a diffusion operator. The reciprocal of the jump rate times the number of sites is the correlation time, therefore, this model can be evaluated over a broad range of motional regimes and crystal orientations. In addition, the Larmor frequency of the spin system, ω_o, is dependent upon the magnitude of the applied magnetic field, which provides another means of testing the chosen model.

When the rate of a motion lies in the intermediate motional regime ($\tau_c^2\omega_o^2 \approx 1$) the dynamics of the spin system (10^3 - 10^7 Hz) are most sensitive to the pulse spacing between the two $\pi/2$ pulses in the quadrupolar echo experiment (§ Chapter 3). Thus, when simulating a spectrum, the evolution of the density matrix of the spin system can be calculated. Using the Bloch equations, the simulated magnetization is (Abragam, 1961; Spiess and Sillescu, 1981; Wittebort et al., 1981; Griffin, 1981):

$$M(\tau) = M(0) \,.\, \exp(i\mathbf{I}_z\omega_o + \mathbf{R}_{ij})\tau \qquad 2.34$$

where τ is the time delay between pulses.

In the extreme narrowing limit ($\tau_c^2\omega_o^2 <<< 1$) where the motions are faster (10^8 - 10^{12} Hz), relaxation experiments are more suitably used to test the motional description. When T_{1Z} is measured, in the inversion-recovery experiment, the Zeeman order builds at an exponential rate (Abragam, 1961):

$$M(t) = M(0) \,.\, [1 - 2\exp(-t / T_{1Z})] \qquad 2.35$$

Essentially, multiplication of $M(\tau)$ in eq. 2.34 by the above factor in the square brackets will simulate the partially-relaxed line shape at different delays, t, between pulses in the inversion recovery experiment (§ Chapter 3).

For a detailed derivation of the formalism, the reader is referred to the original work (Torchia and Szabo, 1982; Wittebort et al., 1987). The essential point is that a rate matrix can be defined for a spin system, which is allowed to evolve under the conditions of a selected NMR experiment. The method allows the rigorous testing of a motional description under a variety of experimental conditions.

Instead of evaluating spectral density functions and discrete motions, order parameter analysis describes the general order of a system, often using force fields and order potentials (Saupe, 1964; Van De Ven and Levine, 1984; Strenk et al., 1985; Pastor et al., 1988a, 1988b). The motions that are considered in this type of approach are less discrete than the statistically independent activity described above by correlation time based formalisms. Although order parameter based formalisms are quantitative, their physical interpretation, by analogy, can be considered classical in nature; the motions tend to be cooperative, not necessarily collective. For complex biological systems, this type of model is preferred by some because it creates a more easily envisioned physical picture. In this dissertation both approaches, spectral density and order parameter analysis, are used to describe the motions of β-DTGL in the liquid crystalline state.

Chapter 3

Methods

3.1 PREPARATION OF MODEL LIPID SYSTEMS FOR NMR STUDIES

3.1.1 Multilamellar Dispersions

Samples prepared in this fashion produce powder-type spectra because the molecules are randomly oriented in the magnetic field.

The lipid mixture (4:1. m/m) of specifically deuterated β-DTGL (generous gift of Dr. H.C. Jarrell, NRC Ottawa; prepared according to Ogawa and Beppu, 1982 and Jarrell et al. 1986) and dipalmitoyl phosphatidyl choline (DPPC, Avanti Polar Lipids, Alabaster, Al) was dissolved in $CHCl_3/CH_3OH$ (2:1, v/v) and dried under a stream of argon and then under vacuum. The residue was dispersed in 1 ml of deuterium-depleted water (^1H_2O) (for ^2H NMR) and lyophilized overnight, to remove any traces of alcohol. The resultant white fluffy material was again hydrated with ^1H_2O and cyclically "freeze-thawed" to homogeneity. Freeze-thawing is the process of heating the sample above the gel to liquid-crystalline phase transition temperature of the lipid system,

vortex mixing, then freezing. Homogeneity was assessed on the basis that reproducible NMR spectra were obtained.

3.1.2 Oriented Multibilayers

Samples prepared in this manner (Jarrell et al., 1987b) produce sharp spectra for each orientation at which the sample is physically set with respect to the magnetic field ($\mathbf{H}_o$); one quadrupolar splitting is observed for each inequivalent ^2H atom.

A given β-DTGL/DPPC lipid mixture (4:1, m/m; 30-60 mg, total lipid) was dissolved in a minimum amount of $CHCl_3/CH_3OH$ (2:1, v/v) and dropped onto 22 X 7 X 0.15 mm glass plates (about 30 plates). After the solvent had evaporated, the plates were stacked in a 10-mm (o.d.) NMR tube and dried under vacuum overnight. The sample was then hydrated by incubation overnight in a vial containing ^1H_2O (for ^2H NMR), at a temperature 5°C above the gel to liquid crystalline phase transition temperature. Afterwards, a drop of ^1H_2O was added to prevent dehydration and the tube was sealed.

The NMR tube was placed in a 10-mm solenoid coil and manually rotated outside of the magnet, the angle was set using a protractor. The exact orientation was determined by ^2H NMR, based on the 90° orientation quadrupolar splitting ($\Delta\nu_Q(90)$), which is measured in powder spectra. When the sample is oriented, the actual orientation (β) can be evaluated because the magnitude of $\Delta\nu_Q(\beta)$ is proportional to $\Delta\nu_Q(90)$, as related through the second order Legendre polynomial (eq 2.2.6).

3.2 BIOMEMBRANES

3.2.1 Growth and Isolation

Anacystis nidulans (Synechococcus sp. 6301) and *A.nidulans* R2 (Synechococcus sp. PCC 7942-R2) were grown autotrophically on BG-11 media (Allen, 1968) at 28°C with a light intensity of 25 $\mu Em^{-2}s^{-1}$ (generous gift of D. Bruce, Dept. Biology, Brock

University, St. Catharines, Ont.). Cells were grown in 2 litre batch cultures and while in logarithmic growth phase perdeuterated palmitic acid (Avanti Polar-Lipids, Pelham, AL) was added, 40:1 (m/m) fatty acid to chlorophyll a (Chl a). Specifically deuterated oleic acid (H. C. Jarrell, NRC, Ottawa) was also added to the growth media of *A.nidulans.*

Forty-eight hours after feeding, the cells were harvested by centrifugation, fragmented with a French pressure cell and thylakoid membranes were isolated by differential and sucrose density gradient steps. In one case *A.nidulans R2* cells were harvested ninety-six hours after perdeuterated palmitic acid feeding. The thylakoid membranes were washed and suspended in 3:7 (v/v) glycerol in 10 mM Hepes pH 7.4 buffer with 5 mM $MgCl_2$ and then stored at -70°C.

3.2.2 Lipid Extraction and Analysis

Total lipids were extracted from the thylakoid membranes (Kahn and Williams, 1977). Wet thylakoid membrane paste (up to 0.5 g wet weight) was put into a teflon sealed glass vial and 4.75 ml of methanol/chloroform/water ($CH_3OH/CHCl_3/H_2O$, 2:1:0.8, v/v/v) was added. The mixture was left at room temperature for 1-2 hrs, with intermittent shaking. After centrifugation, the supernatant extract was decanted into another teflon sealed glass vial and the residue was resuspended in another 4.75 ml of the $CH_3OH/CHCl_3/H_2O$ solvent mixture. After shaking and centrifugation, the combined supernatant extracts were added to 5 ml of $CHCl_3/H_2O$ (1:1, v/v); the mixture was centrifuged. The lower chloroform phase was withdrawn, diluted with benzene (C_6H_6, to aid in the removal of traces of water, and brought to dryness in a rotary evaporator (30-35°C).

The extracted lipids were either methylated for lipid analysis or stored under argon for NMR analysis. The lipids were methylated and analyzed by gas chromatography at the Dept. of Botany, University of Toronto by M. Kahn and J. P. Williams (Kahn and Williams, 1977), using capillary column DB225 (J.W. Scientific).

3.3 PREPARATION OF BIOMEMBRANES FOR NMR STUDIES

3.3.1 Intact Thylakoid Membranes

The green pasty pellets (about 0.5g wet weight) were homogenized in 1 ml of TES buffer made from ^1H_2O and pelleted by centrifugation (18,000 g factor, 20 min). The last step was repeated three times to ensure complete removal of deuterated water. The thylakoid membranes were then suspended in 10 mM TES buffer (with 10 mM NaCl, 5mM EDTA) made from ^1H_2O and sealed in a 10 mm NMR tube.

3.3.2 Extracted Thylakoid Membrane Lipids

A solution of the green lipid extract (lipid plus chlorophyll a, § 3.2.2) dissolved in $CHCl_3$ was added to an NMR tube (10 mm). The solvent was removed under a stream of argon and the residue was completely dried under vacuum (100 - 150 mg dry weight). The sample was then hydrated with about 0.5 ml of 10 mM TES buffer (with 10 mM NaCl, 5mM EDTA) made from ^1H_2O, and the tube was sealed. The sample was subjected to several freeze-thaw cycles to disperse the sample homogeneously in the buffer.

3.4 ^2H NMR SPECTROSCOPY

^2H NMR spectra were acquired on either a "home-built" Fourier transform spectrometer (30.7 MHz) operated by a Nicolet 1280 computer or a Bruker MSL 300 spectrometer (46.1 MHz). The spectral widths were typically between 100 and 200 kHz. Both spectrometers were outfitted with "home-built" probes that were equipped with solenoid coils (90° pulse = 2.3-3.4 μs and 3.9-5.0 μs for the 5 mm and 10 mm coils for both spectrometers, respectively). The solenoid coils are also useful because the sample can be rotated with respect to the applied magnetic field, enabling the study of oriented systems. The sample area of the probes was enclosed in a glass dewar to enable regulation of the sample temperature within about 0.5°C.

3.4.1 The Quadrupolar Echo

For samples which give broad spectra (powder spectra and samples oriented at angles < 20° with respect to the applied magnetic field) much of the information is contained in the first few points of the FID (free induction decay). If the spectral width (sw) used is 200 kHz, the spectrometer dead time has to be less than 5 μs to observe fully the rapidly decaying magnetization. As this is virtually impossible to accomplish electronically, the quadrupolar echo pulse sequence has been developed to overcome the problem (Solomon, 1958):

$$90_x - \tau - 90_y - \text{acquire}$$

This pulse sequence consists of a pair of 90 degree pulses, 90 degrees out of phase with each other and separated by a time τ. The echo FID occurs at a time τ after the second pulse. Quadrature detection and full phase cycling (Griffin, 1981) were used to minimize any phase distortions as the echo signals were recorded. Pulse spacing was typically 60 μs which is longer than the spectrometer dead time yet much shorter than the transverse relaxation time T_{2e}. The recycle time was always greater than 5 T_{1Z}, assuring that the spectra were fully relaxed with respect to T_{1Z}. The recycle delay used for the biomembranes (deuterated acyl chains) was 350 ms. For samples enriched with perdeuterated fatty acids, the spectrum was typically acquired with 100,000 transients. Samples enriched with specifically deuterated fatty acids, however, required more transients in order to have adequate signal to noise; the number of transients were between 200,000 and 600,000, depending on the concentration of the sample.

The carrier frequency was carefully set at the centre of the quadrupolar powder pattern, and the receiver phase adjusted so that all of the FID was observed in only one channel (usually the real channel). This not only simplified the signal phasing of complicated powder spectra after Fourier transformation, but this also allowed for the "folding" of spectra, increasing the signal to noise by a factor of $\sqrt{2}$. Folding is accomplished by zeroing the channel without an FID (usually the imaginary channel)

before Fourier transformation. This is why it is essential that the signal is on resonance and the receiver phase is adjusted so that all of the signal is in one channel only. Folded and unfolded spectra were compared to ensure that no distortion had been introduced by the folding procedure.

3.4.2 Longitudinal Relaxation Time Measurements

The spectra were acquired for oriented {3',3' $^2H_2$} β-DTGL multibilayers in the same manner as above (§ 3.4.1). The repetition time for these experiments was 60 ms because the T_1 is much shorter for deuterons at the glycerol backbone position. The number of transients acquired for each spectrum was about 15,000 for orientations around the "magic angle", 54.7° and 30,000 for all other orientations.

3.4.2.a T_{1Z} : Zeeman Order

T_{1Z} longitudinal relaxation times were obtained via the inversion-recovery technique coupled with the quadrupolar echo sequence (Dufourc et al., 1984):

$$180 - VD - 90_x - \tau - 90_y - \text{acquire}$$

The variable delay (VD) is used to assess the return of Zeeman order to equilibrium; integrated signal intensities were obtained at the different delay times. Assuming that the quadrupolar interaction is the only significant relaxation mechanism, the observed macroscopic longitudinal magnetization (M_{obs}) can be described quantitatively by a single exponential process with the Bloch equation:

$$dM_{obs}/dt = -(M_{obs} - M_0)/T_{1Z} \qquad 3.1$$

Where M_0 is the magnetization at equilibrium and t is time. Integration with $M_{obs} = -M_0$ at $t = 0$ gives (Carr and Purcell, 1954):

$$M_{obs} = M_0 [1 - 2\exp(-t/T_{1Z})]$$

3.4.2.b T_{1Q} : Quadrupolar Order

T_{1Q} longitudinal relaxation times were obtained by measuring the rate of quadrupolar order decay as a function of the variable delay of the spin-alignment experiment (Jeener and Broekaert, 1967) with phase-cycling to eliminate unwanted single and double quantum coherence (Vold et al., 1981):

$$90_x - (2\Delta\nu)^{-1} - 45_y - VD - 45_y - \text{acquire}$$

The spin-alignment experiment was also used with a refocusing 90 degree pulse, which refocuses the magnetization, thereby overcoming the spectrometer dead time problems (Jeffrey, 1981):

$$90_x - (2\Delta\nu)^{-1} - 45_y - VD - 45_y - t_2 - 90_y - \text{acquire}$$

In both experiments Zeeman order returns to equilibrium and quadrupolar order decays during VD. Since the spectrometers used are equipped with quadrature detection, the experimental conditions were such that magnetization associated with Zeeman order was collected in one channel and quadrupolar order was collected in the other (by convention the quadrupolar order was in the imaginary channel). The quadrupolar order information was obtained by zeroing the real channel before transformation. Particular attention was given to ensure that the spectra were centred and that at very long delays ($5T_{1Q}$) there was no signal in the imaginary channel.

The data were processed assuming simple exponential decay; quantitatively the decay of M_{obs} is given by the Bloch equation as ($M_x = M_y = 0$):

$$dM_{obs}(t)/dt = -M_{obs}/T_{1Q} \qquad 3.2$$

Where integration with $M_{obs} = M_0$ at $t = 0$ gives:

$$M_{obs}(t) = M_0 \exp(-t/T_{1Q}) \qquad 3.3$$

3.5 THEORETICAL CALCULATIONS

3.5.1 ^{2}H NMR Lineshape Simulations

Orientation-dependent relaxation profiles ($T_1(\beta)$) and partially relaxed inversion-recovery powder spectra were simulated on a Sun 4-260 computer as described previously (§2.4.4) using a modified lineshape program (Wittebort et al., 1987) which was based on the formalism of Torchia and Szabo (1982). The program was a generous gift of Dr. R.G. Griffin (MIT, Cambridge MA) and was modified for simulations of oriented sample spectra (H. C. Jarrell). Simulated lineshapes were corrected for the finite pulse width of the experimental 90° pulse in the quadrupolar echo sequence (Bloom et al., 1980) and the partially recovered T_{12} spectra were further corrected for the finite width of the 180° pulse (Hiyema et al., 1986).

3.5.2 Conformational Energy Calculations

PFOS (Potential Functions of OligoSaccharides) conformational energy calculations (Tvaroška and Pérez, 1986) were used to evaluate the conformational potential energy the of β-DTGL glucose head group over ϕ, ψ, ω space (§ Chapter 5). These calculations assess the van der Waals interactions between non-bonded atoms (using a Leonard-Jones 6-12 potential), torsional contributions about the glycosidic bond, and an exo-anomeric term (Tvaroška and Pérez, 1986). The program was a generous gift of Dr. J.-R. Brisson (NRC Ottawa, Ont.) and was modified to include a surface term, which calculates the energetics of the head group interacting with membrane surface molecules (§ Chapter 5 and Appendix). All calculations were carried out on a Micro VAX 3500 computer (Digital Equipment Corp., Marlboro, MA).

Part II

Model Membrane Systems

Chapter 4

Glycolipid Dynamics in The Liquid Crystalline State.

A ^{2}H NMR Relaxation Study With Lineshape Analysis.

4.1 INTRODUCTION

Cell surface carbohydrates play a crucial role in cellular biology. This is particularly true in the fields of blood transfusion (Rydberg et al., 1988), membrane structure (Curatolo, 1987), cell-cell recognition (Blackburn et al., 1986), and tumour immunology (Hakomori, 1986). The elucidation of both the three dimensional structure and the dynamical properties of the carbohydrate head groups has been of primary concern, and principal difficulty. Three dimensional structural analysis probes the distribution of conformations of these molecules (§ Chapter 5), whereas dynamical studies involve the investigation of the types, amplitudes, and rates of motion, including conformational equilibria, present in a given system.

Deuterium (^{2}H) NMR has proven to be an extremely valuable tool in studying the dynamics of ordered environments, such as model membrane systems (Smith, 1989; Davis, 1991; Seelig , 1977; Seelig et al. 1980). ^{2}H labelling essentially isolates the molecular segment of interest because the intramolecular ^{2}H quadrupolar interaction dominates the NMR spectrum (Abragam, 1961). As a result, the ^{2}H NMR spectrum is

sensitive to local orientation and to anisotropic motions (Seelig, 1977). This is significant because the time frame of the relevant motions lies within that of the experimental technique ($1\text{-}10^{10}$ s^{-1}) (Abragam, 1961). Furthermore, the ability to measure two longitudinal relaxation times (T_{1Z} and T_{1Q}) makes spin I = 1 nuclei (such as ^2H) potentially more powerful molecular probes than spin I = 1/2 nuclei, which have only one longitudinal relaxation time (T_{1Z}, Jacobsen et al., 1976; Jacobsen and Schaumburg, 1976).

In recent studies of carbohydrate structure and dynamics much attention has been devoted to the glycolipid 1,2-di-*O*-tetradecyl-3-*O*-(β-D-glucopyranosyl-*sn*-glycerol (β-DTGL) (Winsborrow et al., 1991, 1992; Jarrell et al., 1986, 1987a, 1987b) and related compounds (Renou et al., 1989; Carrier et al., 1989). β-DTGL is a reasonable analogue of many biologically relevant glycosphingolipids where the first sugar within the oligosaccharide head group is usually glucose (§ 1.1.1).

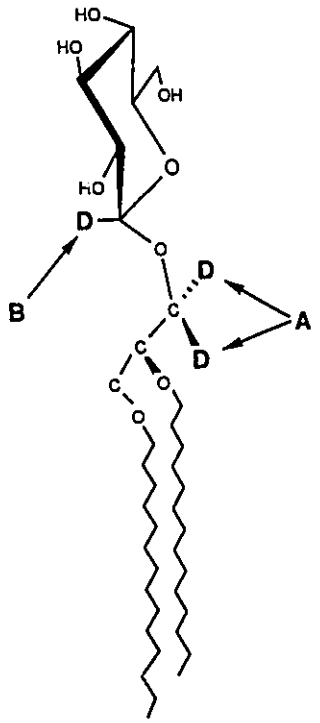

Figure 4.1 Diagrammatic representation of β-DTGL with approximate orientation along the bilayer normal. (A) Deuteration at the glycerol C3' position, {3',3'-$^2H_2$} β-DTGL. (B) Deuteration at the 1 position of glucose, {1-^2H} β-DTGL. Note that primed numbers denote the aglyconic unit.

While NMR relaxation studies can provide a wealth of information about the time scale of molecular motion, such measurements are performed with the goal of extending the physical/chemical description of the system under investigation. In order to utilize fully the potential of such measurements, it is essential to analyze the results within the context of an adequate motional model. Previous work from this laboratory concluded that for β-DTGL, in the gel state, two motions were manifest at the glycerol *sn*-3 position. The motion affecting relaxation is in the fast-limit motional regime ($\omega_o^2\tau_c^2 << 1$); isomerization about the glycerol C2-C3 bond. A slower motion (slow-limit; $\omega_o^2\tau_c^2 >> 1$) involved rotation about the molecular long axis (Auger et al., 1990).

An increase in motional complexity in the more biologically relevant L_α state is anticipated because the segmental order parameter, *S*, at the glycerol backbone C3 position decreases upon transition from gel to fluid L_α state. In turn, *S* of the backbone region is greater than that of the head group region, which is an indication of less restricted motion in the head group region. Specifically, the glycerol backbone *S* values in the gel state, in the L_α state, and then the L_α state head group region for β-DTGL are: ≈ 1, 0.65, 0.45, respectively (Jarrell et al., 1986). Furthermore, it is apparent from the following ^2H NMR spectra that the molecules in the L_α state are undergoing axially symmetric motions ($\eta = 0$), whereas those in the gel state are not ($\eta > 0$; § 2.3.2):

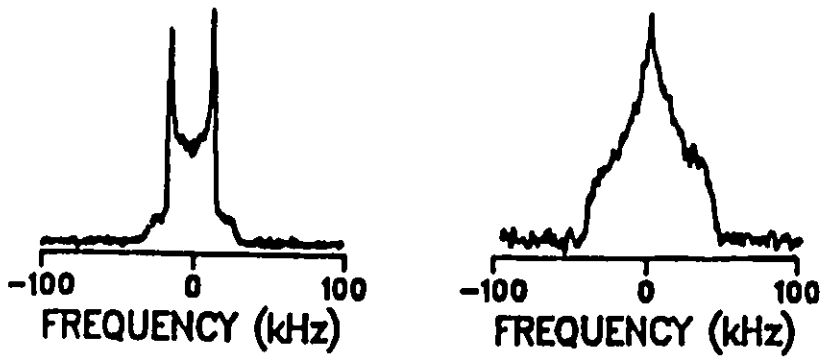

Figure 4.2 **^2H NMR spectra of randomly oriented {3',3'-$^2H_2$} β-DTGL multibilayers.** (*Left*) L_α state, 55°C, spectra are affected by axially symmetric motions ($\eta = 0$). (*Right*) Gel state, 25°C, $\eta > 0$ (non-axially symmetric motions).

In the case of β-DTGL, it is of interest to explore whether the gel state motional description can form the basis for an adequate interpretation of molecular reorientation in the L_α state for both the glycerol and carbohydrate regions of the glycolipid. This is rigorously tested here by using two ^2H NMR observation frequencies, two types of sample preparation (oriented and dispersed multibilayers), and two relaxation experiments (T_{1Z} and T_{1Q}). This study establishes the importance of using oriented samples and the T_{1Q} experiment to obtain unambiguous dynamical information.

4.2 ^2H NMR RELAXATION EXPERIMENTS

4.2.1 Oriented Multibilayers

Both oriented and randomly dispersed multibilayers of β-DTGL, in the L_α state are used. Oriented samples are physically rotated and ^2H NMR spectra corresponding to particular angles between $\mathbf{H}_0$ the order director are obtained:

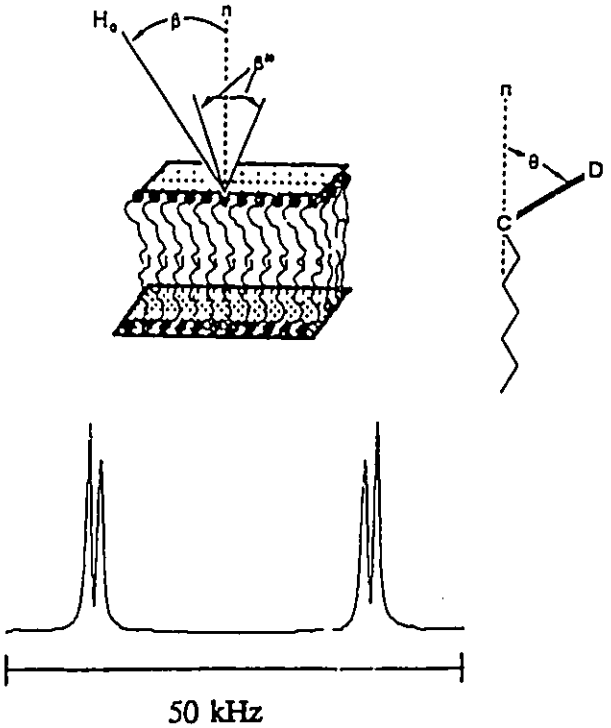

Figure 4.3 ^2H **NMR of oriented multilbilayers.** (*Top left*) Schematic diagram of oriented multibilayers; experimentally β is the angle between the bilayer normal ($\vec{n}$) and the applied magnetic field ($\mathbf{H}_0$) and β'' is representative of a distribution of molecular orientations about $\vec{n}$. (*Right*) Representation of the angle θ, between the C-^2H bond and $\vec{n}$. (*Bottom*) Spectrum of L_α {3',3'-$^2H_2$} β-DTGL oriented at β = 90°. The two quadrupolar splittings indicate that the two ^2H atoms on the glycerol C3 position are inequivalent, θ = 71.7 and 73.7° (Jarrell et al. 1987b).

The class of motional model considered in this study is one in which the C-^{2}H bond reorients about the symmetry axis at a fixed angle θ (Torchia et al., 1982). In the L_α state of {3',3'-^{2}H} β-DTGL the two deuterium atoms on the glycerol C3 position are inequivalent and two splittings can be observed (Figure 4.3). This inequivalence arises because the glycerol backbone is not exactly parallel to the order director. As a consequence, the angles made by the two C-^{2}H bonds (θ) with respect to the order director are different. These angles, however, have been calculated for both positions (73.7° and 72.5°; Jarrell et al., 1987b). For the simulations the average orientation (θ = 73.2°) was used; there was no significant difference observed in the results of the simulations when θ was varied by ± 1.5°.

4.2.2 Oriented Versus Randomly Dispersed Multibilayers

Conventional means of testing models by relaxation studies are via frequency- and temperature-dependent measurements (Dufourc et al., 1986; Brown, 1984). Relaxation is also dependent upon the orientation of the motional symmetry axis with respect to $\mathbf{H}_0$ (T_1 anisotropy). The partially-relaxed ^{2}H NMR spectra from an inversion-recovery experiment of oriented (*left*) and randomly dispersed (*right,* H. C. Jarrell, unpublished results) {3',3' $^2H_2$}β-DTGL multibilayers are presented in Figure 4.4. These data may be used to calculate the orientation-dependent T_{1Z} longitudinal relaxation time.

The anisotropy in relaxation can be observed in the partially-relaxed 'powder' spectra of the randomly oriented multibilayers. Near the null or inversion point the edges of the spectra are positive at a smaller Tau value than the central region (i.e. Figure 4.4, *right*). Unfortunately, in powder spectra the signal to noise (S/N) ratio is the poorest in the region of the null, which makes precise evaluations difficult.

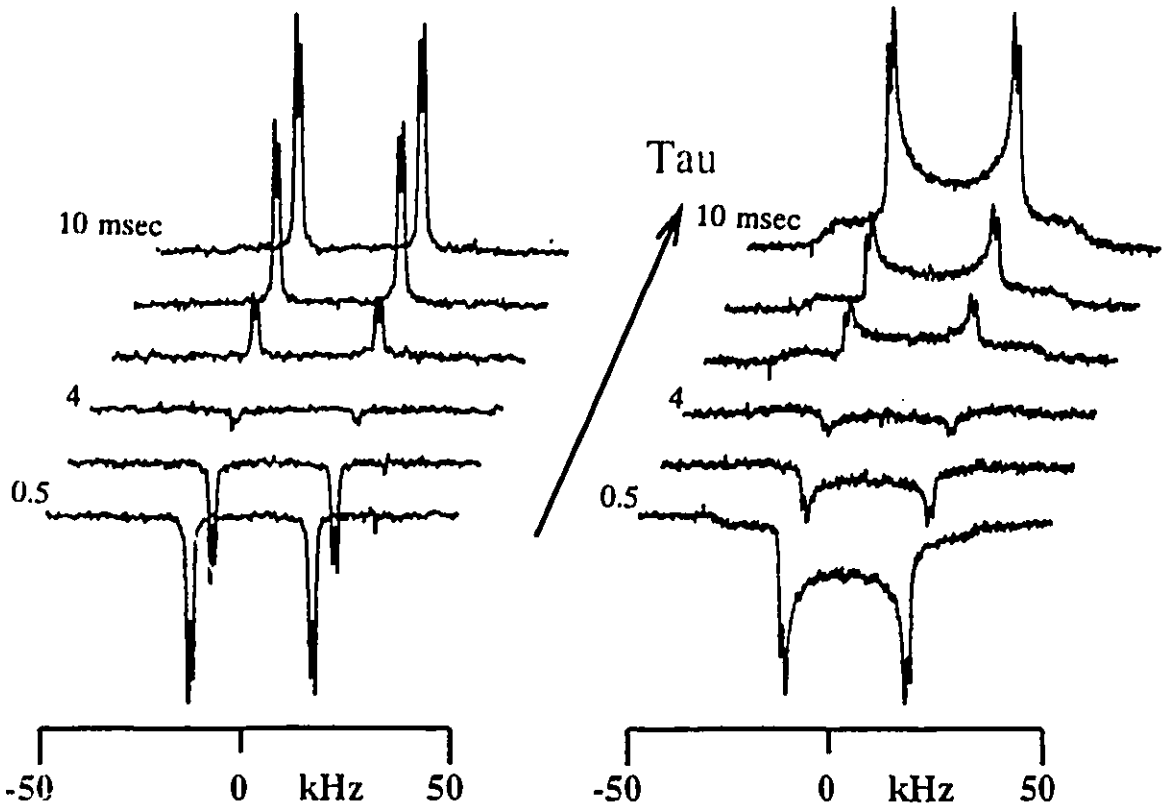

Figure 4.4 Stacked plots of spectra from the inversion-recovery experiment versus the variable delay time, Tau. {3',3' $^2H_2$} β-DTGL/DPPC (4:1, m/m) in the L_α state, at 55°C. (*Left*) Multibilayers are oriented at 90° with respect to $\mathbf{H}_o$. (*Right*) Randomly oriented multibilayers. Tau is the delay between the π and π/2 pulses in the inversion-recovery experiment.

Such determinations are complicated further when there are overlapping spectra due to inequivalent deuterons. For these reasons oriented multibilayers (Figure 4.4, *left*) were used to evaluate the orientation-dependent longitudinal relaxation time, T_{1Z}, over a range of sample orientations, with respect to $\mathbf{H}_o$.

Although it may be time consuming to run an experiment for each desired orientation of an oriented multibilayer sample, the results are unambiguous, the S/N ratio is greatly improved, and overlapping spectra can be resolved. In fact, since the results

of the oriented sample experiments are so reliable both T_{1Z} and T_{1Q} longitudinal relaxation times were determined for a number of β-DTGL sample orientations, in this study. From these data orientation-dependent ($T_1(\beta)$) relaxation profiles were constructed and T_1 anisotropies ($\partial T_1(\beta) = T_1(0) - T_1(90)$) were determined accurately.

T_{1Q} longitudinal relaxation times were measured using the Jeener-Broekaert experiment (§ Chapter 3). The partially-relaxed ^2H NMR spectra from a Jeener-Brokaert experiment of oriented {3',3' $^2H_2$} β-DTGL multibilayers are presented in Figure 4.5. The sample was oriented such that the bilayer normal makes a 25° angle with $\mathbf{H}_o$.

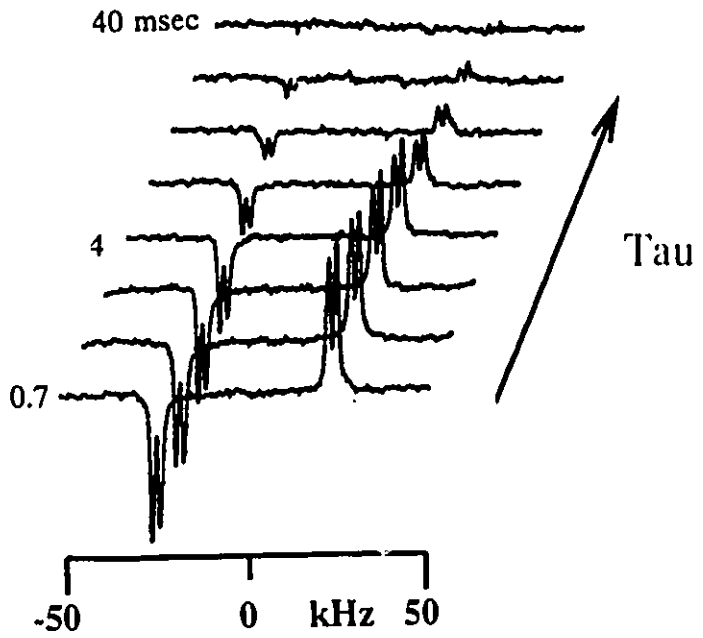

Figure 4.5 Stacked plots of spectra from the Jeener-Broekaert experiment versus the variable delay time, Tau. The part of the FID in the "real channel", with Zeeman coherence, was zeroed before Fourier transformation. The spectra are used to calculate the longitudinal relaxation time T_{1Q}. {3',3' $^2H_2$} β-DTGL/DPPC (4:1, m/m) in the L_α state, at 55°C. Multibilayers are oriented at 25° with respect to $\mathbf{H}_o$. Tau is the delay between the two π/4 pulses in the Jeener-Broekaert experiment.

4.3 THE GLYCEROL BACKBONE REGION

4.3.1 Initial Motional Parameters

Previous work on gel state {3',3'-$^2H_2$} β-DTGL described the dynamics at the glycerol C3 position using two motions: a fast, large angle jump among three sites about the glycerol C2-C3 bond (ie. trans-gauche isomerization) and a slower axial motion of the molecule as a whole (Auger et al. 1990). It was concluded that this fast isomerization (τ_c= $6.7*10^{-10}$ s, fast limit motional regime; $\omega_o^2\tau_c^2 << 1$) among the three sites (populations 0.46, 0.34, 0.20) dominated longitudinal relaxation. The second motion was attributed to rotation about the molecular long axis. Addition of this motion to the simulations of the partially relaxed gel state spectra did not alter the longitudinal relaxation time but was necessary to match line shapes and quadrupolar echo intensities to spectra acquired over the temperature range 25-60°C. The rotation rate was varied in the range of the exchange minimum ($\omega_Q^2\tau_c^2 \approx 1$, $\omega_Q = 2\pi\Delta\nu_Q$, $\Delta\nu_Q$ is the quadrupolar splitting) where the line shape is most sensitive. The fastest axial rotation rate used (τ_c= $3.3*10^{-7}$ s; fast-limit motional regime, ($\omega_Q^2\tau_c^2 << 1$) is fast enough to average the electric field gradient tensor to axial symmetry, but it is too slow to contribute to longitudinal relaxation ($\omega_o^2\tau_c^2 >> 1$, slow-limit T_1 motional regime) (Abragam, 1961; Slichter, 1990).

4.3.2 The Liquid Crystalline State

The above parameters from the gel state study were used as a starting point for the treatment of {3',3'-$^2H_2$} β-DTGL in the L_α state. The simulated and experimental $T_1(\beta)$ relaxation profiles for both T_{1Z} and T_{1Q} obtained at 30.7 MHz are given in Figures 4.6A (T_{1Z}) and 4.7A (T_{1Q}) and at 46.1 MHz in Figures 4.8A (T_{1Z}) and 4.8C (T_{1Q}). In each of the four cases the relative trends in the anisotropies ($\partial T_1(\beta)$) of the simulated relaxation profiles are in agreement with experiment; corroborating the findings of the gel state study. However, the experimental profiles are much less anisotropic than their simulated counterparts, suggesting that there are additional factors influencing the relaxation profiles. This is evident upon consideration of the partially-relaxed T_{1Z} spectra (Figure 4.9B at 30.7 MHz , result not shown for 46.1 MHz); the experimental spectra appear to be more fully recovered than do the simulated spectra.

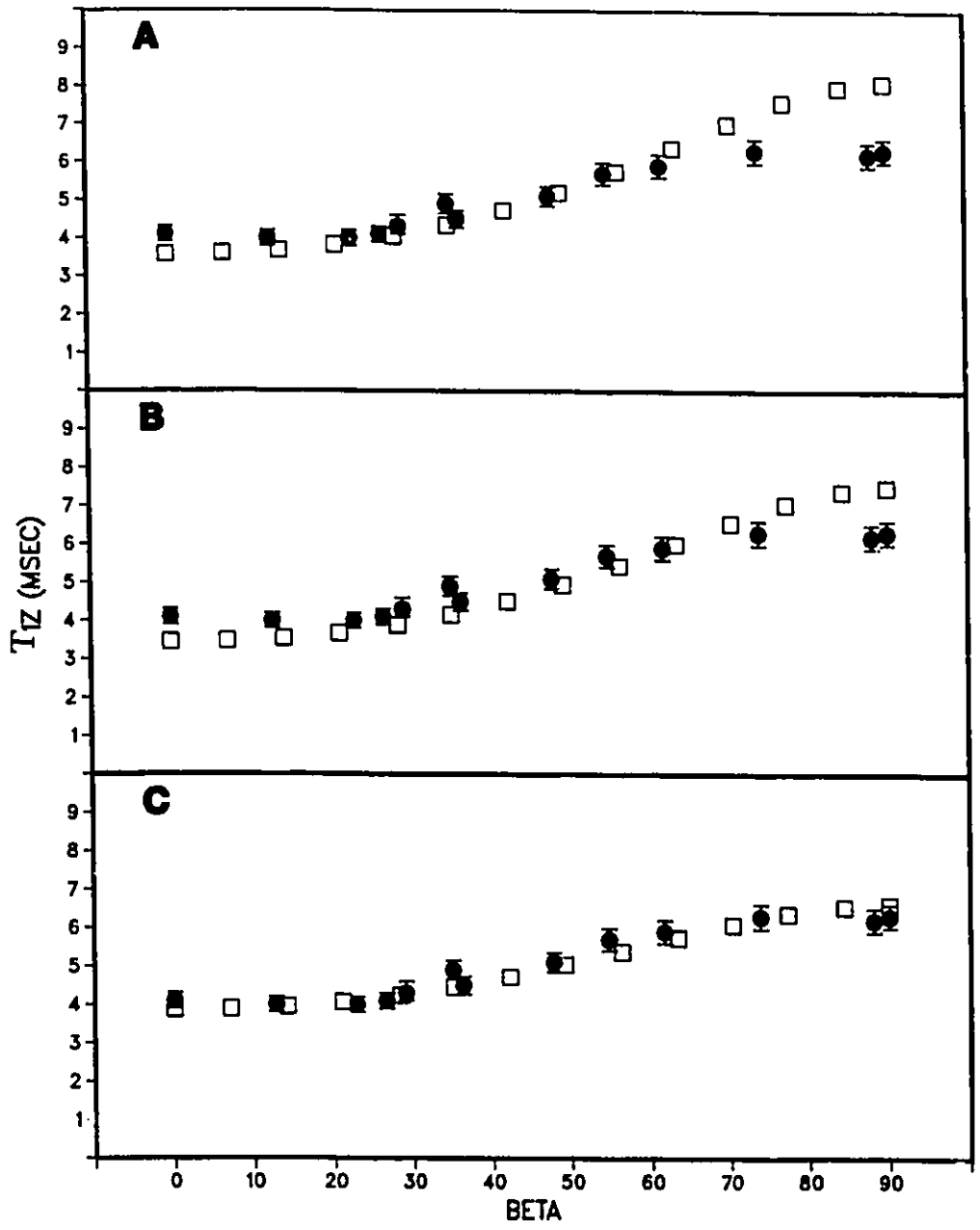

Figure 4.6 Angle-dependent T_{1Z} profiles, oriented multibilayers of {3',3'-$^2H_2$} β-DTGL at 30.7 MHz. Experimental (●) and calculated (□) ^2H T_{1Z} longitudinal relaxation times as a function of β (angle between H_o and bilayer normal). (A) 3 site jump ($\tau_c = 6.7*10^{-10}$ s, fast limit, $\omega_o^2\tau_c^2 << 1$) with site populations 0.46, 0.34, 0.20 plus axial rotation about the molecular long axis ($\tau_c = 3.0*10^{-7}$ s, slow limit, $\omega_o^2\tau_c^2 >> 1$). (B) as in (A) but with increased axial rotation rate ($\tau_c = 8.3*10^{-9}$ s, close to T_1 minimum, $\omega_o^2\tau_c^2 \approx 0.4$). (C) as in (B) plus effects of orientational averaging, $S = 0.65$. Replication of data was reproducible within 2%; experimental error was estimated to be ± 5%.

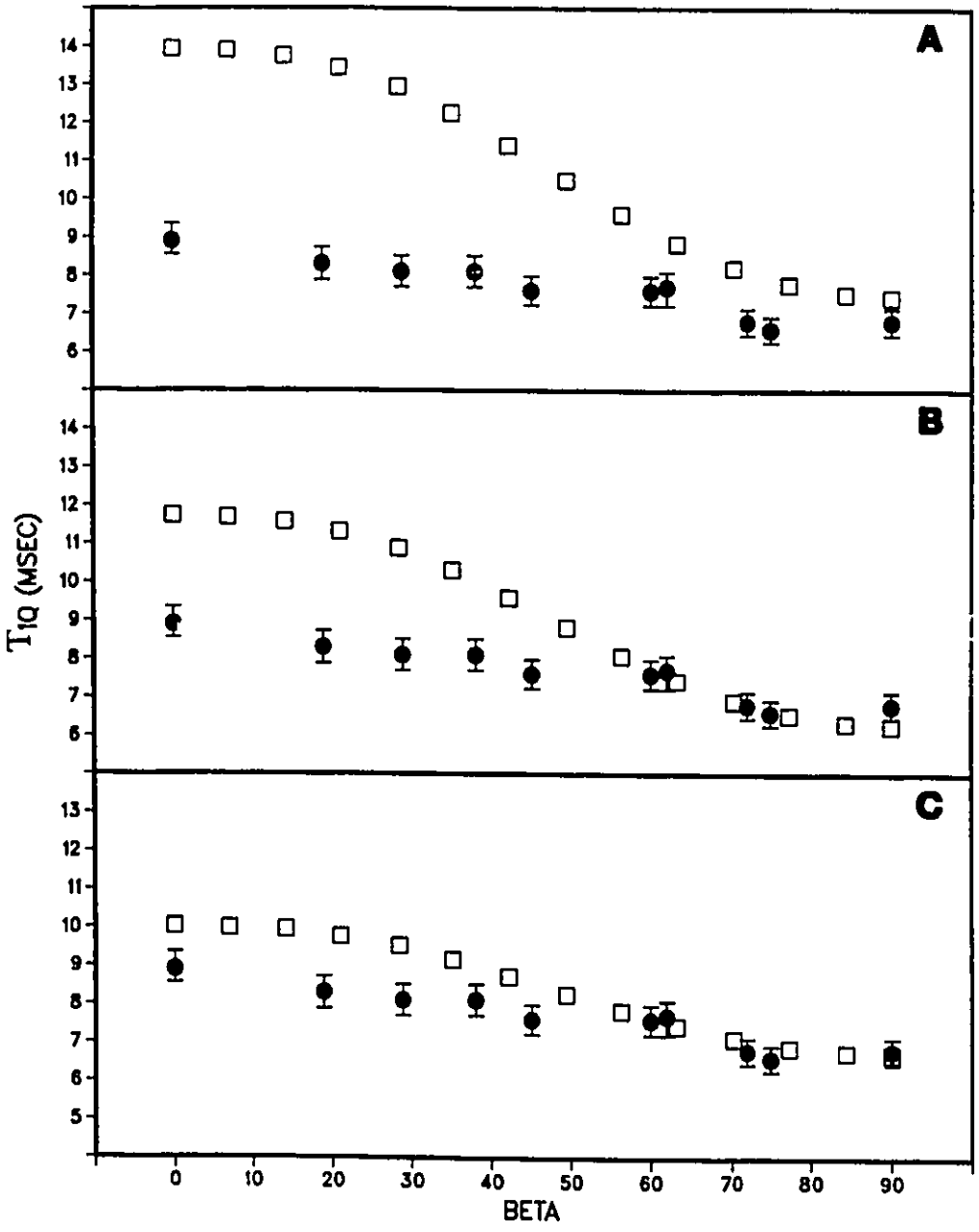

Figure 4.7 Angle-dependent T_{1Q} profiles, oriented multibilayers of {3',3'-$^2H_2$} β-DTGL at 30.7 MHz. Experimental (●) and calculated (□) ^2H quadrupolar longitudinal relaxation times (T_{1Q}) as a function of β (angle between H_o and bilayer normal). (A) 3 site jump ($\tau_c = 6.7*10^{-10}$ s, fast limit, $\omega_o^2\tau_c^2 << 1$) with site populations 0.46, 0.34, 0.20 plus axial rotation about the molecular long axis ($\tau_c = 3.0*10^{-7}$ s, slow limit, $\omega_o^2\tau_c^2 >> 1$). (B) as in (A) but with increased axial rotation rate ($\tau_c = 8.3*10^{-9}$ s, close to T_1 minimum, $\omega_o^2\tau_c^2 \approx 0.4$). (C) as in (B) plus effects of orientational averaging, $S = 0.65$. Replication of data was reproducible within 2%: experimental error was estimated to be ± 5%.

The discrepancy between the simulated and experimental results is not surprising since the segmental order parameter for position C3 of the glycerol moiety of β-DTGL in the gel state ($S \approx 1$) is larger than that of the L_α state ($S = 0.65$) (Jarrell et al., 1987b), suggesting that there is less restricted motion in the L_α state. It is reasonable to assume that the motions used for the gel state are correct; large angle jumps and/or diffusion about the molecular long axis are the two motions used most commonly to describe lipid motions in bilayers (Speyer et al., 1989; Dammers et al., 1988; Hauser et al., 1988; Vold et al., 1988; Wittebort et al., 1987; Siminovitch et al., 1985; Meier et al., 1982; Blume et al., 1982). Obvious modifications to the simulation parameters would be to adjust the rates of the motions already defined.

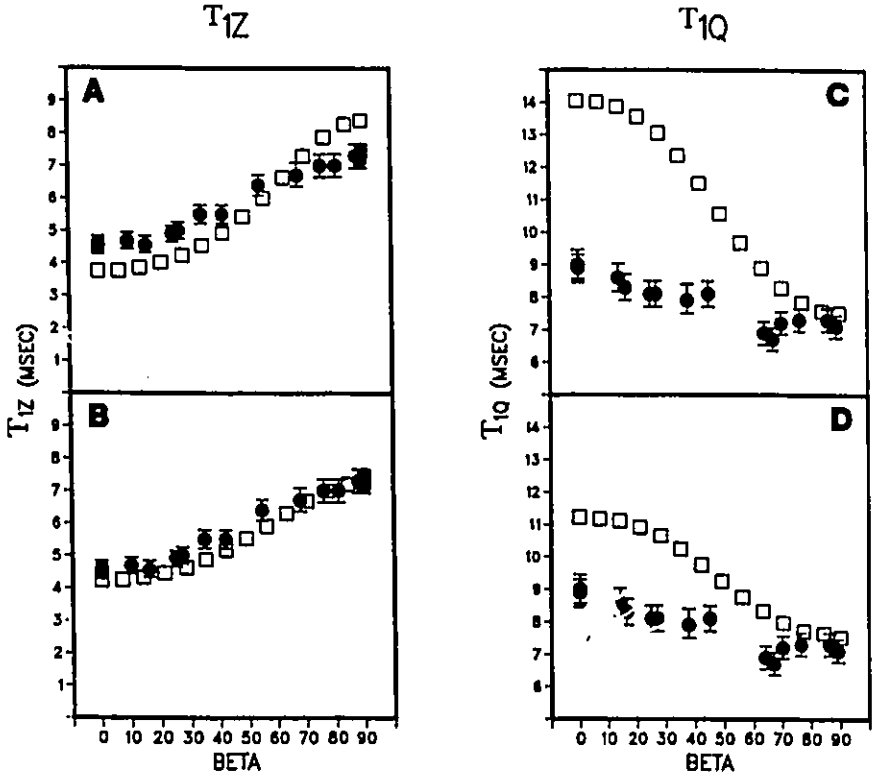

Figure 4.8 Angle-dependent T_{1Z} and T_{1Q} profiles, oriented multibilayers of {3',3'-$^2H_2$} β-DTGL at 46.1 MHz. Experimental (●) and calculated (□) ^2H longitudinal (T_{1Z}, A,B; T_{1Q}, C,D) relaxation times as a function of β. (A and C) 3 site jump ($\tau_c = 6.7*10^{-10}$ s, fast limit, $\omega_o^2\tau_c^2 << 1$) with site populations 0.46, 0.34, 0.20 plus axial rotation about the molecular long axis ($\tau_c = 3.0*10^{-7}$ s, slow limit, $\omega_o^2\tau_c^2 >> 1$). (B and D) All three proposed motions are used: 3 site jump ($\tau_c = 6.7*10^{-10}$ s, fast limit, $\omega_o^2\tau_c^2 << 1$) with site populations 0.46, 0.34, 0.20, axial rotation about the molecular long axis ($\tau_c = 8.3*10^{-9}$ s, close to T_1 minimum, $\omega_o^2\tau_c^2 \approx 0.4$), and effects of orientational averaging, $S = 0.65$. Replication of data was reproducible within 2%, experimental error was estimated to be ± 5%.

Modification of the 3-site jump rate does not attenuate the anisotropy ($\partial T_1(\beta)$) of the relaxation times; only the absolute T_1 values are affected. This is observed for the simulations of both the $T_1(\beta)$ relaxation profiles and the partially relaxed powder spectra. However, increasing the axial rotation rate by two orders of magnitude (τ_c = $8.3*10^{-9}$ s; near the T_1 minimum, $\omega_o^2\tau_c^2 \approx 0.4$) did affect the anisotropies of the relaxation times ($T_1(\beta)$ relaxation profiles (Figures 4.6B (T_{1Z}) and 4.7B (T_{1Q}) at 30.7 MHz; 46.7 MHz results not shown)) and improved agreement between experimental and simulated partially-relaxed T_{1Z} spectra (not shown). Of particular interest is that the attenuation of the anisotropy ($\partial T_1(\beta)$) is most dramatic for the T_{1Q} profile (Figure 4.7B).

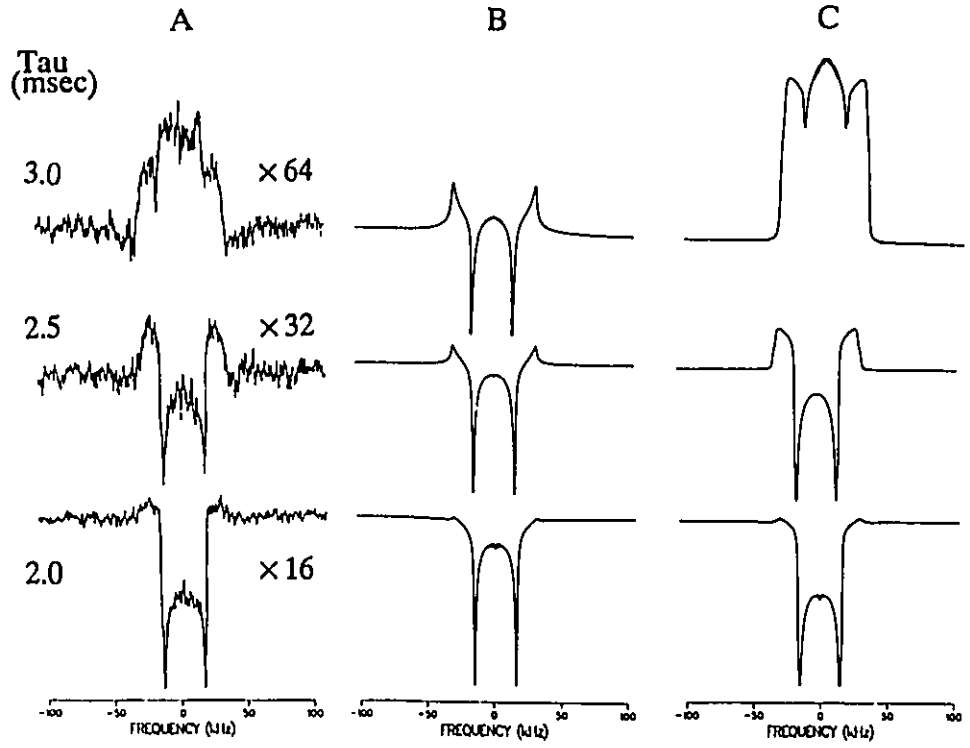

Figure 4.9 T_{1Z} **partially recovered powder spectra of {3',3'-2H$_2$} β-DTGL at 30.7 MHz.** (A) Experimental spectra. (B) simulation of 3 site jump (τ_c = $6.7*10^{-10}$ s, fast limit, $\omega_o^2\tau_c^2 << 1$) with site populations 0.46, 0.34, 0.20 plus axial rotation about the molecular long axis (τ_c = $1.0*10^{-6}$ s, slow limit $\omega_o^2\tau_c^2 >> 1$). (C) 3 site jump (τ_c = $6.7*10^{-10}$ s, fast limit, $\omega_o^2\tau_c^2 << 1$) site populations 0.46, 0.34, 0.20, increased axial rotation about the molecular long axis (τ_c = $8.3*10^{-9}$ s, near T_1 minimum $\omega_o^2\tau_c^2 \approx 0.4$), and effects of orientational averaging (S = 0.65). Tau is the delay between the π and $\pi/2$ pulses in the inversion-recovery experiment.

Even though adjustment of the axial rotation rate did improve the match of the simulated to the experimental $T_1(\beta)$ relaxation profiles and partially relaxed T_{1Z} spectra, it is apparent that additional averaging is required to describe adequately the type of motion that must be occurring in the L_α state of {3',3'-$^2H_2$} β-DTGL.

4.3.3 Additional averaging in the L_α state

In the L_α state there is a distribution of orientations, β'' ($-90° \leq \beta'' \leq +90°$), which the molecular long axis makes with the local bilayer normal (**n**) (Figure 4.3). The orientational distribution, f(β''), can be modelled using a Maier-Saupe restoring potential (Van De Ven et al., 1984) as

$$f(\beta'') = A \exp[U(\beta'')/kT], \qquad 4.1$$

where A is a normalization constant, and k and T have their usual meaning. Assuming axially symmetric ordering, U(β'') is given by

$$U(\beta'') = [\lambda P_2(\cos\beta'')], \qquad 4.2$$

where λ determines molecular ordering and can be calculated from the experimental value of S by iteratively varying λ until the calculated value of the order parameter agrees with experiment according to

$$S = \frac{\int P_2(\cos\beta'') \cdot f(\beta'') \cdot \sin(\beta'')\, d\beta''}{\int f(\beta'') \cdot \sin(\beta'')\, d\beta''} \qquad 4.3$$

The T_{1Z} values in both the gel and L_α states of {3',3'-$^2H_2$} β-DTGL are similar, indicating that additional averaging in the L_α state does not significantly influence longitudinal relaxation. This averaging accounts for the decreased ordering in the L_α state ($S = 0.65$) as compared to the gel state ($S \approx 1$). The above-mentioned fluctuations about the local bilayer normal would lead to orientational averaging of the relaxation rate relative to that expected for a single molecular orientation given only by the

orientation of the local bilayer normal relative to H_o, β. Thus, for a given orientation β' of the local bilayer normal the orientationally averaged relaxation rate would be

$$\langle T_1^{-1}(\beta)\rangle = \sum_{\beta''=-\pi/2}^{\pi/2} T_1^{-1}(\beta) \cdot f(\beta'') , \qquad 4.4$$

where a given orientation of the molecular long axis, β'' relative to the local bilayer normal leads to its having an associated orientation, β', relative to the magnetic field direction and a corresponding relaxation rate. The distribution probability (f(β'')) of molecular orientations about the order director was determined from the molecular order parameter (*S*) (Van De Ven and Levine, 1984; Vold and Vold, 1988). In the limits of *S* equal to 1 and 0, both T_{1Q} and T_{1Z} will exhibit no and complete orientational averaging, respectively.

The application of $T_1(\beta)$ orientational averaging to L_α {3',3'-$^2H_2$} β-DTGL with S = 0.65 results in an attenuation of simulated $T_{1Z}(\beta)$ relaxation profile anisotropies (Figures 4.6C, 30.7 MHz and 4.8B, 46.1 MHz) and leads to a close correspondence with the experimental profiles. Simulations of partially-relaxed inversion recovery spectra also agree very well with the experimental data (Figures 4.9C (30.7 MHz) and 4.10B (46.1 MHz)). In order to obtain better fits for the partially recovered spectra at 30.7 MHz, the tau values (delay between the π and π/2 pulses) had to be lengthened relative to the experimental values (but still within the limits of experimental error); simulated tau values are 2.5, 3.5, 4.2 msec and the experimental values are 2.0, 2.5, 3.0 msec, respectively. The sensitivity of the simulated spectra for a given $T_1(\beta)$ profile to the tau value is not unexpected since T_{1Z} is very short. The spectra near the null point will change very quickly as a function of tau; if the simulated T_{1Z} differs from the experimental value, even within experimental error, the spectra will appear to approach equilibrium at different rates. This is most obvious around the null point (if T_{1Z} is 4.0 msec the null point is 2.8 msec, but for T_{1Z} of 4.4 msec the null point is 3.2 msec). For this reason simulation of experimental line shapes using experimental parameters

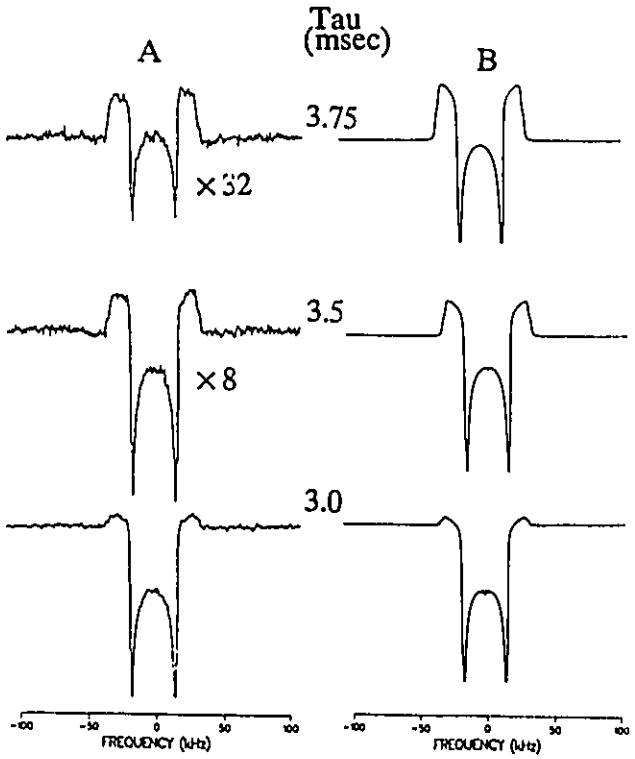

Figure 4.10 T_{1Z} **partially recovered powder spectra of {3',3'-$^2H_2$} β-DTGL at 46.1 MHz.** (A) Experiment. (B) As in Figure 4.8B., all three motions are modelled: 3 site jump ($\tau_c = 6.7*10^{-10}$ s, fast limit, $\omega_o^2\tau_c^2 << 1$) with site populations 0.46, 0.34, 0.20, axial rotation about the molecular long axis ($\tau_c = 8.3*10^{-9}$ s, close to T_1 minimum, $\omega_o^2\tau_c^2 \approx 0.42$), and effects of orientational averaging, $S = 0.65$. Tau is the delay between the π and $\pi/2$ pulses in the inversion-recovery experiment.

is difficult. It is also important to note that although the absolute tau values are longer than their experimental counterparts, the relative anisotropies in the simulated spectra are consistent with those observed experimentally, which is the most important constraint in the lineshape simulation.

There is also a significant attenuation of the simulated $T_{1Q}(\beta)$ profiles when the effects of orientational averaging are included in the calculations. Of the two frequencies used, the fit of the $T_{1Q}(\beta)$ profile at 30.7 MHz (Figure 4.7C) is better than that for 46.1 MHz (Figure 4.6D). This may reflect the sensitivity of the simulation to the axial rotation rate because the correlation time ($\tau_c = 8.3*10^{-9}$) is closer to the T_1

minimum at 30.7 MHz than at 46.1 MHz ($\omega_0^2\tau_c^2$ = 2.56 and 5.76, respectively). It is possible to "fine tune" the simulation parameters, but such a small discrepancy in the T_{1Q} profiles is not significant. A factor of two attenuation of the rotation rate essentially alters the T_{1Q} by a factor of two, whereas the effect on the T_{1Z} simulation is much smaller. At this point, the physical meaning of such small changes in the rates of motion remains to be established; the important feature is the profile shape rather than the absolute values. Hence, no further modifications of the simulations have been attempted to improve the simulated orientation dependent T_{1Q} profiles.

4.4 COMMENTS ON ORIENTED SAMPLES AND THE T_{1Q} EXPERIMENT

The insensitivity of the partially-relaxed powder spectra to changes in the axial rotation rate is significant and justifies the use of oriented samples. It has been demonstrated recently (Baenziger et al., 1988; Bonmatin et al., 1990; Mayer et al, 1990; Pope et al., 1982) that oriented samples, as compared to powder samples, allow orientation-dependent effects to be detected unambiguously and are particularly effective for measuring anisotropic relaxation quantitatively. One reason for this difference is because the powder ^2H spectrum is a superposition of spectra for which the order director is at random angles (β) to the applied magnetic field. For a C-^2H bond executing axially symmetric motions, the observed quadrupolar splitting is given by

$$\Delta\upsilon_Q = \frac{3e^2qQ}{2h} \cdot \frac{(3\cos^2\beta - 1)}{2} \cdot \frac{(3\cos^2\theta - 1)}{2} \cdot S \qquad 4.5$$

e^2qQ is the quadrupolar coupling constant, S is the segmental order parameter and θ is the angle between the order director and the C-^2H bond (Figure 4.3). In the case of a powder spectrum, spectral contributions for β values of 35° and 90° overlap so that only the weighted average relaxation rates ($(T_1(90)^{-1})$ for these orientations can be measured from the spectra directly, $\Delta\upsilon_Q(35)$ and $\Delta\upsilon_Q(90)$ will be equal and their contributions will be superimposed in a powder spectrum. Therefore, any observed T_1

anisotropy, $\partial T_1(\beta)^{-1}$, will not be $T_1(0)^{-1} - T_1(90)^{-1}$ but rather $T_1(0)^{-1} - \overline{T_1(90)}^{-1}$. With an oriented sample only one β orientation is observed at a time (as set by the experimenter), enabling the unambiguous determination of $\partial T_1(\beta)$.

The $T_{1Q}(\beta)$ relaxation profiles also appear to be more sensitive to changes in the simulation parameters than the $T_{1Z}(\beta)$ relaxation profiles. The significance of this difference and utility of T_{1Q} in testing motional models can be assessed from the definition of the resulting relaxation rates in terms of spectral density functions (Jacobsen et al., 1976b):

$$1/T_{1Z} = K[J_1(\omega_0) + 4J_2(2\omega_0)] \qquad 4.6$$

$$1/T_{1Q} = K[3J_1(\omega_0)] \qquad 4.7$$

where $K = \{[3 / 80]*[e^2qQ / hI(2I - 1)]^2\}$, and e^2qQ, h and I have their usual meanings. In equations 4.6 and 4.7, the spectral density functions ($J_m(m\omega_0)$) are contingent upon the orientation of the motional axis relative to the magnetic field direction. The precise nature of this angular dependence relies upon the details of the molecular orientation (Jacobsen et al., 1976b; Torchia and Szabo, 1982). Since $J_1(\omega_0)$ and $J_2(2\omega_0)$ may have partially opposing angular dependencies, T_{1Z}^{-1} (Eq. 4.6) may exhibit a weaker orientational dependence than T_{1Q}^{-1}. This has been demonstrated by Jacobsen et al. (1976b) in the general case of restricted anisotropic motion for a spin 1 nucleus:

$$J_1(\omega_0) = J_1(\omega_0)[\ 1 + (5/7)\langle D_{00}^{(2)}\rangle - (12/7)\langle D_{00}^{(4)}\rangle]. \qquad 4.8$$

$$J_2(2\omega_0) = J_2(2\omega_0)[\ 1 - (5\ 2/7)\langle D_{00}^{(2)}\rangle + (3/7)\langle D_{00}^{(4)}\rangle]. \qquad 4.9$$

where the description of both the orientational dependence and the molecular fluctuations is denoted by the Wigner rotation elements in the angular brackets.
This behavior has also been recognized by Wefing et al. (1984), who noted that the lineshape changes of partially relaxed spectra observed in T_{1Z} experiments may only be minor compared to those observable in T_{1Q} experiments. **The essential point is that**

anisotropy, $\partial T_1(\beta)^{-1}$, will not be $T_1(0)^{-1} - T_1(90)^{-1}$ but rather $T_1(0)^{-1} - \overline{T_1(90)}^{-1}$. With an oriented sample only one β orientation is observed at a time (as set by the experimenter), enabling the unambiguous determination of $\partial T_1(\beta)$.

The $T_{1Q}(\beta)$ relaxation profiles also appear to be more sensitive to changes in the simulation parameters than the $T_{1Z}(\beta)$ relaxation profiles. The significance of this difference and utility of T_{1Q} in testing motional models can be assessed from the definition of the resulting relaxation rates in terms of spectral density functions (Jacobsen et al., 1976b):

$$1/T_{1Z} = K[J_1(\omega_0) + 4J_2(2\omega_0)] \qquad 4.6$$

$$1/T_{1Q} = K[3J_1(\omega_0)] \qquad 4.7$$

where $K = \{[3 / 80]*[e^2qQ / hI(2I - 1)]^2\}$, and e^2qQ, h and I have their usual meanings. In equations 4.6 and 4.7, the spectral density functions ($J_m(m\omega_0)$) are contingent upon the orientation of the motional axis relative to the magnetic field direction. The precise nature of this angular dependence relies upon the details of the molecular orientation (Jacobsen et al., 1976b; Torchia and Szabo, 1982). Since $J_1(\omega_0)$ and $J_2(2\omega_0)$ may have partially opposing angular dependencies, T_{1Z}^{-1} (Eq. 4.6) may exhibit a weaker orientational dependence than T_{1Q}^{-1}. This has been demonstrated by Jacobsen et al. (1976b) in the general case of restricted anisotropic motion for a spin 1 nucleus:

$$J_1(\omega_0) = J_1(\omega_0)[\ 1 + (5/7)\langle D_{00}^{(2)}\rangle - (12/7)\langle D_{00}^{(4)}\rangle]. \qquad 4.8$$

$$J_2(2\omega_0) = J_2(2\omega_0)[\ 1 - (5\ 2/7)\langle D_{00}^{(2)}\rangle + (3/7)\langle D_{00}^{(4)}\rangle]. \qquad 4.9$$

where the description of both the orientational dependence and the molecular fluctuations is denoted by the Wigner rotation elements in the angular brackets.
This behavior has also been recognized by Wefing et al. (1984), who noted that the lineshape changes of partially relaxed spectra observed in T_{1Z} experiments may only be minor compared to those observable in T_{1Q} experiments. **The essential point is that**

the difference in the angular-dependent behavior of T_{1Z} and T_{1Q} would imply that in oriented spectra (and possibly powder spectra), the Jeener-Broekaert experiment may be more useful than the inversion-recovery experiment for discriminating between different motional models. This difference in orientational sensitivity is evident upon comparison of Figures 4.6 and 4.7.

4.5 THE GLUCOSE HEAD GROUP REGION

In the preceding section, a description of molecular reorientation of the glycerol C3 segment was elucidated, which is consistent with longitudinal relaxation measurements in the liquid crystalline state. Since the carbohydrate head group is linked directly to the C3 segment, it is natural to explore the use of the dynamics of the C3 fragments to describe the reorientation of the glucose moiety. Previous work (Jarrell et al., 1987a) showed that there is most likely motion of small amplitude about the glucose-glycerol glycosidic link. As a starting point for this study, this small amplitude motion was ignored and the head group-glycerol segment of β-DTGL was assumed to be rigid with the conformation deduced previously (Jarrell et al., 1987a). Thus the initial isomerization about the glycerol C2-C3 bond, as well as reorientation about the molecular long axis, lead to corresponding reorientation of the head group fragment, which was constrained to be rigid.

Head group reorientation was investigated with {1-$^2H_1$} β-DTGL, in the L_α state, where the deuterium label is at the C1 position of the glucose ring. The lipid was studied as a multilamellar aqueous dispersion. Partially-relaxed T_{1Z} spectra are presented in Figure 4.11 and clearly reveal anisotropic relaxation. Simulations using the above motional model and rates deduced for the glycerol C3 position predict a larger T_{1Z} anisotropy than is seen experimentally (data not shown). Addition of orientational averaging arising from molecular fluctuations about the bilayer normal (S = 0.65), in analogy with that used for the glycerol C3 position, attenuated the predicted T_{1Z} anisotropy and greatly improved the correspondence between the simulated and experimental relaxation profiles (Figure 4.12).

averaging arising from molecular fluctuations about the bilayer normal (S = 0.65), in analogy with that used for the glycerol C3 position, attenuated the predicted T_{1Z} anisotropy and greatly improved the correspondence between the simulated and experimental relaxation profiles (Figure 4.12).

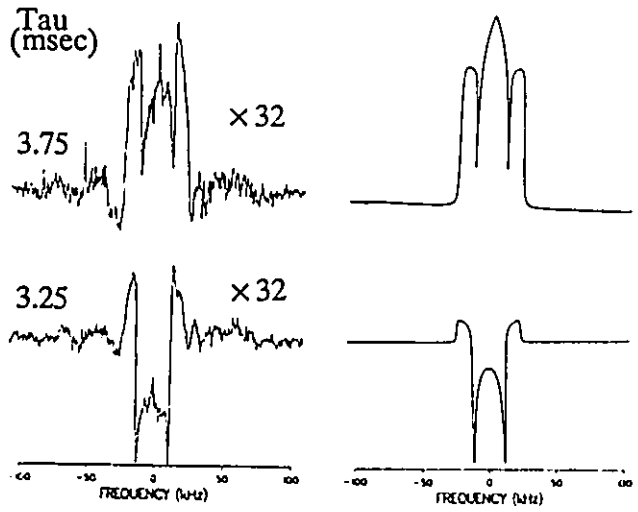

Figure 4.11 T_{1Z} **partially-recovered powder spectra of {1-$^2H_1$} β-DTGL at 30.7 MHz.** (*Left*) Experiment. (*Right*) Calculated spectra. Simulation parameters are same as Figure 4.6c, all three motions are used: 3 site jump ($\tau_c = 6.7*10^{-10}$ s, fast limit, $\omega_o^2\tau_c^2 << 1$) with site populations 0.46, 0.34, 0.20, axial rotation about the molecular long axis ($\tau_c = 8.3*10^{-9}$ s, close to T_1 minimum, $\omega_o^2\tau_c^2 \approx 0.4$), and effects of orientational averaging, S = 0.65. Tau is the delay between the π and π/2 pulses in the inversion-recovery experiment.

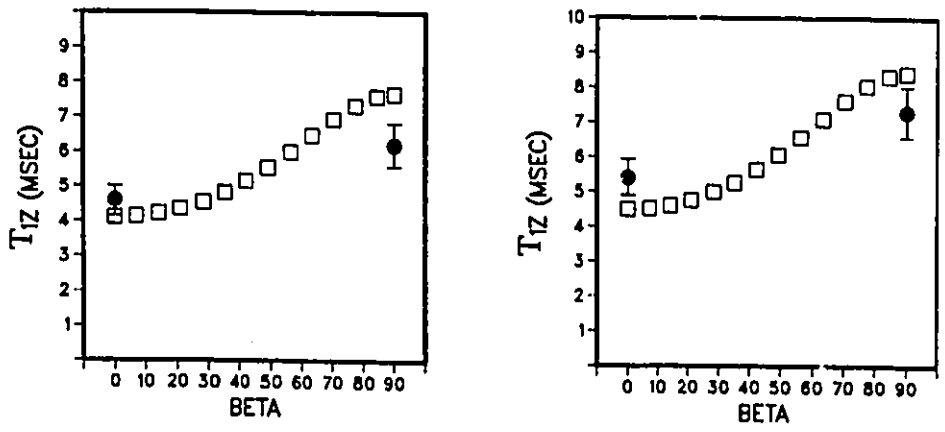

Figure 4.12 Angle-dependent T_{1Z} profiles, from powder spectra of {1-$^2H_1$} β-DTGL at 30.7 MHz (*left*) **and at 46.1 MHz** (*right*). Experimental (●) and calculated (□) ^2H longitudinal relaxation times (T_{1Z} only) as a function of β (angle between H_o and bilayer normal). Simulation parameters are the same as the above spectra. T_{1Z} values are estimated from powder spectra, therefore error is ± 10%.

the T_1 values used are estimated from powder spectra and some error will be associated with $T_1(90)$ in the $T_1(\beta)$ relaxation profile due to spectral overlap associated with β of 35°, 90° (§ 4.4). In fact, quick inspection of the simulated $T_1(\beta)$ relaxation profile indicates that $T_1(35) < T_1(90)$. Removal of the estimated $T_1(35)$ contribution to the experiment $T_1(90)$ value would increase $\partial T_1(\beta)$ and improve the fit of simulated to experimental results.

In general the reorientational model and associated rates elucidated for the glycerol C3 segment also provide a good description of the motion of the glucosyl head group. Close inspection of Figures 4.11 and 4.12 reveals that quantitatively, the simulated results differ from experiment. A potential source of this discrepancy may be the assumption that the glucose-glycerol linkage is rigid. Previous work has shown that for β-DTGL in the L_α state the head group has a segmental order parameter of 0.45, which is smaller than that of the glycerol segment, 0.65 (Jarrell et al., 1987a). The reduced segmental ordering most likely reflects torsional fluctuations of the glucose moiety about the glycosidic bond. It is clear from Figure 4.12 that such motions must be included to improve further the agreement between predicted and experimental relaxation profiles. The following chapter (Chapter 5) presents the results of the potential-energy calculations of the head group conformations about the glycosidic bond with respect to the glycerol backbone. Inclusion of an additional internal jump amongst these sites permit the extension of the present study to a more comprehensive description of head group dynamics. Such an approach has been reported recently in a molecular dynamics study (Edge et al, 1990) which calculated the minimum-energy conformations of disaccharide glycosidic linkages found in glycoproteins.

4.6 COMPARISON WITH PREVIOUS WORK

Limited orientational averaging of T_{1Z} has been used to describe the dynamics of egg phosphatidylcholines (Milburn and Jeffrey, 1989). The dynamics of the phosphodiester moiety are described in terms of two motions, a fast axially symmetric rotation and a slower wobble. The slow wobble which averages the T_1

orientation-dependence is not unlike the molecular reorientations described above. Although this motional model does fit the data, it is probably an oversimplification of the actual behavior.

The present study has the advantage that preliminary investigations of {3',3'-$^2H_2$} β-DTGL in the gel state (Auger et al. 1990) provides a firm basis for describing the L_α dynamics: the molecular motions were refined and a further more complex motion was identified. The three motions described are physically reasonable and have been used either individually or in combination to describe other lipid systems (Mayer et al., 1990; Speyer et al., 1989; Dammers et al., 1988; Hauser et al., 1988; Vold et al., 1988; Wittebort et al., 1987; Meier et al., 1986; Siminovitch et al., 1985; Blume et al., 1982).

Mayer et al. (1990) have elucidated the dynamics of specifically deuterated 1,2-dimyristoyl-*sn*-glycero-3-phosphocholine (DMPC) using T_{1Z} results of oriented multibilayers. They made a comparison of motions in a restricted state (cholesterol present) and a less restricted state (pure DMPC), similar to our comparison of gel and liquid crystalline state β-DTGL. Furthermore, the three basic motions are very similar to those used in the present analysis; internal isomerization (about four sites, versus three), rotation about the molecular long axis, and orientational averaging arising from fluctuations about the bilayer normal. The essential difference in the simulation of dynamic behaviour of the restricted and less restricted DMPC states is the rate of the motions and, most importantly, the effect of the molecular fluctuations, as reflected by the segmental order parameter (the simulations used a population weighted potential, similar to the Maier-Saupe potential used here). The rates of motion used for both states are within an order of magnitude of those used here (as expected since motions around the time frame of the Larmor frequency most affect relaxation). The major difference between the present and the latter study is that the present one has not assigned a correlation time to the orientational averaging process because we assume that these fluctuations are too slow to affect relaxation.

4.7 CONCLUSIONS

It has been possible to apply a motional model deduced for the glycerol C3 position of β-DTGL in the gel state not only to the more fluid L_α state, but also to the analysis of the glucosyl head group ($\{1\text{-}^2H_1\}$) motions of β-DTGL in the L_α state. This translation of modelled motion from the glycerol backbone to the head group is intended to describe the basic "correlated" head group motions with the entire β-DTGL molecule. The following chapter (Chapter 5) completes the description of the more complex torsional motion of the carbohydrate group which is considered to be independent of the other molecular motions defined here.

This study demonstrates the necessity of using both oriented samples and T_{1Q} experiments in testing motional models. Oriented multibilayers not only avoid the effects of fast lateral diffusion over the curved vesicles which may average completely anisotropic longitudinal relaxation (Brown and Davis, 1981), but also provide a means to determine unambiguously the longitudinal $T_1(\beta)$ relaxation profiles in detail. Moreover, the $T_1(\beta)$ profiles will identify more accurately features associated with a particular motional model. Noteably, the T_{1Q} experiment has been useful in testing further the molecular models described. The sensitivity of the $T_{1Q}(\beta)$ relaxation profile to changes in the simulation parameters has proven that T_{1Z} longitudinal relaxation data alone may not be sufficient in this case to discriminate between models for the more detailed molecular motions.

In effect the additional battery of tests (two frequencies, oriented multibilayers, powder spectra lineshapes, and both T_{1Z} and T_{1Q} experiments) have outlined the complex motions of β-DTGL in its biologically relevant liquid crystalline state. While the present study has focused on a simple glycolipid, it suggests that the methodology used may assist in unravelling the conformational and motional aspects of more complex glycolipids in a membranous environment.

Chapter 5

Influence of the Membrane Surface on Glycolipid Conformation and Dynamics.

An Interpretation of NMR Results Using Conformational Energy Calculations.

5.1 INTRODUCTION

Glycolipids typically occur as minor components of the complex heterogeneous matrix of a biological membrane. As a result, the membrane surface may not only influence head group conformation but it also serves as a spatial frame in which the glycolipid is oriented and recognized (Winsborrow et al., 1992). Before addressing the potentially complex motions of the carbohydrate head group of 1,2-di-*O*-tetradecyl-3-*O*-(β-D-glucopyranosyl)-*sn*-glycerol (β-DTGL, Figure 5.1 *left*) in the biologically relevant liquid crystalline phase, a hierarchy of motions of the glycerol backbone (^{2}H-labelled at the glycerol *sn* C3 position) were elucidated (Winsborrow et al., 1991; § Chapter 4). By the analysis of orientation-dependent longitudinal relaxation times (T_{1Z} and T_{1Q}) the following three motions were defined: an internal large-angle three-site jump about the glycerol C2-C3 bond (fast limit, $\omega_o^2\tau_c^2 << 1$), axial rotation around the molecular long

axis (near the T_1 minimum, $\omega_o^2\tau_c^2 \approx 0.42$), and molecular fluctuations about the order director which gives rise to the glycerol (whole molecule) segmental order parameter, $S = 0.65$.

In order to incorporate this model into an overall description of the molecular dynamics the above treatment was also extended to the glucose head group. It had been reported previously that there is additional segmental motion about the glycosidic bond ($S = 0.45$, Jarrell et al. 1987b), but for simplicity the model had considered no motion about the glucose-glycerol linkage (i.e. $S = 1$). The result was a reproduction of the basic relaxation features of the glucose head group, but it was apparent that motion about the glycosidic linkage was taking place and **must** be included to give a more quantitative motional description.

S is a measure of the averaged amplitude of motion that the segment undergoes within the time frame of the experiment, allowing the investigation of ordered systems in large superstructures such as are found in biological membranes. Although experimental results point to some degree of motion about the glycosidic bond ($S = 0.45$), it is not obvious what such motion(s) entails in terms of conformational averaging. S may quantitate the degree of motion, but it does not lead directly to a reasonable physical picture of the molecular motion(s) giving rise to the order parameter. As the next step in defining the molecular details of the recognition processes involving carbohydrates at membrane surfaces, it is very important to appreciate the types, amplitudes, and rates of motion that the head groups may undergo in highly organized structures such as lamellae.

Insight into the conformational averaging that may exist about the glycosidic bond can be gained by means of conformational energy calculations, which define the allowed conformational space for the carbohydrate moiety. Such calculations utilize a potential energy function and determine the energy of particular conformations through pairwise interactions based on the molecular coordinates. The conformational energy

of the structure is minimized by altering the torsional angles about the glycosidic bond (ϕ, ψ, ω, see below; Tvaroška and Pérez, 1986). Application of these calculations to the β-DTGL system can potentially provide an understanding of the nature of the conformational energy surface near the minimum energy structure(s) which may be sampled during conformational exchange.

Recognizing the potential non-rigid nature of the glycosidic bond, Prestegard and co-workers (Scarsdale et al., 1986, 1988) have described an equilibrium between two possible head group conformations of glycolipids in dilute solution. For the calculations they used NOE results in an NMR pseudoenergy approach (Scarsdale et al,. 1986) with the molecular mechanics program AMBER (Assisted Molecular Building with Energy Refinement; Weiner et al., 1986).

In this study, conformational energy calculations have been used to assess the conformational space available to the glucose head group of β-DTGL in a liquid crystalline membrane matrix. ^{2}H NMR quadrupolar splittings are calculated and compared with those observed experimentally. This study demonstrates the importance of including surface interactions when considering the conformational space accessible to cell surface carbohydrates. The empirical approach taken here provides considerable insight at the molecular level, and offers the possibility of exploring even more complex systems.

5.2 COMPUTATIONAL METHODS

5.2.1 The structures

In these calculations, molecular coordinates are not available from experiment for 1,2-di-*O*-tetradecyl-3-*O*-(β-D-glucopyranosyl-*sn*-glycerol (β-DTGL) but they are necessary for the evaluation of the conformational energy. Therefore, two types of

β-DTGL analogues were constructed in the initial phase of the study. The first, 4'-deoxy-gentiobiose, used atom positions taken from the crystal structure of methyl β-D glucopyranoside hemihydrate (Jeffrey and Tagaki, 1977) to construct both the glucose head group and the aglyconic unit (Figure 5.1, *right*, Structure A). The glucose residue that was intended to serve as an analogue to the β-DTGL glycerol fragment was reduced at the C4' position, generating 4'-deoxy glucose. Glucose was linked β 1→ 6 to the 4'-deoxy-glucose, generating 4'-deoxy-gentiobiose. The aglyconic C6', C5', and C4' positions now correspond to the glycerol C3', C2', and C1' β-DTGL positions, respectively. This is a reasonable representation because the atomic species in the interfacial region that are near enough to the head group to affect its energetics are of the correct type. (Primed atoms represent atoms in the aglyconic unit).

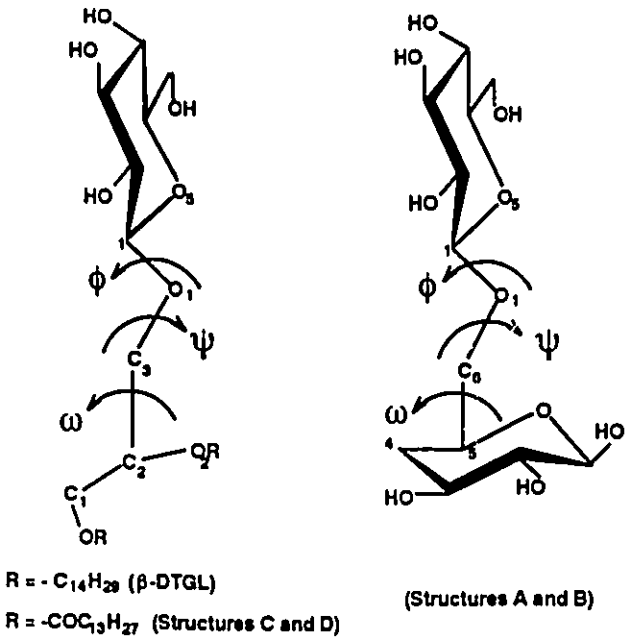

Figure 5.1 β-DTGL molecule and analogue structures. Torsional angles about the glycosidic bond are defined by: ϕ = O5, C1, O1, Cx'; ψ = C1, O1, Cx', C(x-1)'; ω = O1, Cx', C(x-1)', O(x-1)'. Where x represents position number 3 of glycerol and 6 of 4'-deoxy-glucose aglyconic units. Hence, (x-1) represents position number 2' of glycerol and 5' of 4'-deoxy-glucose aglyconic units. *Left*: Structure used in experiment, β-DTGL (R = $-C_{14}H_{29}$), and analogue structures C and D (R = $-COC_{13}H_{27}$). *Right*: Structures A and B, 4'-deoxy-gentiobiose (note that the 4'-deoxy-glucose C6', C5', and C4' positions correspond to the glycerol C3', C2', and C1' atoms, respectively).

A second analogue, 1,2-dilauroyl-3-*O*-(β-D-glucopyranosyl)-*sn*-glycerol (Figure 5.1, *left*, Structure C), was created to represent more closely a lipid molecule and to test the dependence of the results on the choice of models. This molecule was constructed with the same glucose crystal structure but the aglycon is the diacylglycerol portion of the phosphatidyl ethanolamine crystal structure (Elder et al., 1977). This construct is very similar to β-DTGL, except that the lipid chains are ester- and not ether-linked to the glycerol C1' and C2' positions. (Note that in this chapter the aglyconic unit atoms are primed, differentiating them from the carbohydrate portion of a molecule.)

Finally, because of potential concerns in using x-ray crystallographic positions of the above hydrogen atoms, in both cases the glucose structure was also used after the methyl β-D glucopyranoside hemihydrate was relaxed by applying molecular mechanics

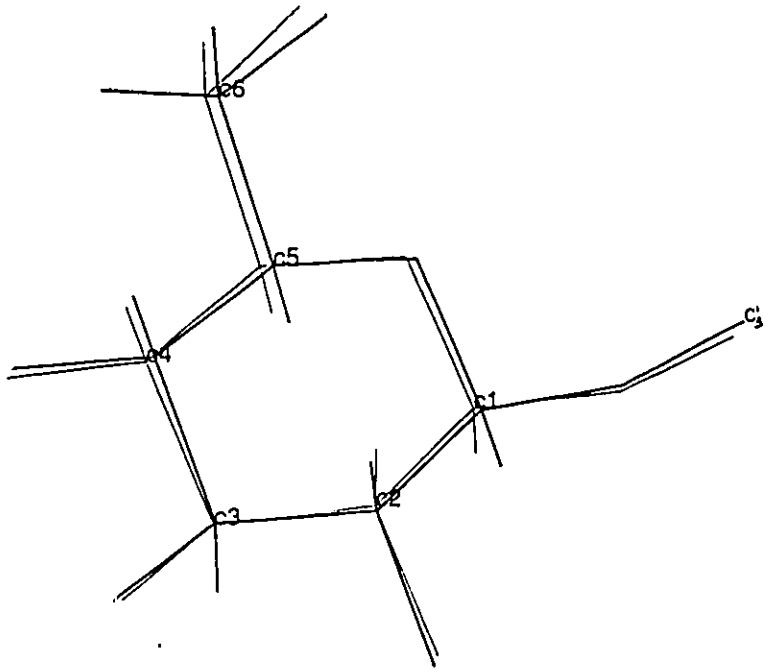

Figure 5.2 Overlay of glucose structures. Light lines are structure using crystal atom positions. Dark lines are structure using crystal atom positions relaxed by MM2.

minimization MM2(87) (Allinger 1977; Lii et al. 1989). Figure 5.2 is an overlay of the two glucose structures used; the main differences are in the positions of the

hydroxymethyl groups and the ring hydroxyl oxygen atoms. Orientation of the hydroxyl hydrogen atoms is not important since they are not considered in the conformational energy calculations. Hence, Structure B is 4'-deoxy-gentiobiose and Structure D is 1,2-dilauroyl-3-*O*-(β-D-glucopyranosyl)-*sn*-glycerol, where the crystal glycose molecule is relaxed by MM2 for both structures. In effect, four β-DTGL analogues were generated (Structures A-D). In all cases the bridging C-O-C angle was 114° and the glucose hydroxymethyl torsional angle was gauche-plus (g^+, defined by O5, C5, C6, O6).

5.2.2 Calculation of Conformational Energy

As a first step to understanding the conformational space that the glucose head group of β-DTGL might occupy, PFOS (Potential Functions of OligoSaccharides) conformational energy calculations (Tvaroška and Pérez, 1986) were used to evaluate the conformational potential energy over ϕ , ψ, ω space (the program is a generous gift of J. R. Brisson, N.R.C.C., Ottawa). These angles are shown in Figure 5.1: ϕ = O5, C1, O1, Cx', ψ = C1, O1, Cx', C(x-1)', and ω = O1, Cx', C(x-1)', O(x-1)'. Where x represents position number 3' of glycerol-containing aglyconic units (Figure 5.1, *left*) or position number 6' of 4'-deoxy-glucose aglyconic units (Figure 5.1, *right*). Hence, (x-1)' represents position numbers 2' and 5' of glycerol and 4'-deoxy-glucose aglyconic units, respectively.

These calculations evaluate the van der Waals interactions between non-bonded atoms (using a Leonard-Jones 6-12 potential), torsional contributions about the glycosidic bond, and an exo-anomeric term (Tvaroška and Pérez, 1986):

$$PFOS = E_{ab} + E_t + E_{exo} \qquad 5.1$$

The torsional contribution had a three-fold periodicity and a barrier V_3 = 1.0 kcal/mol about ϕ, and V_3 = 0.5 kcal/mol about ψ.

The angle ω describes the isomerization about the glycerol C2-C3 bond. In a previous NMR lineshape and relaxation study on β-DTGL in the liquid crystalline state

(Winsborrow et al., 1991) this motion was defined to be a large angle jump with site populations 0.46, 0.34, 0.20; most likely these sites can be characterized by isomerization between the conformers gauche-plus (g^+, 60°), t (trans, 180°), and gauche-minus (g^-, 300°). The angles ϕ and ψ are the angles about the glycosidic bond which were assumed to be fixed in the same study, for the sake of developing a whole body motional model in the liquid crystalline state. In the present calculations ω has the values corresponding to the conformations g^+, t, and g^- as proposed above, and both ϕ and ψ are varied over 360° (with 5° increments).

5.2.3 Surface Potentials

A surface term (E_{surf}) was used which included both a surface barrier (V_s), and an intermolecular energy (E_{im}) between an annulus of six static β-DTGL analogue molecules and the central β-DTGL molecule. E_{im} calculated pairwise non-bonded interactions using a Leonard-Jones 6-12 potential. The annular molecules were translated around the central molecule (Figure 5.3) and then held fixed for the duration of the calculation with the glycerol C2'-C3' (or 4'-deoxy-glucose C5'-C6') bond perpendicular to the membrane surface and the glycerol C2' (or 4'-deoxy-glucose C5') atom at the origin (ϕ = t, ψ = t, ω = t; § Appendix for subroutine).

In addition, a surface barrier (V_s) of 30 kcal/mol, similar to that proposed by Nyholm et al. (1989), was applied at the glycerol C2' (or 4'-deoxy-glucose C5') position which disallowed any conformation where the hydrophilic head group would lie in the hydrophobic lipid region below this position. The potential energy of the system (E_{sys}) is now described by:

$$E_{sys} = PFOS + E_{surf} \qquad 5.2$$

$$E_{surf} = E_{im} + V_s \qquad 5.3$$

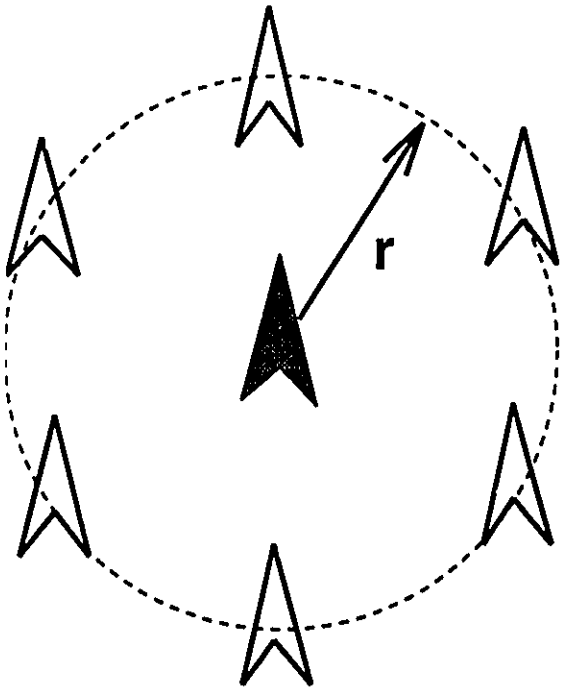

Figure 5.3 Simulated membrane surface. Schematic diagram, as viewed from above, of the central β-DTGL analogue molecule (shaded arrow head) surrounded by six translated surface analogue molecules which are static (ϕ = t, ψ = t, and ω = t). **r** and the dashed circle indicate that the annulus size is variable.

Another feature of this treatment is the variation in the radius of the surface annulus (Figure 5.3). Monolayer and calorimetric studies have estimated the cross sectional area occupied by β-DTGL in the liquid crystalline phase to be 102 ± 4 Å^2/molecule (radius ≈ 5.7 Å; Hinz et al., 1985). Therefore, we placed the annulus of surface molecules within a range of radii, which bracketed twice the cross-sectional radius (7.5 - 15.0 Å), around β-DTGL in order to test the sensitivity of the allowed conformational space to surface constraints.

5.2.4 Calculation of Quadrupolar Splittings

For a deuterated molecular fragment in a partially ordered environment the ^2H NMR spectrum is dominated by the interaction between the deuterium nuclear quadrupole moment (eQ) and the electric field gradient (eq) at the nuclear site. This results in a quadrupolar splitting of the ^2H resonance. The description of the quadrupolar splitting ($\Delta\upsilon_{Qi}$) for C-^2H_i bonds in experimental systems executing axially symmetric motions is (Seelig, 1977):

$$\Delta\upsilon_{Qi} = (3/2h)e^2qQ \,.\, S \,.\, (3\cos^2\theta_i - 1)/2 \,.\, (3\cos^2\beta - 1)/2 \qquad 5.4$$

where e^2qQ is the quadrupolar coupling constant (164 kHz for carbohydrates; Jarrell et al.,1986), θ is the angle between the C-^2H bond and the molecular frame, and β is the angle between the order director ($\vec{\mathbf{n}}$, which is coincident with the molecular long axis) and the applied magnetic field ($\mathbf{H}_o$, Figure 5.4). S is the segmental order parameter (0.45 for the glucose head group; Jarrell et al., 1986), which is a measure of the motional averaging of the molecular fragment with respect to the order director. This is depicted by the shaded region about $\vec{\mathbf{n}}$, in Figure 5.4. Therefore, each deuterated position (i) on the glucopyranose ring of β-DTGL has a quadrupolar splitting ($\Delta\upsilon_{Qi}$), which is dependent upon the corresponding θ_i for each C-^2H bond.

For the calculation of the quadrupolar splitting, it is necessary to know the direction cosine (cos θ) made by a C-^2H vector with the axis about which the order is symmetric ($\vec{\mathbf{n}}$, coincident with the molecular long axis, and also, parallel with the β-DTGL glycerol C2-C3 bond, Jarrell et al., 1987a). For every ϕ, ψ, ω combination a new set of molecular coordinates are generated; hence, the direction cosine and quadrupolar splitting can be evaluated for each glucose C-^2H bond at all conformations (with $\beta = 90°$):

$$\Delta\upsilon_{Qi(\phi,\psi,\omega)} = (3/8h)e^2qQ \,.\, \mathbf{S}_{gl} \,.\, (3\cos^2\theta_i - 1)_{(\phi,\psi,\omega)} \qquad 5.5$$

where e^2qQ and 0 are the same as in equation 5.4, and S_{gl} is the glycerol segmental order parameter (0.65 for this molecule in the liquid crystalline state) which, for this model, is used as the molecular order parameter (Winsborrow et al., 1991).

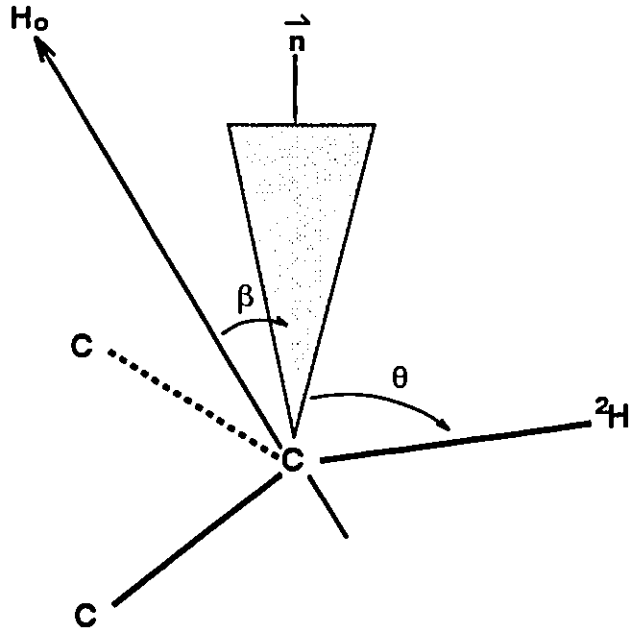

Figure 5.4 Definition of angles. 0 defines the angle that the C-^{2}H bond makes with the order director ($\vec{n}$). β defines the angle that n makes with the applied magnetic field (H_o). The shaded region represents the molecular motional averaging about n which is quantified by S_{mol}.

Both *S* (eq. 5.4) and S_{gl} (eq. 5.5) have been experimentally determined. However, *S* for the sugar ring reflects the motional averaging of the glycerol C3 position and the glucose head group about the glycosidic bond, and S_{gl} reflects only the former motion. Therefore, in order to compare appropriately the experimentally determined quadrupolar splitting, $\Delta\upsilon_{Qi}$ (eq. 5.4), with the calculated one, $\Delta\upsilon_{Qi(\phi,\psi,\omega)}$ (eq. 5.5), the calculated quadrupolar splitting has to include the motional averaging of the head group about the glycosidic bond. This is carried out by averaging $\Delta\upsilon_{Qi(\phi,\psi,\omega)}$ over ϕ, ψ, ω space, as weighted by their conformational populations. The populations of the individual conformers were calculated from their relative energies assuming a Boltzmann distribution:

$$\text{population}(\phi,\psi,\omega) \propto \exp(-\Delta E_{sys}(\phi,\psi,\omega)/kT) \qquad 5.6$$

where $E_{sys}(\phi,\psi,\omega)$ is the conformational energy calculated for a particular ϕ,ψ,ω conformation, and both k and T have their usual meanings. **The averaged calculated quadrupolar splitting, therefore, reflects the predicted degree of conformational averaging about the glycosidic linkage superimposed upon the whole body motions defined by the glycerol backbone.** The resultant quadrupolar splitting for each deuteron may be compared with that observed experimentally to assess the closeness in fit between the predicted and actual internal motional amplitudes.

5.3 RESULTS AND DISCUSSION

5.3.1 Isolated Molecule

For brevity only one set of results of the conformational energy calculations will be presented in detail (from a choice of three ω angles: g^+, t, g^-; and four β-DTGL analogues, Structures A - D); any differences in results between molecular models will be discussed in the text. Figure 5.5 is the ϕ , ψ contour map of Structure A ($\omega = g^+$). The global minimum is at -95°/55°, for ϕ / ψ, respectively. Similar results were produced with the four analogues that were constructed. Moreover, the results for the gentiobiose based analogues (Structures A and B) are similar to those of Neuman et al. (1990) for methyl gentiobioside.

All sets of data indicated that the preferred ϕ conformation was around -80° ± 15° and a broad range of ψ conformations were energetically allowed. It is more readily apparent that there is a "trough" of local minima along ϕ = -90° for Structure A, $\omega = g^+$, (and all other analogues along ϕ = -80° ± 15°) when the population map is considered (Figure 5.6). The populations are evaluated at 55°C (to match the experimental conditions) from the potential energies determined for each conformation, assuming a Boltzmann distribution.

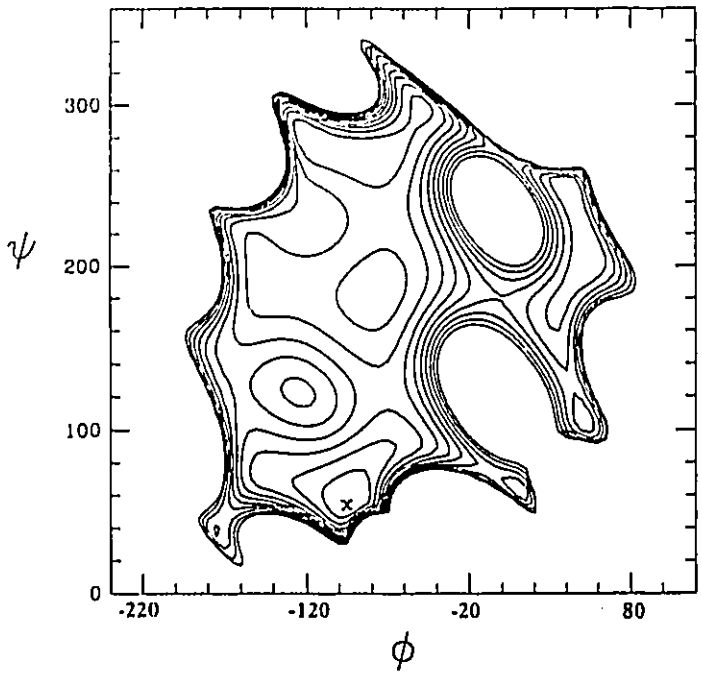

Figure 5.5 Conformational energy as a function of the angles ϕ and ψ for the β-DTGL analogue in vacuo. The analogue molecule is Structure A, 4'-deoxy gentiobiose. There are 10 contour levels, each contour is 1 kcal; X represents the global minimum.

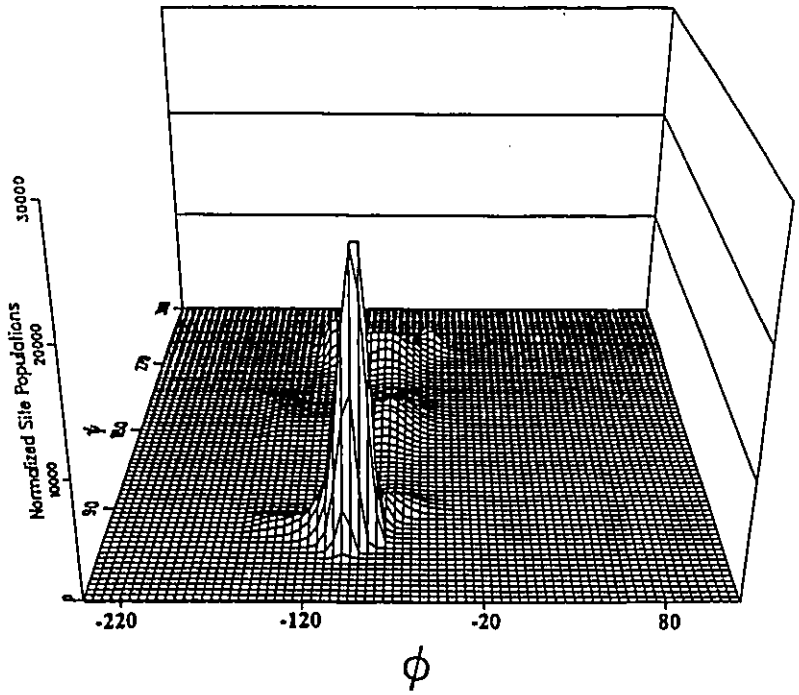

Figure 5.6 ϕ, ψ population map for the β-DTGL analogue in vacuo. The conformational energies of Figure 5.5 have been given a Boltzmann weighting. Note that the most populated sites are ϕ (-110° to -90°) and ψ (40° to 300°).

The ψ range is 40 - 300° for the molecules with the 4'-deoxy glucose aglyconic unit (Structures A and B) and 100 - 270° for the molecules with the diacylglycerol aglyconic unit (Structures C and D). The more restricted conformational space for the latter molecule is not unexpected because this lipid is more bulky at the glycerol backbone due to the carbonyl oxygen atoms which are not present in either Structures A, B, or β-DTGL. In fact, these carbonyl oxygen atoms do experience interactions with the ring hydroxyl oxygen atoms when the van der Waals interactions are examined for the individual pairs of atoms.

The relative populations for the three global minima, $\omega = g^+, t, g^-$, of Structure A are 0.52, 0.32, and 0.16, respectively. Although this compares well with 0.46, 0.34, 0.20, determined independently in NMR lineshape and relaxation studies on β-DTGL in the gel state (Auger et al. 1990), the agreement must be fortuitous since the conformational energy calculations have been only for an isolated molecule. At this point no membrane surface environment considerations have been made and any conclusions concerning the validity of the conformational description would be premature.

5.3.2 Membrane Embedded Molecule

Under conditions in which their biological roles are expressed, these lipids clearly do not exist in vacuo; in a membrane matrix the allowed conformational space is very likely quite different. It is certain that some conformations are not possible, for example, the hydrophilic head group should not be found in the hydrophobic lipid region ($-120° < \phi < 100°$ when $\psi < 140°$) which is energetically unfavourable. In analogy with the approach of Nyholm et al. (1989), when a hydrophilic/hydrophobic barrier was implemented, a 30 kcal/mol penalty was imposed whenever any carbohydrate atoms were positioned below the surface (which begins at glycerol C2' and 4'-deoxy-glucose C5'). A number of additional conformations were disallowed (result not shown) and the

conformational space became more restricted relative to the isolated molecule. However, simply disregarding these conformations in order to simulate a membrane molecule at the membrane surface does not recognize interactions with neighbouring molecules which may influence the conformation(s) allowed.

Through a series of steps where softer surface interactions were applied, a more complicated surface matrix was created by spatially translating six static β-DTGL analogue molecules around the central β-DTGL molecule (Figure 5.3). Monolayer and calorimetric studies have estimated the cross-sectional area occupied by β-DTGL in the liquid crystalline phase to be 102 ± 4 $Å^2$/molecule (radius ≈ 5.6 Å; Hinz et al., 1985). Therefore, the surface molecules were initially positioned 11 Å (2*r) away from the central β-DTGL molecule.

The conformationally averaged $\Delta\upsilon_Q$ values were determined by calculating quadrupolar splittings for the glucose deuterons ($^2H_1$, $^2H_2$, $^2H_3$, and $^2H_4$) for each ϕ, ψ, ω conformation and weighting by their probability, based on the conformational population. In the course of the conformational energy calculations the hydroxymethyl group was maintained at only one conformation (g*). However, it has been established that the exocyclic hydroxymethyl group of glucose in β-DTGL exists in two rotameric forms which are in slow exchange on the ^{2}H-NMR timescale (Jarrell et al., 1987a). Therefore, the quadrupolar splittings due to the hydroxymethyl deuterons have not been calculated.

The calculated splittings for Structure A, 4'-deoxy-gentiobiose (Table 5.1), agree well with those observed experimentally (Jarrell et al., 1987a). In order to test the sensitivity of the conformational space to the surface environment these calculations were carried out for all analogue structures (A-D). A variety of surface conditions were used (Table 5.1): the surface annulus was positioned at a range of radii (7.5 - 15.0 Å) and the static surface molecules were also rotated by 180° about their molecular long axes (Structures E and F).

Table 5.1 Conformationally averaged quadrupolar splittings for different surface constraints

		Quadrupolar Splittings (kHz) of Glucose Deuterons
β-DTGL	^{2}H1	22.9 kHz
	^{2}H2	22.8
Experimental Result[1]	^{2}H3	24.0
	^{2}H4	26.0

		Conformationally Averaged Quadrupolar Splittings (kHz) of Glucose Deuterons							
		Radii of Surface Molecules (Å)							
β-DTGL analogue	^{2}H position	7.5	9.5	10.0	10.5	11.0	11.5	13.0	15.0
	C1	-60.5	**25.1**[2]	**20.1**	**20.2**	**20.6**	18.5	-23.4	-10.7
A	C2	-58.0	**23.9**	**18.7**	**17.7**	**18.1**	12.3	-27.9	-14.0
	C3	-55.8	**26.6**	**21.2**	**20.8**	**20.5**	8.2	-31.4	-15.6
	C4	-55.1	**33.5**	**27.6**	**30.8**	**29.3**	15.0	-34.0	-15.2
	C1	-63.3	**22.6**	**28.0**	**23.2**	7.4	5.0	- 0.8	- 2.8
B	C2	-60.0	**19.5**	**20.7**	**26.7**	5.4	6.5	- 5.3	-1.4
	C3	-56.6	**16.4**	**22.7**	**22.6**	9.8	0.7	-10.6	-4.3
	C4	-55.9	**22.4**	**29.4**	**21.4**	8.2	3.4	-0.9	1.8
	C1		**26.2**	**15.2**	9.7	18.5	19.1		
C	C2		**24.7**	**12.8**	7.3	14.4	13.2		
	C3		**27.5**	**16.4**	11.5	13.7	11.5		
	C4		**35.3**	**27.9**	25.4	19.4	11.5		
	C1		**24.4**	**27.1**	**24.9**	0.4	-1.2		
D	C2		**27.2**	**25.1**	**18.6**	-13.6	-11.9		
	C3		**25.5**	**25.3**	**19.5**	-6.9	-9.0		
	C4		**22.9**	**27.1**	**25.9**	3.9	2.4		
	C1		**29.6**	5.2					
E[3]	C2		**28.5**	1.4					
	C3		**26.6**	3.6					
	C4		**21.3**	15.9					
	C1		36.6	**22.6**					
F[4]	C2		31.1	**18.1**					
	C3		31.5	**14.3**					
	C4		37.4	**22.6**					

1. Jarrell et al. 1987a.
2. Bold indicates calculated quadrupolar splittings that correspond closely with experimental results.
3. **Structure** A with surface molecules rotated 180°. 4. **Structure** B with surface molecules rotated 180°.

As the surface radius was enlarged from 7.5 Å to 15 Å the conformational area of the contour maps for Structure A ($\omega = g^+$, Figure 5.7) progressively grew from a small spot to approach resemblance with the contour of the isolated molecule (Figure 5.5). For brevity only one set of results are presented because the contour plots for the other analogue structures at all three ω positions (g^+, t, g^-) are similar.

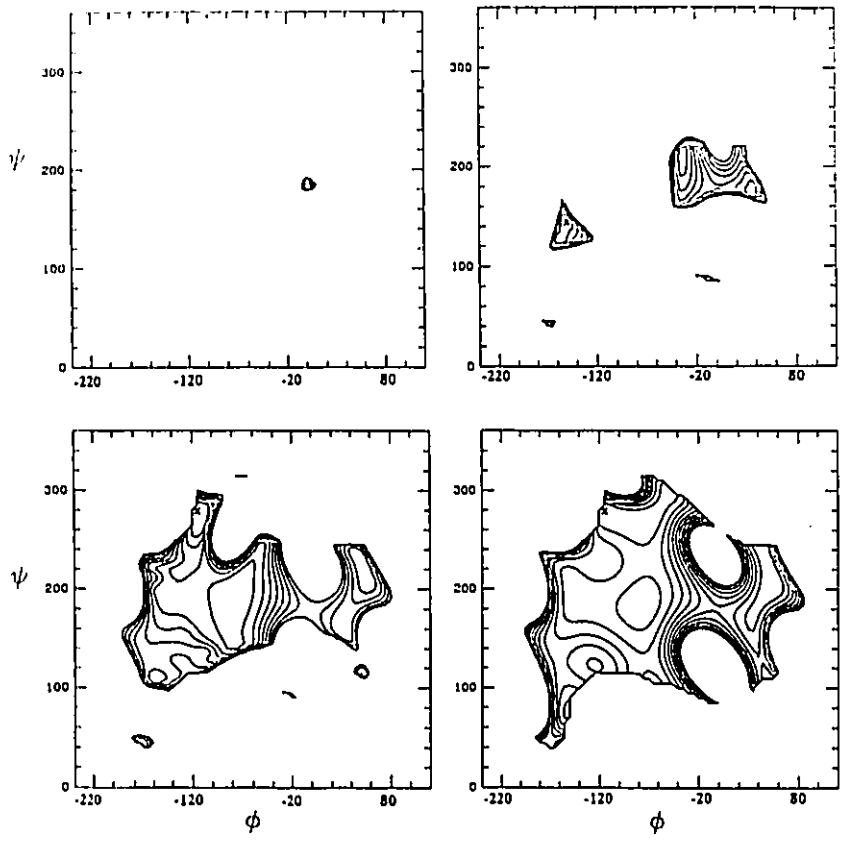

Figure 5.7 Influence of surface space on conformational energy. Conformational energy as a function of the angles ϕ and ψ for the β-DTGL analogue surrounded by an annulus of six surface analogue molecules at a distance of: *top left* 7.0 Å, *top right* 9.5 Å, *bottom left* 11.5 Å, *bottom right* 15.0 Å. The analogue molecule is Structure A (Table 5.1, ω = t). There are 10 contours, each contour is 1 kcal; X represents the global minimum.

The sensitivity of the conformational space to local environment is demonstrated dramatically when the ϕ,ψ population map for membrane-embedded Structure A (r = 9.5 Å, $\omega = g^+$, Figure 5.8) is compared with that of the isolated molecule (Figure 5.6). The conformational space is very restricted when membrane surface interactions are

included in the calculations. The head group conformational space of the membrane-embedded β-DTGL analogue molecule is centred around a conformational well -150° / 145°, ϕ / ψ, with a distribution of populated sites (Figure 5.8): $-170° \leq \phi \leq -130°$ and $120° \leq \psi \leq 155°$. In contrast, the conformational space of the isolated molecule (Figure 5.6) is centred about -95° / 55°, ϕ / ψ, with a much broader distribution of populated sites, particularly in the ψ direction: $-140° \leq \phi \leq -40°$ and $40° \leq \psi \leq 300°$. When ω is set to either g$^-$ or t the conformational space is equally restricted. For ω = g$^-$ the populated sites are centred about $\phi = -80 \pm 20°$ and $\psi = 170 \pm 15°$. In the case of ω = t, ϕ = -70 ± 20° and $\psi = 235 \pm 15°$. The results for the three different ω values clearly demonstrate that the conformational space is restricted relative to the isolated molecule.

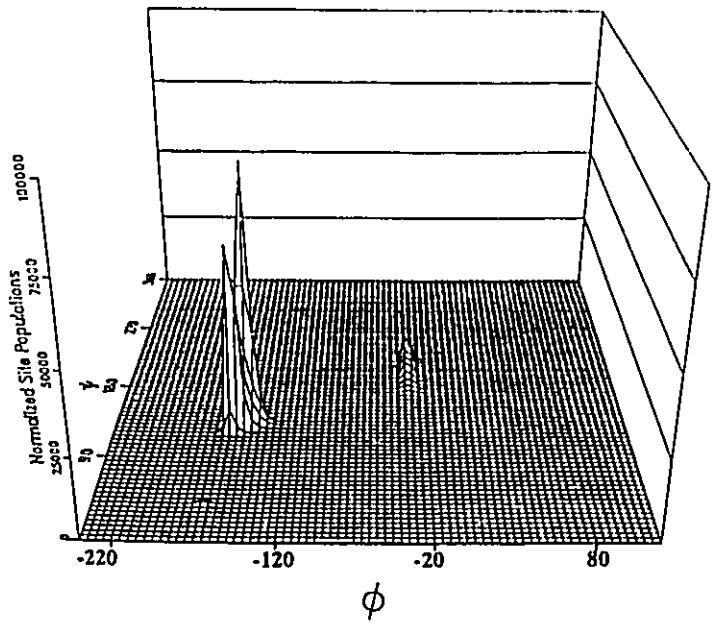

Figure 5.8 ϕ, ψ population map of β-DTGL analogue. Structure A, ω = t, surrounded by an annulus of six surface analogue molecules at a distance of 9.5 Å. Note that the most populated sites are ϕ (-170° to -130°) and ψ (120° to 155°).

In Table 5.1 the calculated quadrupolar splittings that agree most closely with those determined experimentally can be seen in bold print. **The results suggest that the conformational space of all of the central β-DTGL analogue molecules is tolerant**

to the presence of surface molecules within a range of distances (9.5 - 11.0 Å). Upon closer inspection it is apparent that the quadrupolar splittings change more quickly with increasing radius for Structure B than for Structure A (MM2 and crystal glucose atom positions in 4'-deoxy-gentiobiose, respectively, §Figure 5,1). Such rapid changes in the calculated quadrupolar splittings, as displayed with structure B, are usually indicative of a dominant repulsive term (due to the r^{-12} dependence in the Leonard-Jones non-bonding potential). Consideration of the individual interactions reveals that the source of the repulsion is between the glucose hydroxyl oxygen atoms of the central molecule and those of the surface molecules. This implies that the conformational space is very sensitive to its environment, particularly to the positioning of the hydroxyl oxygen atoms.

Although the change in potential energy around the lowest energy conformations may be small (as can be seen in Figure 5.7) this has a dramatic effect on the weighting of the quadrupolar splittings. The angles that the C-^{2}H bond vectors make with the order director in these low energy conformational regions are close to an angle (55.4°, the "magic angle") which causes the quadrupolar splittings to change drastically with small changes in conformation.

The effect of the environment on the conformational space is again noted when the six static surface molecules are rotated by 180° about their molecular long axes (Structures E and F, Table 5.1), effectively changing the apparent nature of the lipid annulus. Not only do the quadrupolar splittings change but the relative sensitivity to the neighbouring hydroxyl oxygen atoms for Structures A and B are reversed: the quadrupolar splittings for Structure A deviate from experiment at a smaller radius (9.5 Å, Structure E) than Structure B (10.5 Å, Structure F). The energy differences around the energy minima are small, again demonstrating the sensitivity of the quadrupolar splitting to conformation in this region where the angle between the C-^{2}H bond and the order director is near the magic angle.

The results of the calculations on the analogue with the diacylglycerol aglyconic unit (Structures C and D, Figure 5.1) demonstrate a trend similar to that observed for the above systems. Note that the results for Structures A and C, with the crystal glucose structure, are very different whereas those for Structures B and D (glucose structure relaxed by MM2) are similar. The conformational space of Structure C is more affected by intramolecular repulsions between the glucose and aglyconic atoms than Structure D. In particular, the glucose O3 hydroxyl oxygen atom and the glycerol C2 carbonyl oxygen atoms contribute strong repulsions to the energetics of the system.

In general, with a molecular annulus spaced 9.5 Å to 11.0 Å around any of the four β-DTGL analogue molecules the conformational space of the head group is centred around a conformational well with a distribution of populated sites: $\phi = -150° \pm 20°$ and $\psi = 145° \pm 15°$ when $\omega = g^+$ (the lowest energy ω conformation) . When $\omega = g^-$ the populated sites are centred about $\phi = -80° \pm 20°$ and $\psi = 170° \pm 15°$, and for ω = t, $\phi = -70° \pm 20°$ and $\psi = 235° \pm 15°$. **It should be reemphasized that although the details (specific conformations and populations) are influenced by the nature of the β-DTGL analogue molecule and annulus, the conclusions are not.**

One final result (not shown) is the effect of positioning the membrane surface with respect to the molecular long axis of the central molecule. The deeper into the membrane the molecule was placed (within 2Å), the more restricted the conformational space became. This approach may be useful in studies concerning the effect of varying lipid chain lengths in membrane systems, lectin binding, and drug-lipid interactions.

5.4 CONFORMATION VERIFICATION

The average head group orientation of glucose in β-DTGL has been determined previously by our research group (Jarrell et al., 1987b). We have sought verification of this result via an independent means. Neutron diffraction is a method which can be

used for such determinations because it is a technique that is based on regular layer separations of ordered but not necessarily crystalline samples (Franks and Lieb, 1982). Moreover, deuterons have a large positive neutron scattering length, specific labelling with deuterium at various positions in a lipid molecule makes it possible to locate the transbilayer position and distribution of the label (Wiener and White, 1991).

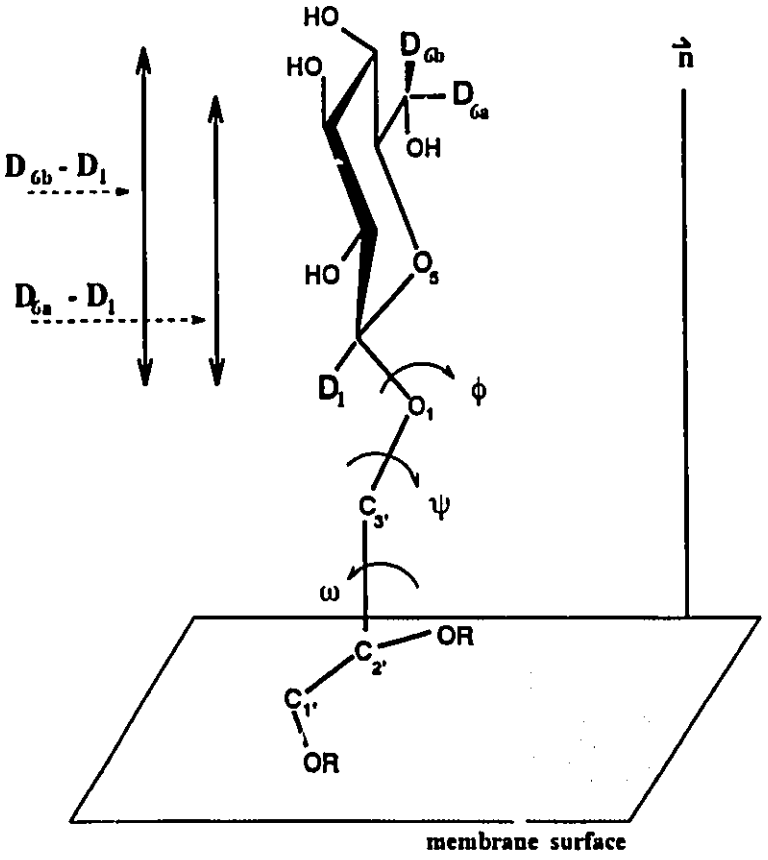

Figure 5.9 Schematic diagram showing the vertical separation between the glucose C1 and C6 deuterons in β-DTGL. D_1 represents the deuteron on C1, D_{6a} and D_{6b} represent the deuterons on C6 of glucose. D_{6a} - D_1 and D_{6b} - D_1 are the vertical separations of the corresponding atoms. The torsional angles are given to show that the conformations of the molecule are averaged over ϕ, ψ, ω space during the time course of the neutron diffraction experiment.

With β-DTGL deuterium labelled at the C1 (D_1) and C6 (D_{6a} and D_{6b}) positions, the neutron diffraction experiments will measure the vertical separation (parallel to the order director, $\vec{n}$) of the deuterons (Figure 5.9). However, the time scale of the neutron diffraction experiment is much longer than the correlation time of the molecular motions; the detected deuterium postion will actually be a distribution of positions, averaged over time. Therefore, an averaged distribution of the two vertical separations, D_{6a} - D_1 and D_{6b} - D_1, will be measured by neutron diffraction because the C6 methoxy group rotates about the C5-C6 bond (Jarrell et al. 1986). The experimentally determined D_6-D_1 separation for β-DTGL is 1.9 ± 1.5 Å (H. C. Jarrell, M. Auger, E. Pebay-Peyroula, and E. J. Dufourc, unpublished results).

Conformational calculations were performed for both a free and a membrane embedded β-DTGL molecule, where the results of the latter calculation agreed well with NMR data (§5.3). The results have been expressed in a format relative to neutron diffraction results. This was effected by subtracting the C1 deuteron molecular coordinate along $\vec{n}$ from that of the C6 deuterons. As in the calculation of the quadrupolar splittings, the separations were weighted by the Boltzmann population corresponding to the particular conformational energies.

The calculated separation probabilities for the free molecule increased gradually from -0.85 to 4.35 Å (Figure 5.10, *top*). However, when the constraints of a membrane surface are included in the calculations, the separation distribution is centred about 2.15Å (Figure 5.10, *bottom*). This result closely resembles that of the neutron diffraction data and supports the conclusions made earlier; the head group conformation of β-DTGL should not be considered as static, but rather as existing in an equilibrium of conformations. The ability of the empirical calculations used to reproduce the experimental results demonstrates further the significance of including membrane surface interactions in the conformational calculations.

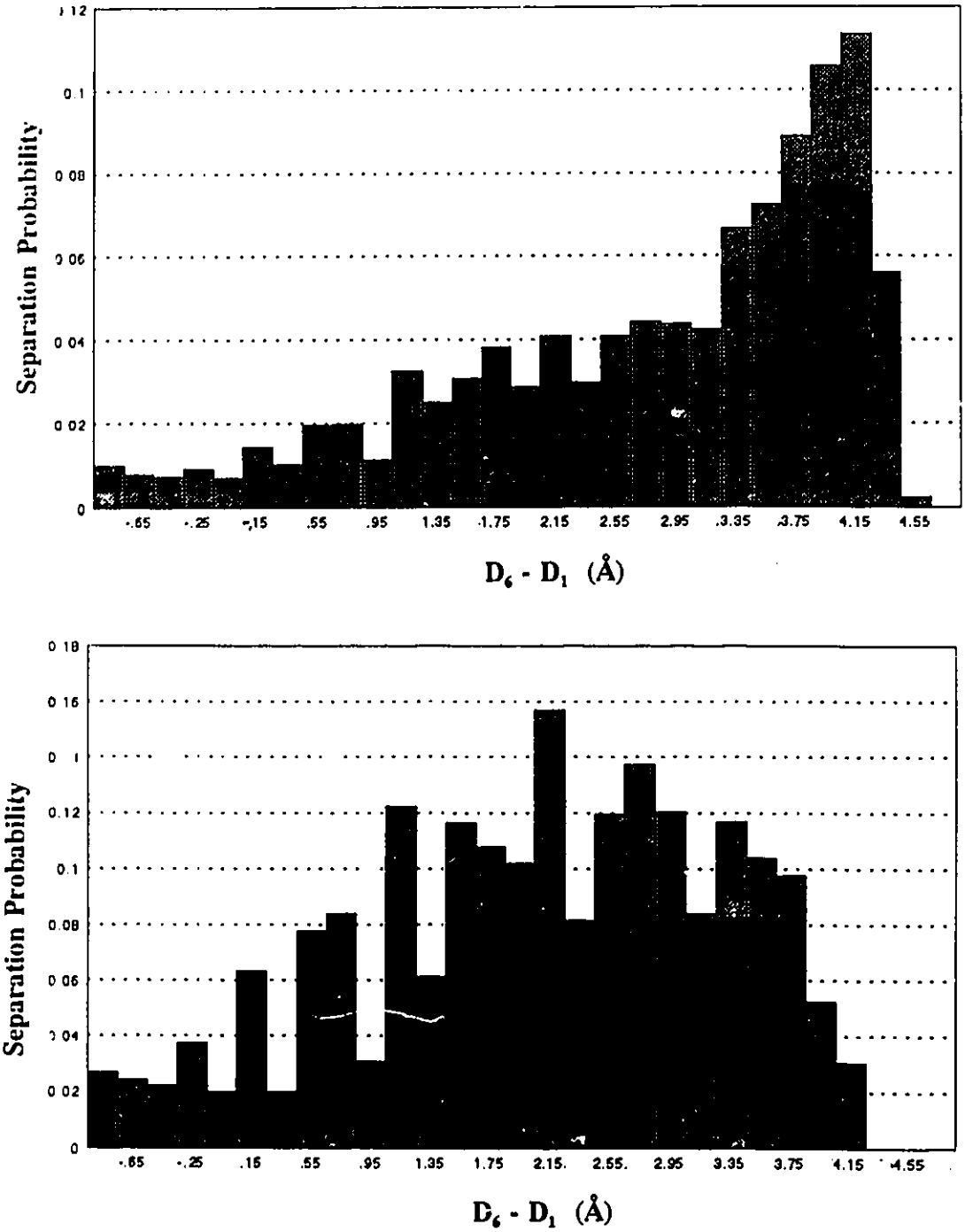

Figure 5.10 Calculated D_6-D_1 separation distributions for a β-DTGL analogue molecule. *Top,* molecule in vacuo. *Bottom,* molecule surrounded by an annulus of six surface analogue molecules at a distance of 11 Å. The separation probabilities are based on a Boltzmann weighting of the corresponding conformational energies. The analogue molecule is Structure A, 4'-deoxy-gentiobiose.

5.5 COMPARISON WITH PREVIOUS WORK

The concept of modelling surface-bound glycolipids has been considered in the HSEA (Hard Sphere ExoAnomeric) analysis of the conformations of blood group A-active glycosphingolipids (Nyholm et al. 1989). A membrane barrier to head group atoms was implemented which disregarded any conformations with any part of the head group below the membrane barrier. This approach was a necessary first step in the description of a membrane surface, but we have now demonstrated the importance of considering the energetics of membrane interactions (intermolecular effects) more specifically.

Another study has included membrane surface energetics in their calculations. Rudolph et al. (1990) used AMBER to identify minimum energy conformations of saccharide/DMPC systems. They modelled saccharide-lipid interactions by calculating intra- and intermolecular energies between lipid molecules and a saccharide molecule. This approach has similar features to ours, but there are three significant differences. First, we have represented the membrane by a hexagon of surface molecules, and whose radius of separation was modified systematically, whereas only one rectangular matrix was used per saccharide in the earlier study. In addition, we propose a complex equilibrium of conformations, whereas, Rudolph et al. focused their attention on a single minimum energy conformation. Finally, we test our results by comparison with experimental observations on a relevant glycolipid system.

In considering the potential non-rigid nature of the glycosidic bond, Prestegard and co-workers (Scarsdale et al., 1986 and 1988) have used an NMR pseudoenergy approach with AMBER to describe an equilibrium between two possible head group conformations of glycolipids in dilute liquid solution. NMR distance constraints were used as a pseudoenergy term which directed the conformational energy minimization calculations. This approach was also used to identify one favoured conformation of membrane surface glycolipid analogues and trehalose in oriented systems (Ram and Prestegard, 1988; Ram et al., 1989; Sanders and Prestegard, 1991). As in our previous

studies a number of simplifying assumptions had to be made in order to approach the more complicated partially ordered systems. However, as a means to testing our assumptions and to prevent any bias in the calculations, we chose to compare the calculated results with those observed in NMR experiments, instead of using the NMR results as part of the minimization procedure.

Molecular dynamics simulations of oligosaccharides in solution have been used to demonstrate that the head groups are not rigid but do exhibit a great deal of flexibility in the picosecond time scale (Edge et al., 1990; Yan and Bush, 1990). This type of calculation would be ideal for completing the dynamic description of the carbohydrate-aglyconic linkage in partially ordered environments. However, the time scale of the motions for the β-DTGL system has been identified, by ^{2}H NMR relaxation studies, to be in the nanosecond range (Winsborrow et al., 1991). Although a molecular dynamics approach is not practical for partially ordered environments, Pastor and co-workers (1988a and 1988b) have demonstrated that a Brownian dynamics simulation can be used to describe quantitatively the motions of membrane bilayer lipid chains in the nanosecond time scale. However, the authors also pointed out that assumptions had been made which obviated conformational energy calculations of head groups. Therefore, at this point in time, neither molecular nor Brownian dynamics simulations are feasible for the ordered glycolipid system most relevant to the biological situation.

5.6 CONCLUSIONS

^{2}H NMR analysis has shown previously that the time scale of the head group motion for liquid crystalline β-DTGL is in the fast limit motional regime ($\omega_o^2\tau_c^2 << 1$) (Winsborrow et al., 1991; § Chapter 4) and that the glycosidic bond of a glycolipid may be flexible. In order to define what is meant by "flexible" a quantitative description of these motions is necessary. At this point the conformational space of the β-DTGL head group is best described as a complex equilibrium of conformations with a distribution

of populated sites for each of the three glycerol C2-C3 conformations (ω = g^+, t, g^-). This implies that there is a hierarchy of motion; rotation about the glycerol C2-C3 bond is coupled with either simultaneous or sequential conformational fluctuations at the glucose head group. The next steps in describing this process are first, to define more quantitatively the process of the conformational equilibrations (libration or discrete jumping, correlation time) and second, to identify any mechanistic correlation between the head group motions and the glycerol backbone rotation.

Admittedly the present approach utilizes an extremely simplified description of the restraints on β-DTGL head group conformations because of the restrictive assumptions that have been made; no solvent was used, the surrounding membrane molecules were held fixed on a lattice, and the interactions have no temporal scale (as incorporated in simulations of molecular and Brownian dynamics). However, the predicted NMR and neutron diffraction parameters are in reasonable agreement with experiment, which indicates that additional insight into the nature and amplitude of the head group motion (not available directly from experiment) is derived from such a simple approach.

The use of an expandable surface annulus has shown that molecular energies are sensitive to spatial packing. Ideally it would be beneficial to explore further the effect of modifying the surface annulus in an attempt to represent more realistically the actual membrane surface (i.e. vary the surface molecule conformations and include other membrane molecules). One feature that was noted but not pursued in this study was the effect of the depth into the membrane that the molecule was positioned. The empirical approach taken here provides considerable insight at the molecular level, and offers the possibility of exploring even more complex systems.

Part III

Biomembranes

Chapter 6

^{2}H NMR and Cyanobacterial Membranes.

Preliminary Physical Studies.

6.1 INTRODUCTION

Biomembranes of blue-green algae are studied by ^{2}H NMR in the following two chapters. This marks a significant departure from the previous two chapters where model membrane systems are considered. The number of components present in model membrane systems is low, typically there are fewer than four components; very precise physical chemical properties can be attributed to specific membrane components. Biomembranes, on the other hand, are complex heterogeneous systems with an incredible number of components. As more is known about model systems and as scientific methods mature, the opportunity for directly studying biomembranes is made possible.

The photosynthetic membranes of green plants and photosynthetic bacteria contribute to the transformation of sunlight energy into chemical energy (Renger, 1983). Cyanobacteria are photoautotrophic prokaryotes. Unlike eukaryotic plant cells, they have only two types of membranes: plasma and thylakoid membranes (Murata and Omata, 1988). The thylakoid membranes contain the structural and functional basis for the light dependent reactions of photosynthesis. Much effort has been made in establishing relationships between their molecular structure and biological function (Coleman et al., 1987; Laskay and Lehoczki, 1986; Mansfield et al., 1987). Thylakoid

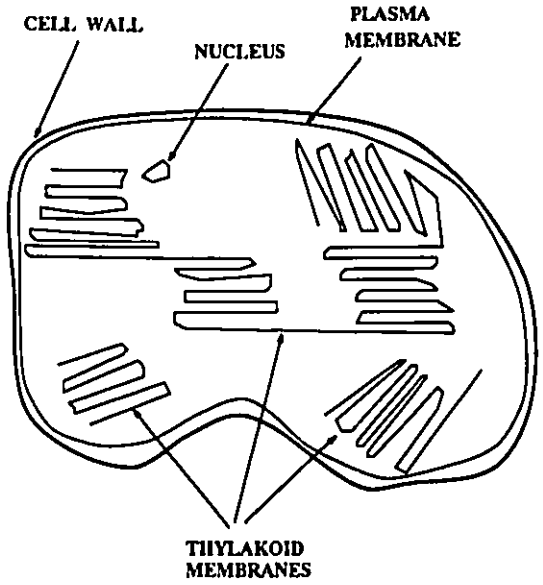

Figure 6.1 Diagram of a cyanobacterium cell.

membranes have two distinct regions. In one region the membranes are appressed, closely stacked, whereas in the other they are non-appressed. Within each region there are different reaction centres, these polypeptide complexes are known as photosystems; they convert light energy to chemical energy via electron transfer. Photosystem I (PSI) is associated with the non-appressed region of thylakoid membranes and is excited by

light of wavelength shorter than 700 nm. PSII requires light of shorter wavelength than 680 nm and is found in the appressed thylakoid membrane region. The response of these organisms to preferential excitation of one photosystem is to compensate by redistributing the absorbed energy more equally between the photosystems. It has been proposed that, in algae, the thylakoid membranes undergo a conformational change to facilitate the interaction between the two photosystems (Biggins, 1983).

For the ^2H NMR investigation of biological membranes, ^2H labelled fatty acids have been incorporated into membrane lipids of unicellular organisms: i.e. *Acholeplasma laidlawii* (Stockton et al, 1977) and *Eschericha coli* (Gally et al., 1980). In this study the thylakoid membranes of *Anacystis nidulans* (Synechococcus sp. 6301) are considered. Membrane labelling was achieved by cultivating for 48 hours in medium supplemented with perdeuterated palmitic acid ($^2H_{31}$ 16:0). The lipids were extracted and lipid analysis as well as ^2H NMR studies were performed. As a means to gain further insight into the factors that influence the phase behaviour of *A.nidulans* thylakoid membranes, temperature-dependent spectra of specifically labelled oleic acid ($18:1^{\Delta 9}$) incorporated into membranes were also obtained.

6.1.1 Membrane Structure

Cyanobacterial thylakoid membranes are composed of approximately 60% (by weight) protein. The four major classes of polar lipids in these membranes are mono- and digalactosyl diacylglycerol (MGDG and DGDG, respectively), sulfoquinovosyl diacylglycerol (SL), and phosphatidylglycerol (PG). The galactolipids compose up to 70% of the thylakoid membrane polar lipids, with about 3:2 MGDG to DGDG. Small amounts of neutral lipids (di- and triglycerides) are also found in these membranes (Gounaris et al., 1986).

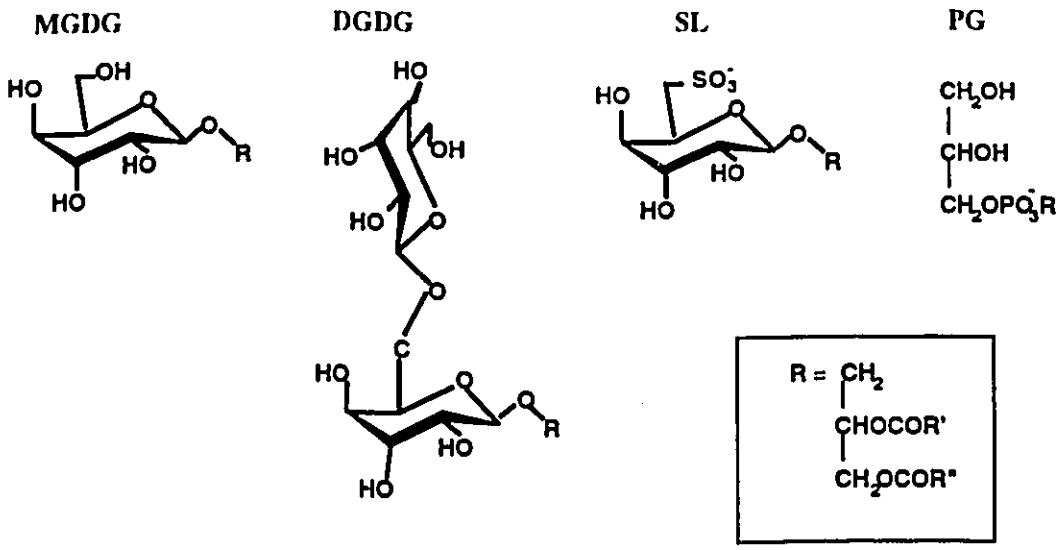

Figure 6.2 Structures of the major classes of polar lipids in cyanobacteria.
R' and R'' represent alkyl chains. At physiological pH both SL and PG are anionic.

Extensive studies have shown that the composition of the thylakoid membranes of *A.nidulans* is influenced by environmental conditions such as growth temperature and exogenous fatty acids added to the growth medium (Quinn and Williams, 1983; Sato and Murata, 1988; Williams et al., 1990; Nicholov et al., 1991). *A.nidulans* are good biosystems to study because of their availability and adaptability.

6.1.2 ^{2}H NMR Review

Deuterium (^{2}H) NMR is an excellent technique for monitoring C-^{2}H bond order and dynamics of biological membranes (§Chapter 2; Smith, 1989 and Davis, 1983). For a C-^{2}H bond executing axially symmetric motions the observed quadrupolar splitting ($\Delta\upsilon_Q(\beta)$) of a randomly dispersed sample is defined by (Seeling, 1977; Petersen and Chan, 1977):

$$\Delta\upsilon_Q(\beta) = (3/8h)e^2qQ \,.\, (3\cos^2\beta - 1) \,.\, S \,.\, (3\cos^2\theta - 1). \qquad 6.1$$

e^2qQ/h is the quadrupolar coupling constant specific to the type of C-^{2}H bond. β is the angle between the molecular long axis and $\mathbf{H}_o$. Usually $\Delta\upsilon_Q(\beta)$ where $\beta = 90°$ is

reported because this splitting corresponds to the most intense feature in a powder spectrum. S is a measure of the orientational order of the segment containing the C-^{2}H bond. θ defines the angle between the C-^{2}H bond and the order director (§2.4.2).

The quadrupolar splitting observed in a ^{2}H NMR spectrum is proportional to the orientational order, S, of the deuterated molecular segment (eq 6.1). Since the orientational order is affected by the temperature-dependent molecular mobility, ^{2}H NMR spectra are acquired as a function of temperature. At low temperatures, when the molecular motions are slow and the membrane lipids are in the highly ordered gel (L_β) state of the lamellar phase there is little orientational averaging. The orientational order parameter, S, is close to the maximum value of 1. With increasing temperature, and thus molecular motions, the orientational averaging increases ($S < 1$). The NMR signals become narrower, characteristic of lipids in the liquid crystalline (L_α) state of the lamellar phase.

6.2 *A.nidulans* ENRICHED WITH PERDEUTERATED PALMITIC ACID

This study of perdeuterated palmitic acid incorporated into membrane lipids is intended to probe the thylakoid membrane structure in a general manner.

6.2.1 Lipid Analysis

Two green (due to chlorophyll a) thylakoid membrane bands were collected after density gradient centrifugation of fractionated *A.nidulans* cells. Only the **top band** (30/39% sucrose interface) was collected for NMR and lipid analysis because the **bottom band** (39/50%) was not sufficiently concentrated. The results of the lipid analysis of the extracted membrane lipids are given in Table 6.1. The table lists the percentage of labelled and unlabelled palmitic (16:0) and palmitoleic (16:1) acids in the four major classes of polar lipids and in the neutral lipids. The fatty acid content also consisted of a minor amount of 14:0, 14:1, 18:0, 18:1 fatty acids (< 15% of total fatty acids); for brevity the data are not shown.

Table 6.1 [a]Fatty acid composition of *Anacystis nidulans* thylakoid membranes (top band). The cells were harvested after 48 hours of growth in perdeuterated palmitic acid supplemented medium.

FATTY ACID (FA)	%FA in the Polar Lipid Fraction:				%FA in Neutral Lipids
	MGDG	DGDG	SL	PG	
d16:0	26.7	5.8	14.4	19.5	49.8
d16:1	1.2	0.0	0.3	1.2	2.8
16:0	27.5	37.0	47.1	38.6	6.5
16:1	31.6	41.7	33.3	30.3	6.7
[b]unsaturated FA %	42.2	53.0	37.6	40.7	24.7
lipid total nmole/mg Chl	1083	353	318	157	434

[a] **d16:0** - perdeuterated palmitic acid
16:0 - naturally occurring palmitic acid
Chl - chlorophyll a
d16:1 - perdeuterated palmitoleic acid
16:1 - naturally occurring palmitoleic acid
[b] Total percentage of unsaturated fatty acids.

After 48 hours of growth in perdeuterated palmitic acid supplemented medium, 26% of the total lipids are deuterated; very little deuterated palmitic acid was desaturated to form deuterated palmitoleic acid. However, the degree of unsaturation in the membranes is high (40%) due to the unlabelled fatty acids (14:1, 16:1, 18:1).

The total lipid content of each lipid class is included at the bottom of Table 6.1 (relative to the amount of chlorophyll a). As a quick reference, the bar graph in Figure 6.3 demonstrates the relative amounts of the lipid classes for both deuterated and total lipid. MGDG is the most abundant lipid and the DGDG, SL, and neutral lipid contents are all similar. The most highly deuterated lipids are MGDG and neutral lipids (NL).

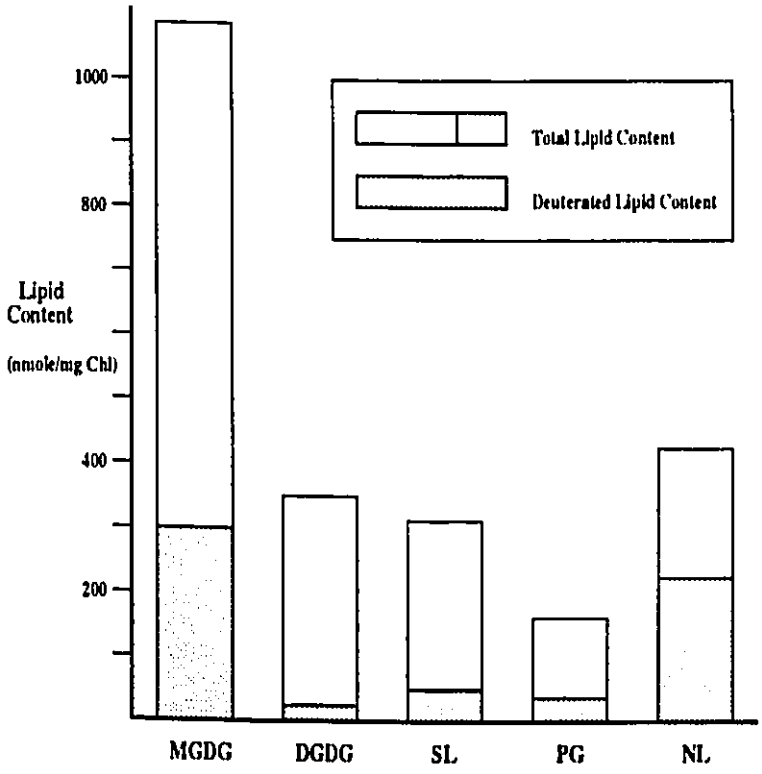

Figure 6.3 Lipid content versus class of lipid in *A.nidulans* thylakoid membranes (top band). Cells were harvested after 48 hours growth in perdeuterated palmitic acid supplemented medium.

6.2.2 ^{2}H NMR Spectroscopy

The ^{2}H NMR spectra of the intact thylakoid membranes isolated from *A.nidulans* were collected as a function of temperature over the range of -10 to 35°C (Figure 6.4), which is the temperature range of biological activity. In the system studied, perdeuterated palmitic acid is incorporated into the membrane lipids; the observed spectra will be a superposition of the spectra corresponding to the different C-^{2}H bonds in the entire molecule of several different lipids. In general, the low temperature ^{2}H NMR spectra of the intact membranes are very broad. For example, at -10°C, the

maximum splitting, $\Delta\nu_Q(0)$, is about 120 kHz (Figure 6.4a). By 30°C the maximum splitting is smaller, approximately 60 kHz (Figure 6.4e). These two spectra are characteristic of lipids in the gel and liquid crystalline states of the lamellar phase, respectively.

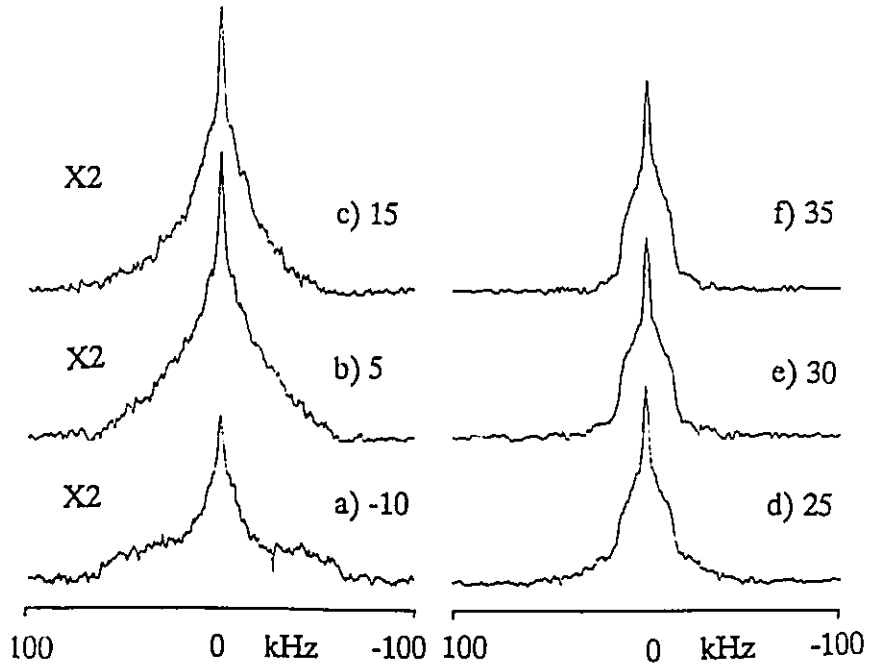

Figure 6.4 ^{2}H NMR spectra of intact *A.nidulans* thylakoid membranes (top band). The cells were harvested after 48 hours of growth in medium supplemented with perdeuterated palmitic acid. Spectra were acquired at a) -10°C, b) 5°C, c) 15°C, d) 25°C, e) 30°C, and f) 35°C.

A continuous narrowing of the ^{2}H NMR spectra with increasing temperature from -10° to 35°C is observed. Between 5° and 30°C both broad (max $\Delta\nu_Q(0) \approx 120$ kHz) and narrow (max $\Delta\nu_Q(0) \approx 60$ kHz) components are present in the spectra of *A.nidulans* thylakoid membranes. The broad spectral component becomes less significant with increasing temperature; indicative of a gradual phase change from the gel to the liquid crystalline state of the lamellar phase. A sharp central component, due to the presence of a non-lamellar lipid phase, is also observed in the spectra. This feature is most prominent at higher temperatures in the extracted lipid spectra (Figure 6.5) and will be discussed later.

Since there is no distinct change in the ^2H NMR spectra of intact *A.nidulans* thylakoid membranes with increasing temperature, it can be inferred that the gel to liquid crystalline phase transition occurs over a broad temperature range from about 5° to 30°C. Although distinct phase transitions have been reported for *A.nidulans* (Murata and Omata, 1988), it is reasonable to anticipate broad phase transitions because the composition of the thylakoid membranes is very heterogeneous, containing up to 60% protein. The same conclusions were made in two studies, electron spin resonance (Nicholov et al., 1991) and differential scanning calorimetry (Furtado et al., 1979), where the lipids of *A.nidulans* thylakoid membranes were observed to undergo broad phase transitions.

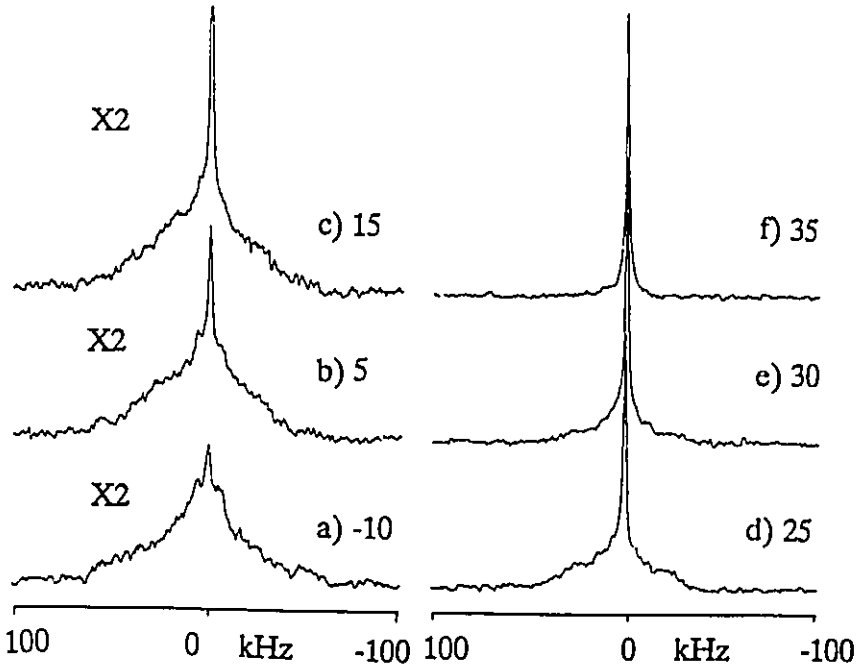

Figure 6.5 ^2H NMR spectra of the extracted lipids from *A.nidulans* thylakoid membrane (top band). The cells were harvested after 48 hours of growth in medium supplemented with perdeuterated palmitic acid. Spectra were acquired at a) -10°C, b) 5°C, c) 15°C, d) 25°C, e) 30°C, and f) 35°C.

To study the intrinsic characteristics of the *A.nidulans* thylakoid membrane **(top band)** lipids, ^2H NMR spectra of the extracted lipids were also obtained from -10° to 75°C. The spectra acquired between -10° and 35°C are presented in Figure 6.5. Significant differences between the spectra of the extracted lipids and those of the intact membranes are observed at temperatures above 15°C, where the central sharp signal in

the extracted lipid spectra is more intense. By 35°C (Figure 6.5f) the central peak is the most significant feature, indicating that at this temperature most of the membrane lipids are in a non-lamellar phase (isotropic, cubic). However, there is still some weak signal intensity on the edges of the central resonance at 75°C (Figure 6.6), suggesting that the non-lamellar phase transition is not complete for *A.nidulans* thylakoid membrane lipids enriched with perdeuterated palmitic acid, even at high temperatures.

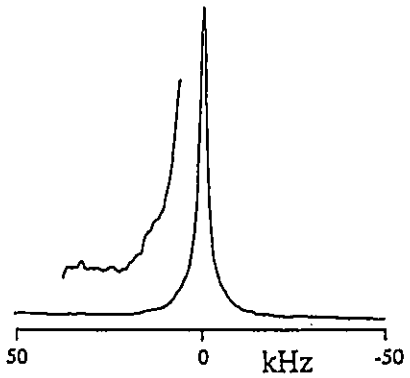

Figure 6.6 ^{2}H NMR spectrum of the extracted lipids from *A.nidulans* thylakoid membrane (top band) at 75°C. The sample was harvested after 48 hours of growth in medium supplemented with perdeuterated palmitic acid.

Solid state ^{2}H NMR spectra are diagnostic of lamellar membrane phases but only indicate the presence and not the kind of non-lamellar phases. It is also difficult to quantify the exact amount of lipid in each of the phases, especially if perdeuterated lipids are considered. When lipids are in the non-lamellar phase, all the signal intensity is focused on the central resonance frequency. However, the spectrum of lipids in the lamellar phase can be spread over 60 to 120 kHz. Therefore the ^{2}H NMR signal of a perdeuterated molecule in a non-lamellar phase will be much more intense than the broad signal of a perdeuterated molecule in the lamellar phase.

Freeze-fracture electron microscopy studies of glycolipids isolated from *A.nidulans* (Mannock et al., 1985) identified heterogeneous pockets in the membranes, which were attributed to inverted micelles embedded in the bilayer matrix. Although inverted micelles would give an isotropic ^{2}H NMR signal, the surrounding bilayer matrix

would not. This type of non-lamellar phase may be present at lower temperatures where complex multi-component spectra are observed (i.e. Figures 6.4b, 6.5b, and 6.7a). However, at higher temperatures (> 65°C) an isotropic signal is the strongest feature observed in the extracted lipid spectra (Figure 6.6); the lipids are most likely in either the cubic or hexagonal phase.

In order to identify specific non-lamellar phases by NMR, either ^{31}P NMR (Smith and Jarrell, 1983), 2D exchange studies (Fenske and Jarrell, 1991), or NMR diffusion studies (Lindblom et al., 1986; Rilfors and Lindblom, 1989) are required. ^{31}P spectra were acquired for these samples (data not shown), they were similar to those obtained for *Halobacterium cutirubrum* (Ekiel et al., 1981). Less than 10% of the thylakoid membrane lipids are phospholipids, therefore the spectra had a poor S/N ratio and little informative data was obtained. Diffusion studies were also attempted on the extracted lipids of *A.nidulans* thylakoid membranes, but the results were not conclusive (B. G. Winsborrow, P.-O Eriksson and G. Lindblom, unpublished data).

6.3 *A.nidulans* AND SPECIFICALLY DEUTERATED OLEIC ACID

6.3.1 Introduction

The heterogeneity of the lipid head groups and fatty acyl chains makes the interpretation of ^{2}H NMR spectra of the thylakoid membranes enriched with perdeuterated palmitic fatty acid difficult. In order to investigate further the physical properties of these membranes, specifically deuterated oleic acid was incorporated into the membrane lipids of *A.nidulans*. Four different cultures were grown, each with oleic acid deuterated at specific positions along the acyl chain: 3-$^{2}H_2$, 8-$^{2}H_2$, 12-$^{2}H_2$, and 18-$^{2}H_3$. This enables the investigation of the membrane structure at different regions in the membrane, from the surface (3-$^{2}H_2$ 18:1) to the membrane bilayer interior (18-$^{2}H_3$ 18:1).

Although the fatty acid content of theses samples was not analyzed, some data are available from another source, for discussion purposes. *A.nidulans* was grown in

medium supplemented with protonated oleic acid (Nicholov et al. 1991), under growth conditions identical to those used in this study. After 48 hours of growth the oleic acid contribution to the total fatty acid content was 77% for MGDG, 69.5% for DGDG, 66.6% for SL, and 68.9% for PG. The oleic acid is both well and uniformly incorporated into the polar thylakoid membrane lipids.

6.3.2 ^{2}H NMR Spectroscopy

The ^{2}H NMR spectra were acquired for each of the samples, from -10° to 35°C for the **top band** of the intact thylakoid membranes and from -10° to 65°C for the extracted lipids. Since the main difference in the spectra of the four sets of samples is the magnitude of the quadrupolar splitting, only some of the ^{2}H NMR spectra of the membranes enriched with 8-$^2H_2$ oleic acid are presented (Figure 6.7). The general line shapes of the spectra for all of the samples are very different from those enriched with perdeuterated palmitic acid. The maximum breadth of the spectra is less than 50 kHz and distinct quadrupolar splittings can be observed in these spectra. There is no evidence of gel state lipids in the spectra, even at -10°C. It is apparent that the gel to liquid crystalline phase transition temperature is lowered considerably by the presence of unsaturated acyl chains. This finding is consistent with the results of a ^{2}H NMR study of *A.laidlawii* cells grown in medium supplemented with deuterated oleic acid. Spectra characteristic of lipids in the gel state were only observed at temperatures below -20°C (Rance et al., 1980).

As was the case for the membranes enriched in palmitic acid, the spectra of the extracted lipids (Figures 6.7c-d) have features similar to those of the intact membranes (Figure 6.7a and b). In addition, the isotropic signal, characteristic of non-lamellar phase lipids, is most prominent in the extracted lipid spectra at higher temperatures. When the baselines of the high temperature spectra are expanded there is no residual signal intensity other than that at the isotropic peak (Figure 6.7e), unlike the spectra of the palmitic acid-enriched samples (Figure 6.6). This indicates that the lamellar to non-lamellar phase transition is complete in the extracted lipid samples of oleic acid enriched

A.nidulans thylakoid membranes at 65°C, and not for palmitic acid-enriched *A.nidulans*. Since the unsaturated lipid content is higher in the samples enriched in oleic acid, this result is not surprising.

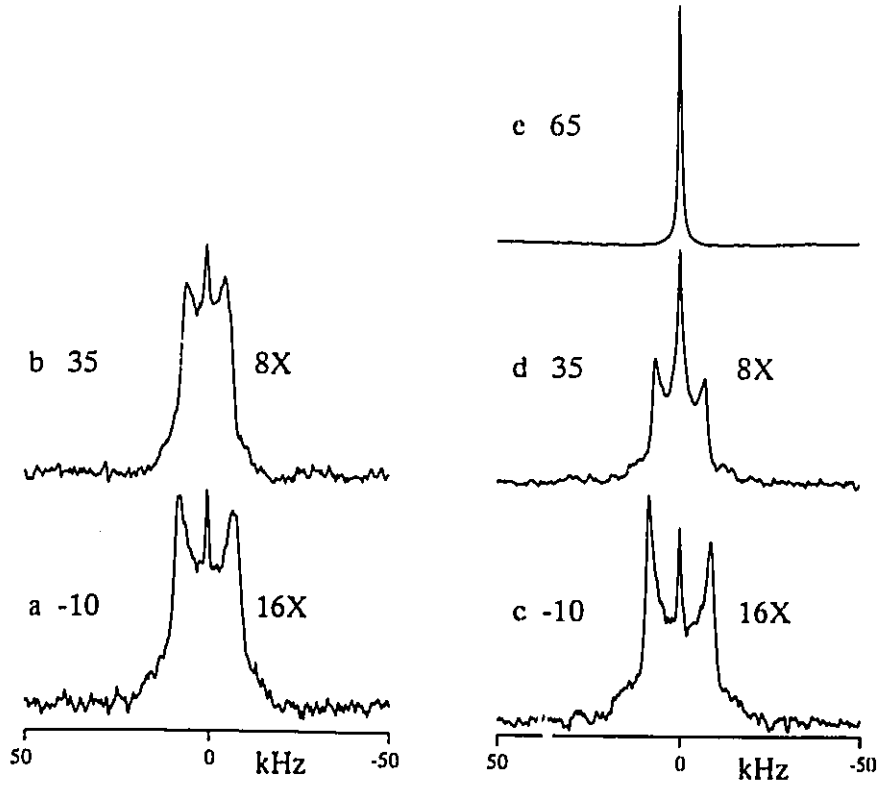

Figure 6.7 ^{2}H NMR spectra of intact thylakoid membranes (top band) and the extracted lipids from {8-$^2H_2$} oleic acid enriched *A.nidulans* cells. Cells were harvested after 48 hours of growth in medium supplemented with {8-$^2H_2$} oleic acid. The spectra of intact thylakoid membranes were acquired at (a) -10°C and (b) 35°C. The spectra of extracted lipids were acquired at (c) -10°C, (d) 35°C, and (e) 65°C.

The ^{2}H NMR data for all the samples are summarized in Figure 6.8, as a plot of the quadrupolar splitting versus temperature. The quadrupolar splitting profiles of the intact membranes of oleic acid fed *A.nidulans* are exactly like those obtained for the oleate moieties in both *A.laidlawii* (Rance et al., 1980) and *E.coli* (Gally et al, 1980). The quadrupolar splittings decrease when the hydrocarbon chain position is deeper into the membrane, reflecting a decrease in orientational order. Motional averaging increases into the membrane interior because there are fewer spatial restrictions in the centre of

the bilayer. Acyl chain motions increase as the sample is heated, which is why the quadrupolar splittings also decrease with heating. Since the spectral intensities did not pass through a minimum with heating, these motions are likely in the fast-limit motional regime ($\omega_Q^2\tau_c^2 << 1$).

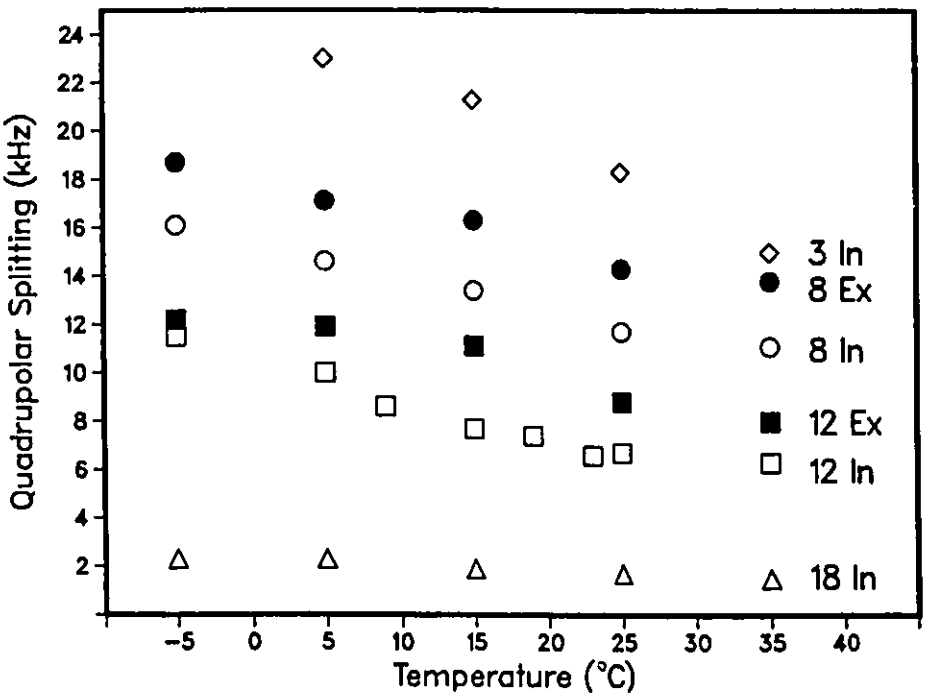

Figure 6.8 ^{2}H NMR quadrupolar splitting versus temperature for *A.nidulans* intact thylakoid membranes (top band) and extracted lipids. Cells were harvested 48 hours after feeding with specifically deuterated oleic acid. ◊, 3-$^2H_2$ 18:1 intact membrane (3In); ○ 8-$^2H_2$ 18:1 intact membrane (8In);● 8-$^2H_2$ 18:1 extracted lipids (8Ex); □ 12-$^2H_2$ 18:1 intact membrane (12In); ■ 12-$^2H_2$ 18:1 extracted lipids (12Ex); ▵ 18-$^2H_3$ 18:1 intact membrane (18In).

The quadrupolar splittings of the extracted lipids (8-$^2H_2$ and 12-$^2H_2$ oleic acid) are greater than those of the corresponding intact membranes (Figure 6.8). This suggests that membrane order is higher in the absence of protein. The phenomenon of decreased order with protein content has been observed in protein reconstitution studies (Gally et al., 1980; Seelig and Seelig, 1978). It is believed that lipids fill voids created by irregularly shaped proteins, thereby increasing the membrane disorder (Bloom and

Smith, 1985). In support of these conclusions, a recent FTIR study of phosphatidylcholine liposomes (Castresana et al., 1991) has also found that the presence of protein increases the motional freedom of the lipid acyl chains.

6.4 CONCLUSIONS AND COMPARISON WITH OTHER WORK

The ^2H NMR spectra and results are very similar to those of *A.laidlawii* membranes grown in media containing myristic acid (Smith et al., 1979; Jarrell et al., 1982) and oleic acid (Rance et al., 1980). The thylakoid membranes of *A.nidulans* cells grown in medium supplemented with unsaturated fatty acid had much lower phase transition temperatures than with the saturated fatty acid enriched membranes. Moreover, the heterogeneous systems undergo broad phase transitions. This is in agreement with a recent ESR study of *A.nidulans* cells (Nicholov et.al., 1991).

An isotropic signal due to lipid in a non-lamellar phase, was observed in all the ^2H NMR spectra. This suggests that lamellar and non-lamellar phases coexist in the thylakoid membranes. In support of this observation, heterogeneous pockets of lipidic particles have been observed in freeze-fracture studies of isolated chloroplast membrane lipids (Sprague and Staehelin, 1984). However, at temperatures above 65°C the only significant signal is the isotropic signal, which suggests that at higher temperatures the lipid phase is likely more homogeneous (i.e. in the hexagonal or cubic phase).

The formation of a non-lamellar phase may be due to a number of factors, such as the nature of the lipid head groups or acyl chain unsaturation. Pure MGDG is well known for its tendency to form non-lamellar phases and pure DGDG, PG, and SL tend to form lamellar phases (Adebodun et al., 1992, Eriksson et al., 1991; Seddon, 1990; Sen et al., 1982). In one freeze-fracture study MGDG required high levels of acyl chain unsaturation in order to form non-lamellar phases (Sen et al., 1981). It has been demonstrated in this study that extracted thylakoid membrane lipids enriched with oleic

acid completely formed a non-lamellar phase at higher temperatures. Many studies of model systems (as reviewed in Davis, 1991) found that unsaturated fatty acids increase membrane fluidity, which results in lower phase transition temperatures. This was also observed here with the *A.nidulans* cells that were grown with oleic acid.

In this study of cyanobacterial membranes, complex heterogeneous systems were investigated, as opposed to the two- and three- component model membrane systems studied in Chapters 4 and 5. In comparison to the model systems, very general conclusions concerning the physical properties of these biomembranes can be made. Although the significance of lipid class on the phase behaviour of the membranes was not considered in this chapter, it will be discussed in the next chapter (Chapter 7).

Chapter 7

More on Cyanobacteria.

A Tale of Two Strains.

7.1 INTRODUCTION

The effect of acyl chain unsaturation on the phase transition temperature of *Anacystis nidulans* thylakoid membrane lipids was discussed in the previous chapter. This chapter considers the thylakoid membrane structure of *Anacystis nidulans R2* (Synechococcus sp. PCC 7942-R2), another strain of *A.nidulans*. Two aspects of membrane structure are studied. Firstly, as a result of these experiments, the effect of head group class on membrane lipid phase behaviour can be more thoroughly appreciated. Secondly, changes in ^{2}H NMR spectra and membrane structure with increasing cell growth period are investigated.

Bishop et al. (1986) have observed that the degree of acyl chain unsaturation is higher for *A.nidulans* than for *A.nidulans R2*. Murata and Omata (1988) have identified two thylakoid membrane bands after density gradient centrifugation of fractionated *A.nidulans* cells: **top band** (30/39% sucrose layer interface) and **bottom band** (39/50% interface). For *Anacystis nidulans R2* cells the banding pattern is the

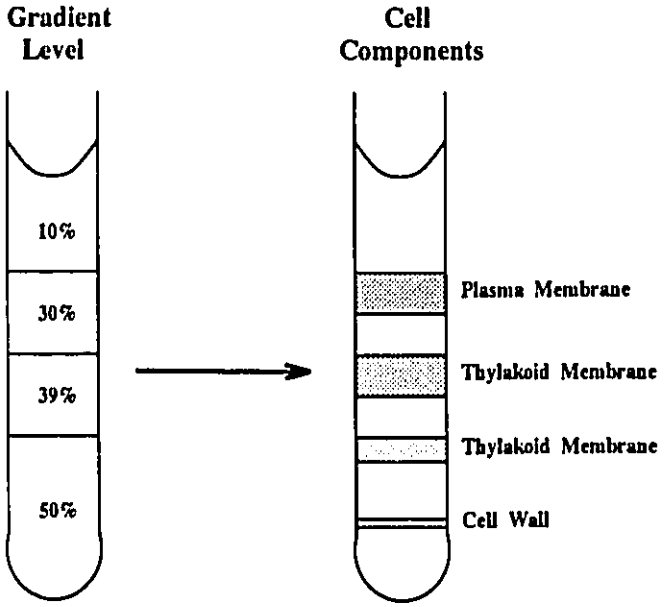

Figure 7.1 Schematic diagram of *A.nidulans* cell components after density gradient centrifugation of fractionated cells. The banding pattern for ruptured *A.nidulans R2* cells is the same, but the amounts of thylakoid membrane in each band is markedly different.

same; the relative amount of thylakoid membranes in the two bands is markedly different (B. G. Winsborrow and D. H. Bruce, unpublished results). The main biological difference between the two strains known up to now is that *A.nidulans R2* readily incorporates exogenous DNA into their cells, and are used for modification/adaptation studies (Wada et al., 1990). Otherwise differences in the lipid composition/function of the thylakoid membranes of the two strains are largely unexplored.

In order to detect differences in the membranes by ^2H NMR, the intact thylakoid membrane fractions (**top** and **bottom** bands) of ruptured *A.nidulans R2* cells were investigated after both 48 and 96 hours of culture in medium containing perdeuterated palmitic acid ($^2H_{31}$ 16:0). Afterwards, their lipids were extracted and lipid analysis as well as ^2H NMR studies were performed. Although these systems are very complex, when the results are pooled with those of *A.nidulans* (§Chapter 6), conclusions can be made relating lipid head group class and lipid phase behaviour.

7.2 *A.nidulans* R2: 48 HOUR GROWTH PERIOD

A.nidulans R2 cells were harvested after 48 hours of growth in medium supplemented with perdeuterated palmitic acid. Two thylakoid membrane bands were collected after density gradient centrifugation of fractionated *A.nidulans R2* cells. The **bottom band** (39/50% sucrose interface) had more material than the **top band** (30/39%). Two thylakoid membrane bands were also observed for fractionated *A.nidulans* cells (§Chapter 6) but only the **top band** (30/39%) was collected because the **bottom band** (39/50%) did not contain sufficient material for further analysis.

7.2.1 Lipid Analysis

The results of the extracted lipid analysis of *A.nidulans R2* thylakoid membranes are given in Tables 7.1 (**top band**) and 7.2 (**bottom band**). Each table lists the percentage of labelled and unlabelled palmitic (16:0) and palmitoleic (16:1) acids in the four major classes of polar lipids and in the neutral lipids (glycerides). The total amount of lipid per sample, normalized relative to the amount of chlorophyll a, is given at the bottom of each table. As a visual aid, the .nolar proportions of the lipids are summarized in the bar graphs of Figures 7.2 (**top band**) and 7.3 (**bottom band**). Note that the percentages do not add up to 100% since, for clarity, the less abundant fatty acids (14:0, 14:1, 18:0, 18:1) are not included. The total unsaturation is given, which does include the 14:1 and 18:1 contributions.

Table 7.1 [a]Fatty acid composition of *Anacystis nidulans R2* thylakoid membranes (top band). The cells were harvested after 48 hours of growth in perdeuterated palmitic acid supplemented medium.

FATTY ACID (FA)	% FA in the Polar Lipid Fraction: MGDG	DGDG	SL	PG	%FA in Neutral Lipids
d16:0	40.6	11.2	20.7	37.9	51.1
d16:1	0.9	0.3	0.0	0.9	1.9
16:0	26.4	43.4	51.1	34.0	11.5
16:1	22.8	32.7	18.5	16.8	5.6
[b]unsaturated FA%	28.9	41.3	23.3	23.9	20.5
total lipid nmole/mg Chl	2156	146	69	388	817

Table 7.2 [a]Fatty acid composition of *Anacystis nidulans R2* thylakoid membranes (bottom band). Cells were harvested after 48 hours of growth in perdeuterated palmitic acid supplemented medium.

FATTY ACID (FA)	% FA in the Polar Lipid Fraction: MGDG	DGDG	SL	PG	%FA in Neutral Lipids
d16:0	45.6	13.8	23.4	44.7	91.5
d16:1	0.7	0.0	0.0	0.0	0.3
16:0	26.7	46.5	53.2	34.8	3.5
16:1	18.8	29.6	22.2	12.6	1.9
[b]unsaturated FA %	18.8	36.3	23.3	16.6	3.3
total lipid nmole/mg Chl	3720	399	420	506	8303

[a] **d16:0** - perdeuterated palmitic acid
16:0 - naturally occurring palmitic acid
Chl - c hlorophyll a
d16:1 - perdeuterated palmitoleic acid
16:1 - naturally occurring palmitoleic acid
[b] Total percentage of unsaturated fatty acid.

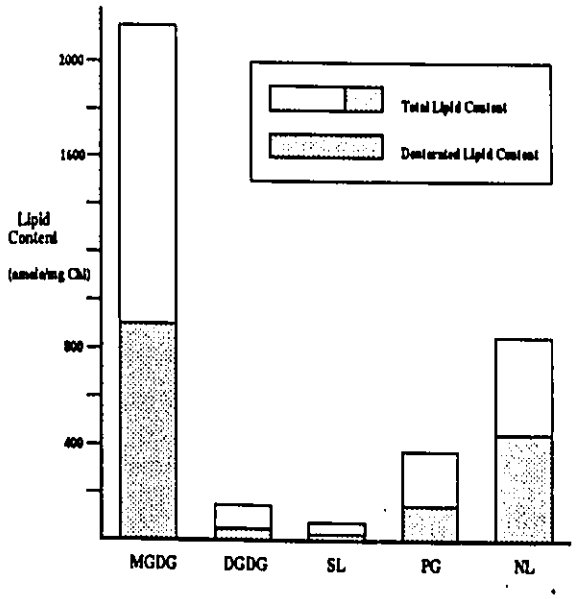

Figure 7.2 Lipid content versus class of lipid in *A.nidulans R2* thylakoid membranes (top band). Cells were harvested after 48 hours of growth in perdeuterated palmitic acid supplemented medium.

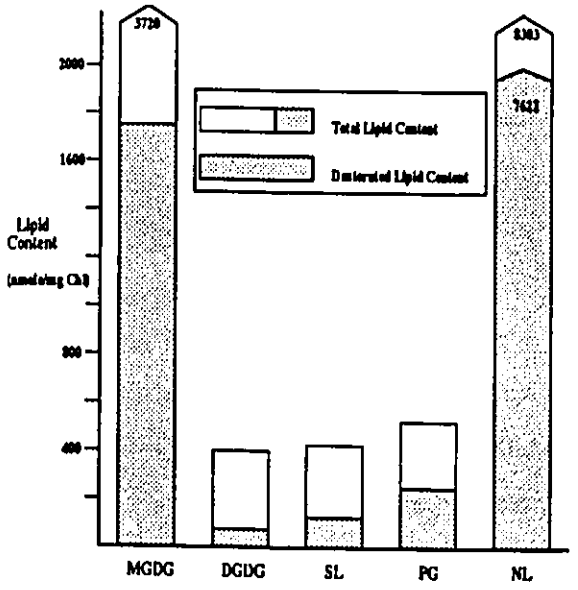

Figure 7.3 Lipid content versus class of lipid in *A.nidulans R2* thylakoid membranes (bottom band). Cells were harvested after 48 hours of growth in perdeuterated palmitic acid supplemented medium.

The MGDG:DGDG (mono-:digalactosyl diacylglycerol) ratio is high for both thylakoid membrane fractions. The PG (phosphatidylglycerol) level in both samples (**top** and **bottom bands**) is also similar. However, the relative proportion of SL (sulfoquinovosyl diacylglycerol) is markedly different; very little SL is found in the *A.nidulans R2* **top band** sample. There is considerably more neutral lipid (glycerides) present in the *A.nidulans R2* **bottom band** sample than in the **top band.** Relative to total lipid content (polar plus neutral lipids) the neutral lipid fraction makes up 62% of the *A.nidulans R2* **bottom band** sample, whereas that for the **top band** sample is 25%. Lastly, 27% of the lipids in the **top band** are unsaturated, as compared to only 10% unsaturation in the **bottom band.**

7.2.2 ^{2}H NMR Spectroscopy

The ^{2}H NMR spectra of the thylakoid membranes isolated from *A.nidulans R2* (**top** and **bottom bands**) were collected as a function of temperature over the range from -10° to 35°C for the intact membranes and from -10° to 65°C for the extracted lipids. The spectra obtained are very similar to those obtained previously from the thylakoid membranes (**top band**) of *A.nidulans* (§Chapter 6) and the membranes of *A.laidlawii* grown in media containing myristic acid (Smith et al., 1979; Jarrell et al., 1982). Therefore, for brevity, only the spectra acquired at 0° and 35°C are presented for *A.nidulans R2* **top band** (Figure 7.4) and *A.nidulans R2* **bottom band** (Figure 7.5).

In general, all ^{2}H NMR spectra have a very broad component (≈ 120 kHz), most prominent at 0°C and a narrower component (≈ 60 kHz), most prominent at 35°C, indicative of gel and liquid crystalline states in the lamellar phase, respectively. A sharp central component, due to the presence of a non-lamellar phase lipid, is observed in all spectra, especially at higher temperatures.

The only significant difference between the spectra of the extracted lipids and intact membranes is observed at temperatures above 25°C for the **bottom band**; the central sharp signal in the extracted lipid spectra (spectrum d) is more intense.

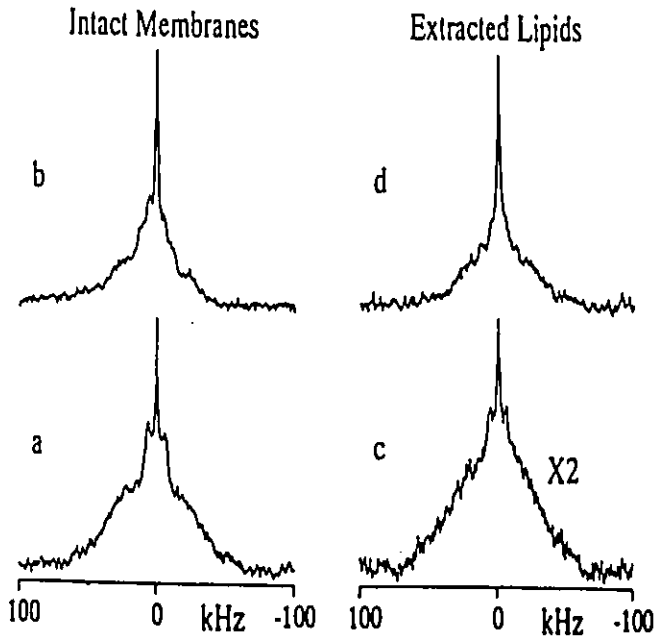

Figure 7.4 ^{2}H NMR spectra of *A.nidulans R2* thylakoid membranes (top band). The sample was harvested after 48 hours of growth in medium supplemented with perdeuterated palmitic acid. Intact membrane spectra presented here were acquired at a) 0°C and b) 35°C; extracted lipid spectra are presented at c) 0°C and d) 35°C.

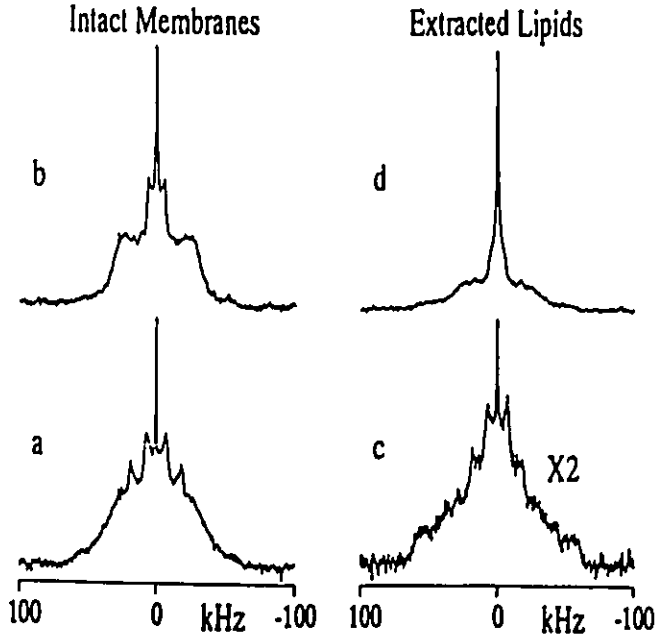

Figure 7.5 ^{2}H NMR spectra of *A.nidulans R2* thylakoid membranes (bottom band). The sample was harvested after 48 hours of growth in medium supplemented with perdeuterated palmitic acid. Intact membrane spectra presented here were acquired at a) 0°C and b) 35°C; extracted lipid spectra are presented at c) 0°C and d) 35°C.

It is noteworthy that additional spectral features are observed in the lower temperature spectra of the *A.nidulans R2* **bottom band** sample and not the **top band**. At 0°C (Figure 7.5a and c) the resolvable quadrupolar splittings are 38 and 12 kHz. Since these features appear in the spectra of both the intact membranes and extracted lipids, this is not likely a physical effect of the presence of membrane protein. Moreover, similar ^2H NMR spectra have been observed in another study where diacylglycerol was added to model DMPC model membrane systems (DeBoeck and Zidovetsky, 1989). Lipid analysis in this present study reveals that in fact, there is considerably more deuterated neutral lipid (including diacylglycerol) in the *A.nidulans R2* **bottom band** sample than in the **top band** (Figures 7.2 and 7.3). One possible explanation for these distinct spectral features is that at least some of the neutral lipids form heterogeneous pockets in the membrane. In the freeze-fracture analysis of thylakoid membranes, lipidic particles and heterogeneous membrane regions have indeed been observed (Sen et.al., 1982; Quinn and Williams, 1983).

Another difference between the spectra of the two samples is the breadth of the higher temperature spectra. For example, at 35°C the ^2H NMR spectrum of the intact membranes for the **top band** sample (Figure 7.4b) is narrower than that of the **bottom band** sample (Figure 7.5b). This suggests that the phase transition of the **top band** lipids is occurring at a lower temperature than the **bottom band** lipids. As established in Chapter 6, increased unsaturation decreases phase transition temperatures. The **top band** of lipids *A.nidulans R2* thylakoid membranes are, in fact, more unsaturated than the **bottom band** membranes (27% vs. 10%, respectively).

7.3 *A.nidulans* R2: 96 HOUR GROWTH PERIOD

Prokaryotes follow a common pathway in the formation of thylakoid membrane lipids; fatty acids are first incorporated into diacylglycerol, which are then coupled with various headgroups, producing membrane lipids (Browse and Sommerville, 1991). After

48 hours of growth spectral features diagnostic of diacylglycerol were observed for the **bottom band** sample. The next step in the biosynthesis of membrane lipids is the addition of a head group. MGDG is synthesized first and then it may be glycosylated to produce DGDG (Gounaris et al., 1986). In an attempt to trace lipid metabolism in thylakoid membrane lipids, *A.nidulans R2* was harvested 96 hours after growth in medium supplemented with perdeuterated palmitic acid. As in the 48 hour experiment, *A.nidulans R2* cells had two thylakoid membrane bands, but the **bottom fraction** (39/50% interface) was less concentrated after 96 hours of growth (similar to *A.nidulans* after 48 hours of growth, §Chapter 6).

7.3.1 Lipid Analysis

The results of the extracted lipid analysis are given in Tables 7.3 (**top band**) and 7.4 (**bottom band**). As a visual aid, molar proportions of the lipids from these tables are summarized in the bar graphs of Figures 7.6 (**top band**) and 7.7 (**bottom band**).

After 96 hours of growth in perdeuterated palmitic acid supplemented medium the unsaturated fatty acid levels are higher in both the **top** and **bottom bands**. 32% of the lipids in the **top band** thylakoid membranes are unsaturated (cf. 27% at 48 hours), whereas there is 21% unsaturation (cf. 10% at 48 hours) in the **bottom band.**

The neutral lipid levels are lower than after only 48 hours of growth. The level is particularly low for the **bottom band** membranes, which is one quarter of that at 48 hours. While the MGDG content in the **top band** is fairly similar after 48 and 96 hours, the MGDG content at 96 hours in the **bottom band** is one third of that observed at 48 hours. With an increased growth period, DGDG levels are higher and SL levels are lower for both bands. Finally, the production of PG in the **bottom band** is 10 times lower after 96 hours than after 48 hours. In contrast, the PG content of the **top band** is twice as high after 96 nours than after 48 hours.

Table 7.3 [a]Fatty acid composition of *Anacystis nidulans R2* thylakoid membranes (top band). The cells were harvested after 96 hours of growth in perdeuterated palmitic acid supplemented medium.

FATTY ACID (FA)	% FA in the Polar Lipid Fraction: MGDG	DGDG	SL	PG	%FA in Neutral Lipids
d16:0	39.3	12.9	17.6	32.1	10.0
d16:1	1.1	0.0	0.0	0.0	2.6
16:0	29.9	41.2	55.0	38.8	15.2
16:1	16.7	32.6	60.9	50.2	3.4
[b]unsaturated FA %	23.9	43.3	12.0	22.4	56.4
total lipid nmole/mg Chl	1874	215	17	603	731

Table 7.4 [a]Fatty acid composition of *Anacystis nidulans R2* thylakoid membranes (bottom band). The cells were harvested after 96 hours of growth in perdeuterated palmitic acid supplemented medium.

FATTY ACID (FA)	% FA in the Polar Lipid Fraction: MGDG	DGDG	SL	PG	%FA in Neutral Lipids
d16:0	35.7	17.3	28.4	19.2	20.2
d16:1	1.3	1.1	2.0	0.6	6.1
16:0	29.3	37.7	35.2	51.1	35.9
16:1	21.9	29.3	13.7	19.2	9.3
[b]unsaturated FA %	29.2	40.0	27.8	24.4	34.1
total lipid nmole/mg Chl	1474	417	281	114	350

[a] **d16:0** - perdeuterated palmitic acid
16:0 - naturally occurring palmitic acid
Chl - chlorophyll a
d16:1 - perdeuterated palmitoleic acid
16:1 - naturally occurring palmitoleic acid
[b]Total percentage of unsaturated fatty acid.

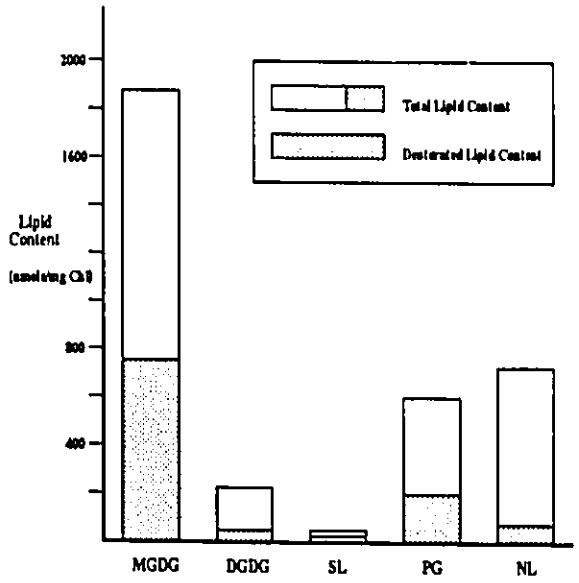

Figure 7.6 Lipid content versus class of lipid in *A.nidulans R2* thylakoid membranes (top band). Cells were harvested after 96 hours of growth in perdeuterated palmitic acid supplemented medium.

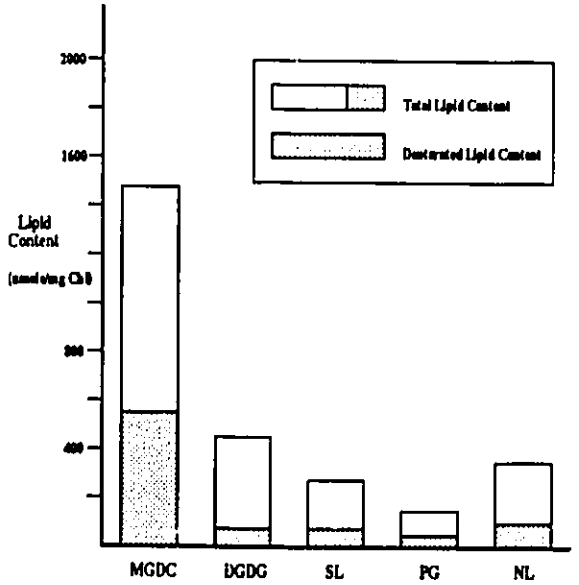

Figure 7.7 Lipid content versus class of lipid in *A.nidulans R2* thylakoid membranes (bottom band). Cells were harvested after 96 hours of growth in perdeuterated palmitic acid supplemented medium.

A knowledge of the relative amounts of lipids in the membranes after the two growth periods may also be important for the interpretation of the NMR data. The following are lists of the relative lipid contents of the *A.nidulans* R2 thylakoid membranes after 48 and 96 hours of growth. The molar ratios can be estimated from the bar graphs on the preceding pages. Although the actual lipid levels of the **top band** thylakoid membranes changed, the relative polar lipid ratios did not.

48 Hours		96 Hours	
SL < DGDG < PG < NL < MGDG	→	SL < DGDG < PG < NL < MGDG	7.1

However, for the **bottom band** thylakoid membranes the relative DGDG and PG contents are reversed. Also note that the neutral lipid (NL) level is at a lower relative molar amount after 96 hours.

48 Hours		96 Hours	
DGDG < SL < PG < MGDG < NL	→	PG < SL < NL < DGDG < MGDG	7.2

These differences in relative lipid content indicate significant changes in the rate of lipid synthesis in the two thylakoid membrane bands over time. It will be interesting to see what effect, if any, that these changes have on the ^2H NMR spectra.

7.3.2 ^2H NMR Spectroscopy

Temperature-dependent ^2H NMR spectra of *A.nidulans R2* **top band** thylakoid membranes were obtained after 96 hours of growth. Spectra of the intact membranes acquired at 0° and 35°C are presented in Figures 7.8a and b, respectively. There is no significant difference between these spectra and those acquired after 48 hours (Figures 7.4a and b). The spectra of the **top band** extracted lipids (Figure 7.8c and d) are also similar to the extracted lipid spectra acquired after 48 hours (Figures 7.4c and d).

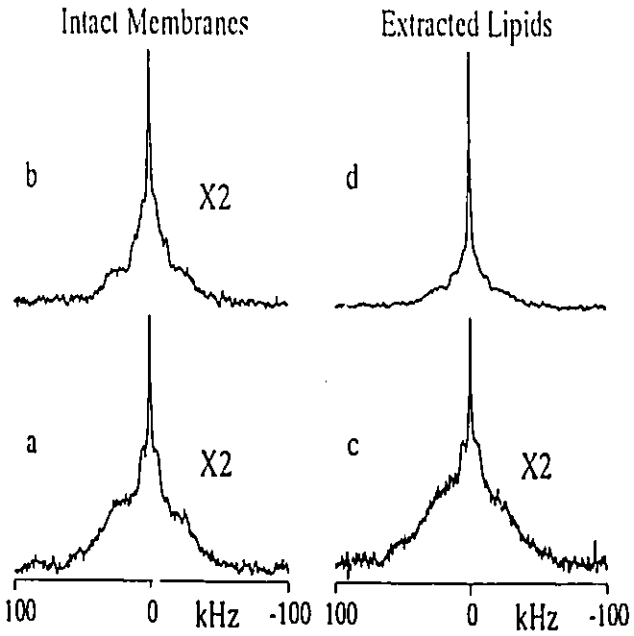

Figure 7.8 ^{2}H NMR spectra of *A.nidulans R2* thylakoid membranes (top band). The sample was harvested after 96 hours of growth in medium supplemented with perdeuterated palmitic acid. Intact membrane spectra presented here were acquired at a) 0°C and b) 35°C; extracted lipid spectra are presented at c) 0°C and d) 35°C.

Pure MGDG is well known for its tendency to form non-lamellar phases and pure DGDG forms lamellar phases (Eriksson et al., 1991; Sprague and Staehelin, 1984; Sen et al., 1982). PG and SL also tend to form lamellar phases (Shipley et al., 1973; Gruner and Jain, 1985; Seddon, 1990; Adebodun et al., 1992). The similarity in the spectra of the **top band** thylakoid membranes after both growth periods is an interesting result. It may indicate that the factors that induce the membrane lipids to form non-lamellar phases are either unchanged or any changes may have opposing spectral effects.

For example, it may have been expected that there would be less lipid in a non-lamellar phase after 96 hours because the MGDG level is lower than that of the 48 hour sample. Additionally, the DGDG and PG levels are elevated, which should stabilize the lamellar structure. In contrast, after 96 hours, there appears to be no diminution of the isotropic signal, due to a non-lamellar phase. However, one freeze-fracture study (Sen et al., 1981) found that MGDG required elevated levels of unsaturation to form non-lamellar phases. The 96 hour sample is slightly more saturated than the 48 hour sample

(32% vs. 27%), which may offset the tendency to form a lamellar phase. Notwithstanding this observation, it would be premature to base any conclusions on just one factor. Another possible explanation is that the relative lipid ratios of the **top band** are the same after both growth periods (eq 7.1), which may be the decisive factor for the lipid phase behaviour.

The *A.nidulans R2* **bottom band** intact membrane spectra after 96 hours of growth (Figures 7.9a and b) are very different from those after 48 hours of growth (Figures 7.5a and b). The narrow symmetrically placed peaks observed in the low temperature 48 hour growth spectra (i.e. Figure 7.5a) are not present in any of the spectra after 96 hours. This result is not surprising because the neutral lipid content is much lower after 96 hours than 48 hours and the extra peaks were attributed to the presence of elevated diacylglycerol levels (§7.2.2).

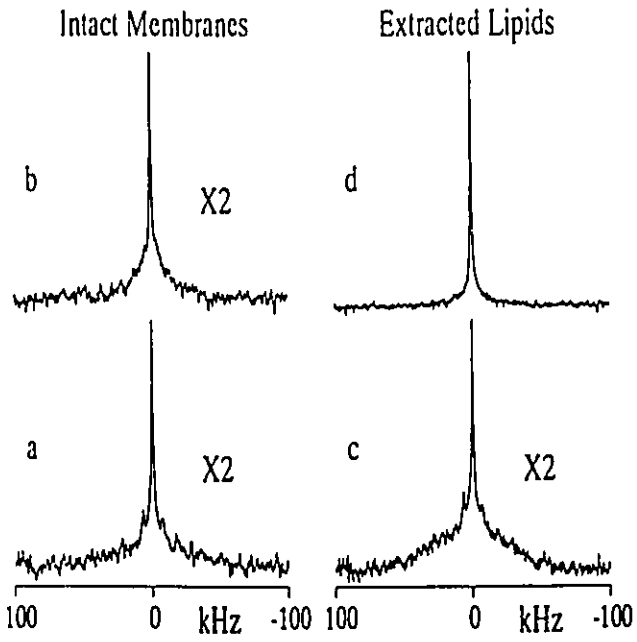

Figure 7.9 ^{2}H NMR spectra of *A.nidulans R2* thylakoid membranes (bottom band). The sample was harvested after 96 hours of growth in medium supplemented with perdeuterated palmitic acid. Intact membrane spectra presented here were acquired at a) 0°C and b) 35°C; extracted lipid spectra are presented at c) 0°C and d) 35°C.

The extracted lipid spectra are also quite different, at 35°C the central isotropic signal is the predominant feature in the spectrum of the 96 hour growth *A.nidulans R2* **bottom band** sample (Figure 7.9d). This may be caused by the higher unsaturation in the 96 hour sample, which is double that of the 48 hour sample (21% vs. 10%, respectively). Furthermore, the relative lipid ratios after both growth periods are also very different (eq 7.2). Again one is confronted with the situation that there are too many variables to consider in these complex systems. At this point, it could prove most efficacious to compile all of the available data before drawing any conclusions. This is accomplished in the following section where the NMR and lipid analysis data from *A.nidulans* (Chapter 6) and *A.nidulans R2* thylakoid membranes comprise a sufficient data base to make correlations between lipid content and NMR spectral behaviour.

7.4 *A.nidulans* versus *A.nidulans R2*

A.nidulans cells were harvested after 48 hours growth in perdeuterated palmitic acid supplemented medium (§ Chapter 6). After density gradient centrifugation of fractionated cells only the **top band** of thylakoid membranes was sufficiently concentrated for further analysis by NMR. Whereas for *A.nidulans R2,* after 48 and 96 hours, both the **top** and **bottom bands** of thylakoid membranes were used for NMR analysis. Hence, there are five different sets of thylakoid membrane data available for comparison. Two observations can be made when the ^{2}H NMR spectra of all five samples are considered.

First, the gel to liquid crystalline phase transition temperature range is lowest for intact *A.nidulans* **top band** thylakoid membranes (0° to 30°C). For either band of *A.nidulans R2,* some lipids are still in the gel state at 35°C. The presence of *A.nidulans R2* lipids in the gel state at higher temperatures is suggestive of membrane features which restrict acyl chain mobility such as a smaller percentage of unsaturated fatty acids

in *A.nidulans R2* or an abundance of lipid head groups that inhibit motion. The most unsaturated sample is from the *A.nidulans* **top band** thylakoid membranes with 40% unsaturated fatty acid content. The *A.nidulans R2* **top band** samples are 27% and 32% unsaturated after 48 and 96 hour growth periods, respectively. Finally, the *A.nidulans R2* **bottom band** sample is the most saturated with 10% and 21% unsaturation after 48 and 96 hours, respectively. Since it has been established that increased unsaturation does decrease the temperature of the lipid phase transition temperatures, it is reasonable to observe that the gel to liquid crystalline phase transition temperature range is lowest for *A.nidulans* **top band** thylakoid membranes.

The second notable observation is that the ^{2}H NMR spectra of the *A.nidulans* **top band** thylakoid membranes (Figures 7.4 and 5) are unlike those of the **top band** membranes in the *A.nidulans R2* samples (Figures 7.4 and 7.8). Rather, the *A.nidulans* **top band** spectra are most similar to the spectra of the *A.nidulans R2* **bottom band** sample after 96 hours of growth (Figure 7.9). For example, the appearance of the central isotropic signal, indicative of non-lamellar phases, at 35°C in the extracted lipid spectra is particularly noticeable for only *A.nidulans* and *A.nidulans R2* **bottom band** (96 hours). If unsaturation was the only factor affecting lipid phases, the phase behaviour of all of the **top band** samples in *A.nidulans R2* would be similar to that of *A.nidulans*. With only one half the unsaturation the *A.nidulans R2* **bottom band** (96 hours) extracted lipids form non-lamellar phases at lower temperatures, like *A.nidulans*. Therefore the lipid phase behaviour is likely a head group effect.

Interestingly the relative lipid ratios are similar for *A.nidulans* **top band** (48 hours growth) and *A.nidulans R2* **bottom band** (96 hours growth). The only difference is that the NL content for the *A.nidulans R2* **bottom band** 96 hour sample (eq 7.2) is slightly higher than that of the *A.nidulans* **top band** sample:

	48 Hours	
A.nidulans **top band**	PG < SL < DGDG < NL < MGDG	7.3

In this study, the thylakoid membrane lipids with higher DGDG levels actually tended to form non-lamellar phases as opposed to lamellar phases (*A.nidulans* and 96 hour **bottom band** *A.nidulans R2*). However, in both samples PG is least abundant lipid, which may be correlated with the formation of the non-lamellar phase. PG is an anionic lipid (Figure 6.2) it could be anticipated that the electrostatic interactions may be resistant to the non-planar packing of non-lamellar phases. Since the spectra of extracted lipids have a more intense isotropic signal, this may be an indication of the stabilizing effect of interactions between membrane protein and the negatively charged PG. Alternatively, this result may also be due to the loss of membrane asymmetry with the removal of membrane proteins.

7.5 COMPARISON WITH OTHER WORK

Since the PG and SL contents in thylakoid membranes do not tend to be as high as the MGDG and DGDG contents, their effect on lipid phase behaviour has not been thoroughly considered. For example, Borovyagin et al. (1988) have used ^{31}P NMR and electron-microscopy studies to show that the polymorphism of MGDG, PG, and DGDG model membranes is influenced by chlorophyll a and b. They found that chlorophyll-glycolipid interactions induce non-lamellar membrane structures, and that DGDG retards the formation of non-lamellar phases. However, they did not consider the effect of the relative concentration of PG on the membrane structure.

In a more recent study of model membrane systems Webb and Green (1990) have shown that both anionic lipids (PG and SL) inhibit aggregation of DGDG vesicles. They concluded that in the model system and probably in biological systems both PG and SL require the lamellar structure to accommodate the electrostatic interactions. This is consistent with our findings that non-lamellar phases form when there are decreased levels of PG in the thylakoid membranes of *A.nidulans R2*. With regards to lipid

function in biological membranes, aggregation in model systems may be related to the stacking (appression) of thylakoid membranes in plants and algae. Brandt and Eichenberger (1991) have demonstrated that the heterogeneous distribution of lipids in the thylakoid membranes of *Eugiena gracilis* has an effect on membrane appression. Although the specific effect of PG was not considered a connection has been made between lipid composition and membrane function.

7.6 CONCLUSIONS

In this body of work *A.nidulans R2* cells were harvested after 48 and 96 hours of growth in perdeuterated palmitic acid supplemented medium. This is an efficient means of probing the interior of the membrane because the function of the thylakoid membranes was not affected by the incorporation of these deuterated fatty acids (B. G. Winsborrow and D. H. Bruce, unpublished results).

Of all the thylakoid membrane lipids, only the effect of the presence of diacylglycerol was directly observed in the ^2H NMR spectra. Distinct spectral features were detected in the spectra of the *A.nidulans R2* **(bottom band)** 48 hour growth sample, where elevated diacylglycerol levels were also present. Interestingly, after 96 hours the diacylglycerol levels were much lower and their NMR signals were not detected.

Although pure DGDG is known to stabilize lamellar membrane phases, it appears as though PG is more influential in stabilizing the lamellar membrane structure in these systems. This effect was more noticeable for the spectra of extracted lipids; in the absence of protein and with low PG levels, the lipids formed non-lamellar phases at lower temperatures. No effect of SL has been observed, but this does not lead to the conclusion that SL does not play an important role in membrane structure or function.

Biological differences between the two strains of cyanobacteria are largely unexplained. The observed differences in the membrane structure and composition after 48 and 96 hours of growth might be one starting point for the investigation of biological differences. These results do form a basis for future work, which will be discussed in the following chapter.

Part IV

Conclusions

Chapter 8

Concluding Remarks

The focus of this dissertation has been the biophysical analysis of two related research subjects: a model membrane glycolipid system and glycolipid-rich biomembranes. The objective in the study of the model system was to provide a biological understanding of the molecular conformation and dynamics at the membrane surface. The biomembrane project is ideally the first stage in a series of many where the ultimate goal is to define the conformational changes in algal thylakoid membranes during photosynthetic activity. The following summarizes the findings made in this body of work. Often, when one research question is answered, it lays the foundation for many more: therefore, a discussion of future research possibilities is also included.

8.1 β-DTGL: A MODEL MEMBRANE SYSTEM

This research group has been attempting to provide a quantitative description of the nature of the molecular motions of the glycolipid 1,2-di-*O*-tetradecyl-3-*O*-(β-D glucopyranosyl)-*sn*-glycerol (β-DTGL) and other related glycolipids in the biologically relevant liquid crystalline state (Jarrell et al., 1986, 1987a,b; Carrier et al., 1989; Renou et al., 1989; Auger et al., 1990; Winsborrow et al., 1991, 1992). The results presented here are the culmination of the group's efforts over a period of six years. The driving force for this work is that an understanding of glycolipid conformation and dynamics at the membrane surface could advance many fields of study, such as, membrane structure (Curatolo, 1987), cell-cell recognition (Blackburn et al., 1986), and tumour immunology (Hakamori, 1986).

Two disparate but complementary approaches were taken when defining the liquid crystalline state dynamics and glucose head group conformational space of β-DTGL at the membrane surface. The former study analyzed ^{2}H NMR powder lineshapes and relaxation data (§Chapter 4; Winsborrow et al., 1991). The latter compared conformational energy calculations with ^{2}H NMR and neutron diffraction data (§Chapter 5; Winsborrow et al., 1992).

8.1.1 Liquid Crystalline State Dynamics

Analysis of the powder lineshapes and oriented sample relaxation data for the glycerol backbone region of β-DTGL was performed. The dynamics of glycerol at the C3 position, in the gel state, have been described by large angle jumps about the glycerol C2-C3 bond with a correlation time in the fast-limit motional regime ($\omega_o^2\tau_c^2 << 1$) and site populations 0.46, 0.34, 0.20 (Auger et al., 1990). The present data show that in the liquid crystalline state the internal jump rate is maintained, and two additional motions are necessary to describe the dependence of the relaxation rate on the orientation of the order director with respect to $\mathbf{H}_o$. These are rotation about the molecular long axis with a correlation time in the slow-limit motional regime very near

the T_1 minimum ($\omega_0^2\tau_c^2 \approx 0.42$), and molecular fluctuations about the director (modeled by a Maier-Saupe restoration potential).

The results strongly uphold the choice of motional model and indicate the utility of both oriented samples and the T_{1Q} experiment. Oriented multibilayers avoid the effects of fast lateral diffusion over the curved vesicles, which may average completely anisotropic longitudinal relaxation (Brown and Davis, 1981). They also provide a means to determine unambiguously the longitudinal $T_1(\beta)$ relaxation profiles in detail. Moreover, the $T_1(\beta)$ profiles will identify more accurately features associated with a particular motional model. Notably, the T_{1Q} experiment has been useful in testing further the molecular models described. The sensitivity of the $T_{1Q}(\beta)$ relaxation profile to changes in the simulation parameters has proven that T_{1Z} relaxation data alone may not be sufficient to discriminate between motional models.

This study has attempted to provide a stringent test of the motional model chosen earlier because relaxation data were obtained at two ^2H NMR frequencies, using two relaxation experiments (T_{1Z} and T_{1Q}) and two types of sample preparation (oriented and dispersed multibilayers).

8.1.2 The Glucose Head Group Conformational Space

The above treatment was also extended to the glucose head group region where additional segmental motion about the glycosidic bond had been reported previously (Jarrell et al., 1987b). While the two motions dominating relaxation at the glycerol C3 segment reproduce the general relaxation features of the glucose head group, the results suggest that the glycosidic bond of a glycolipid may be flexible to some degree. In order to define what is meant by "flexible" a quantitative description of these motions is necessary. To this end conformational energy calculations were performed.

Conformational energies were calculated as the glucose head group was rotated over all of the possible glycosidic torsional bond angles. For the calculations the

molecule was held in a membrane matrix, which was approximated by placing an annulus of six molecules around the molecule of interest. The use of an expandable surface annulus has shown that molecular energies are sensitive to spatial packing. At this point the conformational space of the β-DTGL head group is best described as a complex equilibrium of conformations with a distribution of populated sites for each of the three glycerol C2-C3 conformations (ω = g^+, t, g^-). This implies that there is a hierarchy of motion; rotation about the glycerol C2-C3 bond is coupled with either simultaneous or sequential conformational fluctuations at the glucose head group.

Admittedly this approach utilizes an extremely simplified description of the restraints on β-DTGL head group conformations because of the restrictive assumptions that have been made; no solvent was used and the surrounding membrane molecules were held fixed on a lattice. However, the predicted NMR and neutron diffraction parameters are in reasonable agreement with experiment, which indicates that additional insight into the nature and amplitude of the head group motion (not available directly from experiment) is derived from such a simple approach.

8.1.3 Suggestions For Future Work

Glycobiology is at the level where complex biological interactions should be investigated in a biologically relevant medium. Molecular recognition is an excellent example of the type of interaction that can be investigated by NMR. The identification of this type of interaction requires the ability to study the molecular environment at the membrane surface. The average head group conformation of β-DTGL has been previously determined by ^2H NMR (Jarrell et al., 1987b). In the analysis, the ^1H-^2H dipolar coupling values were estimated; although the assumptions made were reasonable it is worthwhile to test the previous results and to evaluate the head group orientation via a different means. One possibility is with ^{13}C NMR. ^{13}C-^{13}C dipolar coupling is a second rank tensorial interaction (§ Chapter 2), which has the potential of yielding geometrical information about the molecule of interest.

Sanders and Prestegard (1991) were able to make a conformational analysis of β-D-dodecyl glucopyranoside solubilized in a magnetically orientable membrane system, CHAPSO (§1.2.2). The average head group orientation was elucidated by the evaluation of ^{2}H quadrupolar couplings, ^{13}C-^{1}H dipolar splittings, and ^{13}C-^{13}C dipolar splittings obtained by 1D and 2D NMR methods. The same approach can be used to determine the head group conformation of β-DTGL, synthesized with ^{13}C labelled glucose. Preliminary results indicate that ^{13}C-^{1}H dipolar couplings between glucose atoms, in the liquid crystalline state, can be detected in 2D Separated Local Field experiments (data not presented). Ideally, ^{13}C-^{13}C dipolar couplings will also be measured in 2D multiple quantum experiments. Although time was not available to complete this work, this is an excellent strategy for determining the average β-DTGL head group conformation.

The β-DTGL head group flexibility has been established. The next steps in describing the dynamics at the membrane surface are first, to define more quantitatively the process of the conformational equilibrations (libration or discrete jumping, correlation time) and second, to identify any mechanistic correlation between the head group motions and the glycerol backbone rotation. Simulations of molecular and Brownian dynamics have been used for these purposes, but they are not practical for partially ordered environments (§1.4). However, it is not unreasonable to expect that in the future the capabilities of these simulations will be able to cope with the demands of modelling accurately biological systems.

The approach taken in the conformational energy calculations provides considerable insight at the molecular level, and offers the possibility of exploring even more complex systems. For example, in an attempt to represent more realistically the actual membrane surface it would be beneficial to consider further the effect of modifying the surface matrix, which was used in the calculations (i.e. vary the surface molecule conformations and include other membrane molecules). One feature that was noted but not pursued in this study was the effect of positioning the height of the molecule under consideration with respect to the membrane surface. The effects of

glycolipid positioning in the membrane is used in the study of complement-dependent immune reactions of liposomes. Molecular interactions are sensitive to the depth in the membrane at which the active glycolipid is positioned (Alving et al., 1980).

8.2 BIOMEMBRANES

8.2.1 Cyanobacteria

Algal thylakoid membranes are known for their ability to undergo conformational changes during periods of photosynthetic activity (Biggins 1983). An understanding of these systems has been realized through the numerous physical studies that have been performed on model membrane systems, which contain the major thylakoid membrane lipids (§6.4, 7.3.2, 7.5). The ultimate goal of the biomembrane project is to use ^2H NMR to study conformational changes in thylakoid membranes during photosynthetic activity. Such an undertaking has been made viable by the pioneering work of Smith and co-workers in the study of biological membranes by ^2H NMR (Stockton et al., 1977; Smith et al., 1979; Rance et al., 1980; Jarrell et al., 1982).

This project is in the first stages of development, therefore, the more modest but attainable short term goal is to observe directly the structure and phase behaviour of two strains of cyanobacterial thylakoid membranes, *Anacystis nidulans* and *A.nidulans R2*. *A.nidulans* cells were harvested after 48 hours and *A.nidulans R2* cells after both 48 and 96 hours of growth in perdeuterated palmitic acid supplemented medium. *A.nidulans* was also grown, for 48 hours, in medium supplemented with specifically deuterated oleic acid. This is an efficient means of probing the interior of the membrane because the function of the thylakoid membranes was not affected by the incorporation of these deuterated fatty acids (B. G. Winsborrow, D. H. Bruce, unpublished results).

The ^2H NMR spectra are very similar to those of membranes of *A.laidlawii* grown in media containing myristic acid (Smith et al., 1979; Jarrell et al., 1982) and oleic acid (Rance et al., 1980). In both the previous studies and this study, it was found

that acyl chain unsaturation lowers the phase transition temperature of the membranes. The thylakoid membranes of *A. nidulans* cells grown in medium supplemented with oleic acid had much lower phase transition temperatures than did membranes supplemented with palmitic acid. Moreover, the heterogeneous systems undergo broad phase transitions, which is also in agreement with a recent ESR study of *A.nidulans* cells (Nicholov et.al., 1991).

Distinct spectral features were detected in the intact membrane and extracted lipid spectra of the *A.nidulans R2* (**bottom band**) 48 hour growth thylakoid membranes, where elevated diacylglycerol levels were also present. These spectral features are associated with membrane diacylglycerol levels for two reasons. First, after 96 hours of growth, the diacylglycerol levels were much lower and their NMR signals were not detected. Second, a model membrane study of diacylglycerol/DMPC systems has similar ^{2}H NMR spectra (De Boeck and Zidovetzky, 1989). Of all the thylakoid membrane lipids, only the presence of diacylglycerol was directly observed in the ^{2}H NMR spectra.

An isotropic signal due to lipid in a non-lamellar phase, was also observed in all the ^{2}H NMR spectra. This suggests that lamellar and non-lamellar phases coexist in the thylakoid membranes. In support of this observation, heterogeneous pockets of lipidic particles have been observed in freeze-fracture studies of chloroplast membrane lipid extracts (Sprague and Staehelin, 1984). However, at temperatures above 65°C the only significant signal is the isotropic signal, which suggests that at higher temperatures the lipid phase is likely more homogeneous (i.e in the cubic phase).

Although pure DGDG is known to stabilize lamellar membrane phases, it appears as though PG is more influential in stabilizing the lamellar membrane structure in these systems. This effect was more noticeable for the spectra of extracted lipids; in the absence of protein and with low PG levels, the lipids formed non-lamellar phases at lower temperatures. No effect of SL has been observed, but this does not lead to the

conclusion that SL does not play an important role in membrane structure or function.

Two basic criteria have been used to relate the physical properties measured by ^2H NMR to the heterogeneous thylakoid membrane structure: acyl chain unsaturation and lipid head group class. In the study of model systems the identification of the effects that unsaturation and different lipid head groups have on the membrane phase behaviour is straightforward because the number of variables are few. In complex biological systems, however, this is more challenging. In these studies elevated unsaturation was correlated with decreased gel to liquid crystalline state transition temperatures. Additionally, the head group class was related to the formation of non-lamellar phases; PG stabilizes strongly the lamellar phase. Although the spatial requirements of the lipid head group dictates which phase that the membrane will tend to form, increased acyl chain unsaturation facilitates the formation of these phases.

8.2.2 Suggestions For Future Work

Thylakoid membranes incorporated with specifically deuterated fatty acids gave simpler spectra, which were much easier to interpret than those of perdeuterated lipids. Although perdeuterated fatty acids were used in these studies to assess quickly the feasibility of studying thylakoid membranes by ^2H NMR, any future work would benefit from the use of specific labels. Another means of simplifying spectra is to physically orient the membranes for the NMR experiments. This can be managed easily by squeezing membranes in agar gel.

One biosynthetic pathway in thylakoid membranes is the glycosylation of diacylglycerol to form MGDG, which can then be glycosylated to produce DGDG. Lipid analysis did indicate that this pathway may have been followed. There was a concomitant rise and fall of diacylglycerol and MGDG levels, with a continued increase in DGDG levels over 96 hours of growth. In addition, SL is essentially MGDG that has been sulfonated at the glucose C6 position. If cells were grown in medium supplemented with ^{13}C labelled glucose, perhaps production of MGDG, DGDG, and SL

could be traced. This may also provide the opportunity to observe the effect of the glycolipids on the membrane phase behaviour.

The biological differences between the two strains of cyanobacteria are largely unexplained. Although the thylakoid membrane lipid analysis and ^2H NMR spectra of *A. nidulans R2* **(top band)** cells are similar after both 48 and 96 hours of growth in labelled medium, those of *A.nidulans R2* **(bottom band)** are not. Moreover, the results of *A. nidulans* **(top band)** after 48 hours growth are similar to those of *A. nidulans R2* **(bottom band)** after 96 hours. These observations are curious and might be one starting point for the investigation of biological differences. The growth cycle of a cell is less than 24 hours and more differences between the two strains may be observed if these cells are harvested after three or six hour growth periods, as in the work of Brandt and Eichenberger (1991).

8.3 PARTING COMMENTS

Biophysical studies imply that there will be a convergence of two diverse perspectives. One is physical or mechanical in nature. The types of questions asked can be viewed as being microscopic: "how exactly does a molecule move?", or "what molecular segments are rotating?", or "what is the rate of motion?". On the other hand, the second perspective has a biological slant. The research questions are structured to gain a macroscopic understanding: "when a molecule moves in a particular way, what is the effect on the rest of the organism?", or "how important is this information for life function and interactions?". The physical results are specific and quantitative, whereas the biological results are more general and qualitative. In a true biophysical study, both elements are present and the results are mutually inclusive. This dissertation has been a successful endeavour in embodying the multifarious biophysical concepts of membranes, as studied by ^2H NMR.

APPENDIX

Subroutine to calculate surface interactions.

This subroutine is included in a program that calculates PFOS (Potential Functions of OligoSaccharides) conformational energies (Tvaroška and Pérez, 1986). The program was a generous gift of Dr. Jean-Robert Brisson (NRC Ottawa, Ont.).

```
      subroutine surfpe
c
c calculates interaction of glycon for linkage vl with surface
c incorporated subroutine pepfos to calculate softer surface
c interaction

      include 'aainc.for'
      integer fv     !output file for hb
      integer i,iii          !loop variable
      integer iv, jv  !some variable for pecode
      integer ii             !glycon residue #
      integer m              !surface hexagon atom #
      integer p      !number of surface atoms in molecules
      integer  ii1, ii2 !range of atom #s for glycon residue
      integer nbcode(MAtm,MAtm)
      character*4 garb
      integer garba
      common /zpec/ nbcode

      real pi, hexang, hexangm, hex(6,3)
      real difx, dify, difz, dif2, dif6
      real difa, difb, difxtes

!
      OPEN(unit=61, file=surfile,status='old',form='formatted')
!
      do 16 P = 1,gatm
```

```
          Read(61,9200,end=888)
     1  garb, surfmat(P,1),surfmat(P,2),surfmat(P,3),npecode(P),
     1  garba

16        continue
9200      format(A4,3F15.6,I5,I10)
!
888    continue
!         write(6,*) 'end of file'
          pesurf = 0
          do 40 i= 1, GlyRes(vl,0)
           ii  = GlyRes(vl,i)
           ii1 = FirstA(ii)
           ii2 = LastA(ii)
           do 30 iii = ii1,ii2        !atoms in glycon residue

              iv = abs(PECode(iii))
!                 jv = 2                      !2 is surface oxygen (OH)

            do 20 P = 1,gatm
                  jv = abs(npecode(P))  !pecode for surf atoms

                  difx = cx(iii) - surfmat(P,1)  !calc. dist.
                  dify = cy(iii) - surfmat(P,2)  !of molecule
                  difz = cz(iii) - surfmat(P,3)  !from surf. mols.
!
                  difxtes = cx(iii) - del

!calculations include an interaction with surface molecules.
!Note that a surface penalty is included in the program.
!This way the molecule is not allowed to rotate below the surface.
!Penalty and del are input at the onset of running CCH.

            if(difxtes.le.0.0) pesurf = pesurf + penalty
                              !this maintains surface barrier
           if(pesurf.gt.50.0) goto 10
                  dif2 = difx*difx + dify*dify + difz*difz
            if(dif2.gt.49.) goto 10

              dif6 = dif2*dif2*dif2

                  difa = - lja(iv,jv)/dif6 !active for surf attr'n
                  difb = ljb(iv,jv)/(dif6*dif6)

          pesurf = pesurf + difa + difb
10     continue

          if(pesurf.gt.50.0) return


20        continue
30        continue
40        continue
      return


      end
```

```
c*****************************************************************

          subroutine splitcal

C  FOR SHORT MOLECULE - GENTIOBIOSE ATOM CODE
c
c  calculate the quadrupolar splittings of the c1 of glucose in
c  gentiobiose, actual program will calculate all splittings
c  for glucose, for simplicity the subroutine has been truncated

          include 'aainc.for'
          include 'aahinc.for'
          include 'fdevinc.for'
          real rcha, rrcha    !bond length of c-h bond, and reciprocal
          real sxa, ctha, cth2a, p2tha, p2beta, cons
          real sya, cthya, sza, cthza, sx2a, sy2a, sz2a
          real rchi, rrchi    !bond length of c-h bond, and reciprocal
          real sxi, cthi, cth2i, p2thi
          real syi, cthyi, szi, cthzi, sx2i, sy2i, sz2i
          integer nbcode(MAtm,MAtm)
          common /zpec/ nbcode


          qcc = 164.          !quad coupling constant for CDOH
          smol = 0.65         !mol order parameter for bdtgl glycerol
          p2beta = -0.5       !P2 term for beta = 90 deg
          cons = 1.5*qcc*p2beta*smol

!1

          sxa = cx(24) - cx(36)  !code for 2C1 and 2H1 of
                                 !glucose in BDTGL
          sya = cy(24) - cy(36)
          sza = cz(24) - cz(36)

          sx2a = sxa*sxa
          sy2a = sya*sya
          sz2a = sza*sza



          rcha = (sx2a + sy2a + sz2a)**0.5
          rrcha = 1/rcha

          ctha = sxa*rrcha

          cth2a =ctha*ctha
          p2tha = (3.*cth2a -1.)*0.5

          qsplita = cons*p2tha


          return
          end
```

```
c*****************************************************************
                    subroutine deutdist

C  ATOM CODE FOR SHORT MOLECULE - GENTIOBIOSE
c  this calculates the distance between the H1 and H6A or B of
C  glucose.  The resulting matrices will be used with the pop
c  ulation matrix to plot population vs distance.  this will be
c  used to analyze neutron diffraction results.

          include 'aainc.for'
          include 'aahinc.for'
          integer nbcode(Matm,Matm)
          common /zpec/ nbcode

           dlta = cx(41) - cx(36)
           dltb = cx(42) - cx(36)

           return
           end


c*****************************************************************
```

REFERENCES

Abragam, A. 1961. The Principles of Nuclear Magnetism. Clarendon Press, Oxford. 599 pp.

Adebodun, F., J. Chung, B. Montez, E. Oldfield, and X. Shan. 1992. Spectroscopic studies of lipids and biological membranes: carbon-13 and proton magic-angle spinning nuclear magnetic resonance study of glycolipid-water systems. *Biochem.* 31:4502-4509.

Allen, M. M. 1968. Simple conditions for growth of unicellular blue-green algae on plates. *J. Phycol.* 4:1-4.

Allinger, N. L. 1977. Conformational analysis. 130. MM2. A hydrocarbon force field utilizing V_1 and V_2 torsional terms. *J. Am. Chem. Soc.* 99:8127-8134.

Alving, C. R., K. A. Urban, and R. L. Richards. 1980. Influence of temperature on complement-dependent immune damage to liposomes. *Biochim. Biophys. Acta* 600:117-125.

Auger, M. A., D. Carrier, I. C. P. Smith, and H. C. Jarrell. 1990. Elucidation of motional modes in glycoglycerolipid bilayers: a ^2H NMR relaxation and line-shape study. *J. Am. Chem. Soc.* 112:1373-1381.

Baenziger, J. E., I. C. P. Smith, R. J. Hill, and H. C. Jarrell. 1988. Direct measurement of deuterium-deuterium dipolar coupling and analysis of the ordering of a specifically deuterated diunsaturated lipid. *J. Am. Chem. Soc.* 110:8229-8231.

Biggins, J. 1977. Kinetic behaviour of P-700 during induction of photosynthesis in algae. *Biochim. Biophys. Acta.* 459:442-450.

Biggins, J. 1983. Mechanism of the light state transition in photosynthesis. 1. Analysis of the kinetics of cytochrome-F oxidation state-1 and state-2 in the red alga, *Porphyridium cruentum*. *Biochim. Biophys. Acta* 724:111-117.

Biodart, M., A. Hochapfel, and M. Laurent. 1988. An actualized survey of micellar nematic lyophases. *Mol. Cryst. Liq. Cryst.* 154:61-67.

Bishop, D. G., J. R. Kendrick, T. Kondo, and N. Murata. 1986. Thermal properties of membrane lipids from two cyanobacteria, *Anacystis nidulans* and *Synechococcus* sp. *Plant Cell Physiol.* 27:1593-1598.

Blackburn, C. C., P. Swank-Hill, R. L. Schnaar. 1986. Gangliosides support neural retinal cell adhesion. *J. Biol. Chem.* 261:2873-2881.

Bloembergen, N., E. M. Purcell and R. V. Pound. 1948. Relaxation effect in nuclear magnetic absorption. *Phys. Rev.* 73:679-95.

Bloom, M. and I. C. P. Smith. 1985. Manifestations of lipid-protein interaction in deuterium NMR. *In* Progress in Protein-Lipid Interactions. Watts and De Pont, editors. Elsevier Science Publishers, Amsterdam. 61-88.

Blume, A., D. M. Rice, R. J. Wittebort, and R. G. Griffin. 1982. Molecular dynamics and conformation in the gel and liquid-crystalline phases of phosphatidylethanolamine bilayers. *Biochem.* 21:6220-6230.

Bonmatin J. M, I. C. P. Smith, H. C. Jarrell, and D. S. Siminovitch. 1990. Use of a comprehensive approach to molecular dynamics in ordered lipid systems: cholesterol reorientation in ordered lipid bilayers. A ^{2}H NMR relaxation case study. *J. Am. Chem. Soc.* 112:1697-1704.

Borovyagin, V. L., Y. S. Tarakhovsky, and I. A. Vasilenko. 1988. Polymorphism in galactolipid/phosphatidylglycerol model membranes initiated by chlorophyll: ^{31}P-NMR and electron-microscopy studies. *Biochim.Biophys. Acta* 939:111-123.

Brady J. W. 1987. Molecular dynamics simulations of β-*D*-glucopyranose. *Carbo. Res.* 165:306-312.

Brandt, P. and W. Eichenberger. 1991. Developmental heterogeneity of the lipid distribution in the thylakoid membranes of *Euglena gracilis*. *Physiol. Plant.* 82:594-598.

Branton, D. 1966. Fracture faces of frozen membranes. *Proc. Natl. Acad. Sci. USA* 55:1048-1056.

Brown, M. F. and J. H. Davis. 1981. Orientation and frequency dependence of the deuterium spin-lattice relaxation in multilamellar phospholipid dispersions: implications for dynamic models of membrane structure. *Chem. Phys. Lett.* 79:431-435.

Brown, M. J. 1984. Theory of spin-lattice relaxation in lipid bilayers and biological membranes. Dipolar relaxation. *J. Chem. Phys.* 80:2808-2831.

Browse, J. and C. Somerville. 1991. Glycerolipid synthesis: biochemistry and regulation. *Annu. Rev. Plant Physio. Plant Mol. Biol.* 42:467-506.

Carrier, D., J. B. Giziewicz, D. M. Moir, I. C. P. Smith, and H. C. Jarrell. 1989. Dynamics and orientation of glycolipid headgroups by ^{2}H NMR: gentiobiose. *Biochim. Biophys. Acta* 983:100-108.

Castresana, J., J. M. Valpuesta, J. L. R. Arrondo, and F. M. Goñi. 1991. An infrared spectroscopic study of specifically deuterated fatty-acyl methyl groups in phosphatidylcholine liposomes. *Biochim. Biophys. Acta* 1065:29-34.

Cheresh, D. A., R. Pytela, M. D. Pierschbacher, F. G. Klier, E. Ruoslhati, and R. A. Reisfeld. 1987. An arg-gly-asp-directed receptor on the surface of human melanoma cells exists in a divalent cation-dependent functional complex with the disialoganglioside GD2. *J. Cell Biol.* 105:1163- 1173.

Coleman, W. J, Govindjee, and H. S. Gutowsky. 1987. The location of the chloride binding sites in the oxygen-evolving complex of spinach Photosystem II. *Biochim. Biophys. Acta.* 894:453-459.

Cullis, P. R., B. de Kruijff, M. J. Hope, A. J. Verkleij, R. Nayar, S. B. Farren, Tilcock, C., Madden, T. D., and Ballly, M. B. 1983. Structural properties of lipids and their functional roles in biological membranes. *in* Membrane Fluidity in Biology. R. C. Aloia, Ed, Vol 1, Academic Press, NY. p 39-81.

Curatolo, W. 1987. The physical properties of glycolipids. *Biochim. Biophys. Acta.* 906:111-136.

Dammers, A. J., Y. K. Levine, K. Balasubramanian, and A. H. Beth. 1988. A planar rotor model for cholestane spin label motion in phospholipid multibilayers with high order. *Chem. Phys.* 127:149-160.

Danielli, J. F. and Davson, H. 1935. The permeability of thin films. *J. Cell. Comp. Physiol.* 5:495-508.

Darnell, J., Lodish, H., and Baltimore, D. 1990. Molecular Cell Biology, 2nd Ed.,Scientific American Books, NY, 1105 pp.

Davis, J. H., Nichol, C. P., Weeks, G., and Bloom, M. 1979. Study of the cytoplasmic and outer membranes of *Escherichia coli* by deuterium magnetic resonance. *Biochem.* 18:2103-2112.

Davis, J. H. 1983. The description of membrane lipid conformation, order, and dynamics by ^{2}H-NMR. *Biochim. Biophys. Acta.* 737:117-171.

Davis, J. H. 1991. Deuterium nuclear magnetic resonance spectroscopy in partially ordered systems. *In* Isotopes in the Physical and Biomedical Sciences, Vol 2. E.Buncel and J. R. Jones, editors. Elsevier Science Publishers B.V., Amsterdam. 99-157.

De Boeck, H. and R. Zidovetzki. 1989. Effects of diacylglycerols on the structure of phosphatidylcholine bilayers: a ^{2}H and ^{31}P NMR study. *Biochem.* 28:7439-7446.

de Kruijff, B. 1987. Polymorphic regulation of membrane lipid composition. *Nature.* 329:587-588.

Diesenhofer, J. 1981. Crystallographic refinement and atomic models of a human Fc fragment and its complex with Fragment B of protein A from *Staphylococcus aureus* at 2.9- and 2.8-Å resolution. *Biochem.* 20:2361-2379.

Dufourc, E. J., I. C. P. Smith, and H. C. Jarrell. 1984a. Role of cyclopropane moieties in the lipid properties of biological membranes: a ^{2}H NMR structural and dynamical approach. *Biochem.* 23:2300-2309.

Dufourc, E., H. C. Jarrell, and I. C. P. Smith. 1984b. Structural and dynamical details of cholesterol-lipid interaction as revealed by deuterium NMR. *Biochem.* 23:6062-6071.

Dufourc, E. J., and I. C. P. Smith. 1986. A detailed analysis of the motions of cholesterol in biological membranes by ^{2}H NMR relaxation. *Chem. Phys. Lip.* 41:123-135.

Edge, C. J., U. C. Singh, R. Bazzo, G. L. Taylor, R. A. Dwek, and T. W. Rademacher. 1990. 500-picosecond molecular dynamics in water of the mana1->2mana glycosidic linkage present in asn-linked oligomannose-type structures on glycoproteins. *Biochem.* 29:1971-1974.

Ekiel I., Marsh, D., Smallbone, B. W., Kates. M., and I. C. P. Smith. 1981. The state of the lipids in the purple membrane of *Halobacterium cutirubrum* as seen by ^{31}P NMR. *Biochem. Biophys. Res. Comm.* 100:105-110.

Elder, M., P. Hitchcock, R. Mason, and G. G. Shipley. 1977. A Refinement analysis of the crystallography of the phospholipid 1,2-dilauroyl-DL-phosphatidylethanolamine, and some remarks on lipid-lipid and lipid-protein interactions. *Proc. R. Soc. Lond. A.* 354:157-170.

Emsley, J. W., and J. C. London. 1975. NMR Spectroscopy Using Liquid Crystal Solvents. Pergamon Press, New York. 367 pp.

Eriksson, P.-O., L. Rilfors, A. Wieslander, A. Lundberg, and G. Lindblom. 1991. Order and dynamics in mixtures of membrane glucolipids from *Acholeplasma laidlawii* studies by ^{2}H NMR. *Biochem.* 30:4916-4924.

Fenske, D. B. and H. C. Jarrell. 1991. Phosphorous-31 two-dimensional solid-state exchange NMR. Application to model membrane and biological systems. *Biophys. J.* 59:55-69.

Frye, L. D. and M. Edidin. 1969. Rapid intermixing of cell surface antigens after formation of mouse-human heterokaryans. *J. Cell Sci.* 7:319-335.

Furtado, D., W. P. Williams, A. P. R. Brain, and P. J. Quinn. 1979. Phase separations in membranes of *Anacystis nidulans* grown at different temperatures. *Biochim. Biophys. Acta* 555:352-357.

Gally, H. U., G. Pluchke, P. Overath, and J. Seelig. 1979. Stucture of *Escherichia coli* membranes and cells as studied by deuterium magnetic resonance. *Biochem.* 18:5605-5610.

Gennis, R. B. 1989. Biomembranes. Molecular Structure and Function. C. R. Cantor, Ed., Springer-Verlag, NY, 533 pp.

Gorter, E. and F. Grendel. 1925. On bimolecular layers of lipoids on the chromocytes of the blood. *J. Exp. Med.* 41:439-443.

Gounaris, K., J. Barber, and J. L. Harwood. 1986. The thylakoid membranes of higher plant chloroplasts. *Biochem. J.* 237:313-326.

Griffin, R. G. 1981. Solid state nuclear magnetic resonance in lipid bilayers. *Methods Enzymol.* 72:109-174

Gruner, S. M., and M. K. Jain. 1985. X-ray diffraction demonstrates that phosphatidyldiacylglycerol and phosphatidylcholesterol are not lamellar above the main transition temperature. *Biochim. Biophys. Acta* 818:352-355.

Hakomori, S. 1984. Glycosphingolipids as differentiation-dependent, tumor-associated markers and as regulators of cell proliferation. *TIBS* 9:453-458.

Hakomori, S. 1986. Tumor-associated antigens, their metabolism and organization. *Chem. Phys. Lipids* 42:209-233.

Hanahan, D. J. 1986. Platelet activating factor: a biologically active phosphoglyceride. *Ann. Rev. Biochem.* 55:483-509.

Hauser, H., I. Pascher, and S. Sundell. 1988. Preferred conformation and dynamics of the glycerol backbone in phospholipids. An NMR and X-ray single-crystal analysis. *Biochem.* 27:9166-9174.

Hinz, H.-J., L. Six, K.-P. Ruess, and M. Liefländer. 1985. Head-group contributions to bilayer stability: monolayer and calorimetric studies of synthetic, stereochemically uniform glucolipids. *Biochem.* 24:306-313.

Hiyama, Y., J. V. Silverton, D. A. Torchia, J. T. Gerig, and S. J. Hammond. 1986. Molecular structure and dynamics of crystalline *p*-fluoro-D,L-phenylalanine. A combined X-ray/NMR investigation. *J. Am. Chem. Soc.* 108:2715-2723.

Hore, P. J., E. T. Watson, J. Bioden Pedersen, and A. J. Hoff. 1986. Line-shape analysis of polarized electron paramagnetic resonance spectra of the primary reactants of bacterial photosynthesis. *Biochim. Biophys. Acta* 849:70-76.

Huber, R. 1980. Spatial structure of immunoglobulin molecules. *Klin. Wochenschrift* 58:5217-5230.

Jacobsen, J. P. and K. Schaumburg. 1976. Spin-lattice relaxation time measurements of D_2O in a lyotropic phase. *J. Mag. Reson.* 23:173-180.

Jacobsen, J. P., H. K. Bildsoe, and K. Schaumburg. 1976. Application of density matrix formalism in NMR spectroscopy. II The one-spin-1 case in anisotropic phase. *J. Mag. Reson.* 23:153-164.

Jacobson, K. 1983. Lateral diffusion in membranes. *Cell Motility.* 3:367-373.

Jarrell, H. C., K. W. Butler, R. A. Byrd, R. Deslauriers, I. Ekiel, and I. C. P. Smith. 1982. A ^{2}H NMR study of *Acholeplasma laidlawii* membranes highly enriched in myristic acid. *Biochim. Biophys. Acta* 688:622-636.

Jarrell, H. C., J. B. Giziewicz, and I. C. P. Smith. 1986. Structure and dynamics of a glyceroglycolipid: a ^{2}H NMR study of head group orientation, ordering, and effect on lipid aggregate structure. *Biochem. 25*:3950-3957.

Jarrell, H.C., A. J. Wand, J. B. Giziewicz, and I. C. P. Smith. 1987a. The dependence of glyceroglycolipid orientation and dynamics on head-group structure. *Biochim. Biophys. Acta.* 897:69-82.

Jarrell, H. C., P. A. Jovall, J. B. Giziewicz, L. A. Turner, and I. C. P. Smith. 1987b. Determination of conformational properties of glycolipid head groups by ^{2}H NMR of oriented multibilayers. *Biochem. 26*:1805-1811.

Jeener, J. and P. Broekaert. 1967. Nuclear magnetic resonance in solids: thermodynamic effects of a pair of rf pulses. *Phys. Rev.* 157:232-240.

Jeffrey, G. A. and S. Takagi. 1977. The crystal and molecular structure of methyl β-D-Glucopyranoside hemihydrate. *Acta Cryst.* B33:738-742.

Jeffrey, K. R. 1981. Nuclear magnetic relaxation in a spin 1 system. *Bull. Mag. Res.* 3:69-82.

Kahn, M. and J. P. Williams. 1977. Improved thin-layer chromatographic method for the separation of major phospholipids and glycolipids from plant lipid extracts and phosphatidyl glycerol and bis(monoacylglyceryl) phosphate from animal lipid extracts. *J. Chromatog.* 140:179-185.

Khanna, R., S. Rajan, Govindjee, and H. S. Gutowsky. 1981. NMR and ESR of thylakoid membranes. *in* Photosynthesis II. Electron Transport and Photophosphorylation. G. Akoyunoglou, Ed. Balaban Int., Philadelphia, Pa. 307-316.

Khintchine, A. 1934. Korrelationstheorie der stationären statistischen prozess. *Math. Ann.* 109:604-615.

Laitinen, J., R. Lopponen, J. Merenmies, and H. Rauvala. 1987. Binding of laminin to brain gangliosides and inhibition of laminin-neuron interaction by the gangliosides. *FEBS Lett.* 217:94-100.

Laskay, G, and E. Lehoczki. 1986. Correlation between linolenic-acid deficiency in chloroplast membrane lipids and decreasing photosynthetic activity in barley. *Biochim. Biophys. Acta* 849:77-84.

Lemieux, R. U., K. Bock, L. T. J. Delbaere, S. Koto, and V. S. Rao. 1980. The conformations of oligosaccharides related to the ABH and Lewis human blood group determinants. *Can. J. Chem.* 58:631-652.

Lemieux, R. U., and K. Bock. 1983. The conformational-analysis of oligosaccharides by H^1 NMR and HSEA calculations. *Arch. Bioch.* 22:125-134.

Lindblom, G., I. Brentel, M. Sjölund, G. Wikander, and A. Weislander. 1986. Phase equilibria of membrane lipids from *Acholeplasma laidlawii*: importance of a single lipid forming nonlamellar phases. *Biochem.* 25:7502-7510.

Lindblom, G. and Rilfors, L. 1988. Cubic phases and isotropic structures formed by membrane lipids - possible relevance. *Biochim. Biophys. Acta.* 988:221-256.

Lii, J. H., S. Gallion, C. Bender, H. Wikstrom, L. N. Allinger, K. M. Flurchick, and M. M. Teeter. 1989. Molecular mechanics (MM2) calculations on peptides and on the protein crambin using the cyber 205. *J. Comput. Chem.* 10:503-513.

Luz, Z., R. Puopko, and E. T. Samulski. 1981. Deuterium NMR and molecular ordering in the cholesteryl alkanoates mesophases. *J. Chem. Phys.* 74:5825-5837.

Mannock, D. A., A. P. R. Brain, and W. P. Williams. 1985. The phase behaviour of 1,2-diacyl-3-monogalactosyl-*sn*-glycerol derivatives. *Biochim. Biophys. Acta* 817:289-298.

Mansfield, R. W., J. H. A. Nugent, and M. C. W. Evans. 1987. ESR characteristics of Photosystem I in deuterium oxide: further evidence that electron acceptor A_1 is a quinone. *Biochim. Biophys. Acta* 894:515-523.

Mayer, C., G. Grobner, K. Muller, K. Weisz, and G. Kothe. 1990. Orientation-dependent deuteron spin-lattice relaxation times in bilayer membranes: characterization of the overall lipid motion. *Chem. Phys. Lett.* 165:155-161.

Mehring, M. 1983. Principles of High Resolution NMR in Solids. 2nd Ed. Springer-Verlag. N.Y., 342 pp.

Meier, P., E. Ohmes, and G. Kothe. 1986. Multipulse dynamic nuclear magnetic resonance of phospholipid membranes. *J. Chem. Phys.* 85:3598-3614.

Meyer, B. 1990. Conformational aspects of oligosaccharides. *Topics Curr. Chem.* 154:141-208.

Milburn, M. P., and K. R. Jeffrey. 1989. Dynamics of the phosphate group in phospholipid bilayers. A ^{31}P angular dependent nuclear spin relaxation time study. *Biophys. J.* 56:543-549.

Murata, N. and T. Omata. 1988. Isolation of cyanobacterial plasma membranes. *Meth. Enzym.* 167:245-251.

Nabedryk, E., S. Andrianambinintsoa, and J. Breton. 1984. Transmembrane orientation of α-helices in the thylakoid membrane and in the light-harvesting complex. *Biochim. Biophys. Acta* 765:380-387.

Neuman, A., F. Longchambon, O. Abbes, H. Gillier-Pandraud, S. Pérez, D. Rouzaud, and P. Sinaÿ. 1990. Conformational features of *C*-Gentiobioside. *Carb. Res.* 195:187-197.

Nicholov R., E. E. Maissan, and J. P. Williams. 1991. The dynamic properties of *Anacystis nidulans* thylakoids containing increased levels of oleic acid in the membrane glycerolipids. *J. Plant Physiol.* 137:711-716.

Nyholm, P.-G., B. E. Samuelsson, M. Breimer, and I. Pascher. 1989. Conformational analysis of blood group A-active glycosphingolipids using HSEA-calculations. The possible significance of the core oligosaccharide chain for the presentation and recognition of the A-determinant. *J.Mol.Rec.* 2:103-113.

Ogawa, T., and K. Beppu. 1982. Synthesis of glycoglycerolipids: 3-*O*-mannooligosyl-1,2-di-*O*-tetradecyl-*sn*-glycerol. *Agric. Biol. Chem.* 46:263-268.

Olden, K., B. A. Bernard, M. J. Humphries, T. K. Yeo, S. L. White, S. A. Newton, H. C. Bauer, H. C., and J. B. Parent. 1985. Function of glycolipid glycans. *Trends Bioch. Sci.* 10:78-83.

Overton, E. 1895. Über die osmotischen eigenschaften der lebenden pflanzen und tierzelle. *Vjsch. Naturf. Ges. Zurich.* 40:159-201.

Pastor, R. W., R. M. Venable, and M. Karplus. 1988. Brownian dynamics simulation of a lipid chain in a membrane bilayer. *J. Chem. Phys.* 89:1112-1127.

Pastor, R. W., R. M. Venable, and M. Karplus. 1988. A simulation based model of NMR T_1 relaxation in lipid bilayer vesicles. *J. Chem. Phys.* 89:1128-1146.

Perczel, A., J. G. Ágyán, M. Kajtár, W. Viviani, J.-L. Rivail, J.-F. Marcoccia, and I. G. Csizmadia. Peptide models. 1. Topology of selected peptide conformational potential energy surfaces (glycine and alanine derivatives). *J. Am. Chem. Soc.* 113:6256-6265.

Péréz, S., F. Taravel, and C. Vergelati. 1985. Experimental evidences of solvent induced conformational changes in maltose. *Nouv. J. Chim.* 9:561-564

Perly, B., I. C. P. Smith, and H. C. Jarrell. 1985. Acyl chain dynamics of phosphatidylethanolamines containing oleic acid and dihydrosterculic acid: ^{2}H NMR relaxation studies. *Biochem.* 24:4659-4665.

Petersen, N. O. and S. I. Chan. 1977. More on motional states of lipid bilayer membranes- interpretation of order parameters obtained from nuclear magnetic resonance experiments. *Biochem.* 16:2657-2667.

Piomelli, D., A. Volterra, N. Dale, S. A. Siegelbaum, E. R. Kandel, J. H. Schwartz, and F. Belardetti. 1987. Lipoxygenase metabolites of arachidonic acid as second messengers for presynaptic inhibition of *Aplysia* sensory cells. *Nature.* 328:38-43.

Pope, J. M., L. Walker, B. A. Cornell, and F. Separovic. 1982. A study of the angular dependence of NMR relaxation times in macroscopically oriented lyotropic liquid crystal lamellar phases. *Mol. Cryst. Liq. Cryst.* 89:137-150.

Puopko, R., Z. Luz, N. Spielberg, and H. Zimmermann. 1989. Structure and dynamics of pyramidic liquid crystals by deuterium NMR and X-ray diffraction. *J. Am. Chem. Soc.* 111:6094-6105.

Quinn, P. J. and W. P. Williams. 1983. The structural role of lipids in photosynthetic membranes. *Biochim. Biophys. Acta.* 737:223-266.

Ram, P., and J. H. Prestegard. 1988. Head-group orientation of a glycolipid analogue from deuterium NMR data. *J. Am. Chem. Soc.* 110:2383-2388.

Ram, P., L. Mazzola, and J. H. Prestegard. 1989. Orientational analysis of micelle-associated trehalose using an NMR-pseudoenergy approach. *J. Am. Chem. Soc.* 111:3176-3182.

Rance, M., K. R. Jeffrey, A. P. Tulloch, K. W. Butler, and I. C. P. Smith. 1980. Orientational order of unsaturated lipids in the membranes of *Acholeplasma laidlawii* as observed by ^{2}H NMR. *Biochim. Biophys. Acta* 600:245-262.

Renger, G. 1983. Photobiophysics. *in* Biophysics. W. Hoppe, W. Lohmann, H. Markl, and H. Ziegler, Eds. Springer-Verlag, N.Y., p 515-565.

Renou, J. P., J. B. Giziewicz, I. C. P. Smith, and H. C. Jarrell. 1989. Glycolipid membrane surface structure: orientation, conformation, and motion of a disaccharide headgroup. *Biochem.* 28:1804-1814.

Rose, M. E. 1957. Elementary Theory of Angular Momentum. Wiley, N.Y. 248 pp.

Rudolph, B.R., I.Chandrasekhar, B. P. Gaber, and M. Nagumo. 1990. Molecular modelling of saccharide-lipid interactions. *Chemistry and Physics of Lipids.* 53:243-261.

Rydberg, L., M. E. Briemer, and B. E. Samuelsson. 1988. Antibody response in an ABO-incompatible blood transfusion. *Transfusion.* 28:483-488.

Sato, N. and N. Murata. 1988. Membrane lipids. *Meth. Enzym.* 167:251-259.

Sanders, II., C.R., and J. H. Prestegard. 1991. Orientation and dynamics of β-dodecyl glucopyranoside in phospholipid bilayers by oriented sample NMR and order matrix analysis. *J. Am. Chem. Soc.* 113:1987-1996.

Saupe, V. A. 1964. Kernresonanzen in kristallinen flüssigkeiten und in kristallinflüssigen lösungen. Teil I. *Zeits. Naturforschg.* 19a:161-171.

Scarsdale, J.N., R. K. Yu, and J. H. Prestegard. 1986. Structural analysis of a glycolipid head group with one- and two-state NMR pseudoenergy approaches. *J. Am. Chem. Soc.* 108:6778-6784.

Scarsdale, J.N., J. H. Prestegard, and R. K. Yu. 1988. A molecular mechanics-NMR pseudoenergy approach to the solution conformation of glycolipids. *J. Comp. Chem.* 9:133-147.

Schmidt, C., B. Blümich, and H. W. Spiess. 1988. Deuteron two-dimensional exchange NMR in solids. *J. Magn. Res.* 79:269-290.

Seddon, J. M. 1990. Structure of the inverted hexagonal (H_{II}) phase, and non-lamellar phase transitions of lipids. *Biochim. Biophys. Acta* 1031:1-69.

Seelig, A. and J. Seelig. 1974. The dynamic structure of fatty acyl chins in a phospholipid bilayer measured by deuterium magnetic resonance. *Biochem.* 13:4839-4845.

Seelig, J. and A. Seelig. 1975. Bilayers of dipalmitoyl-3-*sn*-phosphatidylcholine conformational differences between the fatty acyl chains. *Biochim. Biophys. Acta.* 406:1-5.

Seelig, J. 1977. Deuterium magnetic resonance: theory and application to lipid membranes. *Quart. Rev. Biophys.* 10:353-418.

Seelig, J. and A. Seelig. 1980. Lipid conformation in model membranes and biological membranes. *Quart. Rev. Biophys.* 13:19-61.

Seelig, J. and P. M. Macdonald. 1981. Phospholipids and proteins in biological membranes. ^{2}H NMR as a method to study structure, dynamics, and interactions. *Prog. NMR Spec.* 14:113-136.

Sen, A., W. P. Williams, and P. J. Quinn. 1981. The structure and thermotropic properties of pure 1,2-diacylgalactosylglycerols in aqueous systems. *Biochim. Biophys. Acta* 663:380-389.

Sen, A., W. P. Williams, A. P. R. Brain, and P. J. Quinn. 1982. Bilayer and non-bilayer transformations in aqueous dispersions of mixed *sn*-3-galactosyldiacylglycerols isolated from chloroplasts. A freeze-fracture study. *Biochim. Biophys. Acta* 685:297-306.

Shipley, G. G., J. P. Green, and B. W. Nichols. 1973. The phase behaviour of monogalactosyl, digalactosyl. and sulphoquinovosyl diglycerides. *Biochim. Biophys. Acta.* 311:531-544.

Siminovitch, D. J., M. J. Ruocco, E. T. Oljeniczak, S. K. Das Gupta, and R. G. Griffin. 1985. Anisotropic spin-lattice relaxation in lipid bilayers: a solid state ^{2}H nmr lineshape study. *Chem. Phys. Lett.* 119:251-255.

Singer, S. J. and G. L. Nicholson. 1972. The fluid mosaic model of the structure of cell membranes. *Science.* 175:720-731.

Slichter, C. P. 1990. Principles of Magnetic Resonance. Springer-Verlag, New York. 655 pp.

Smith, I. C. P., K. W. Butler, A. P. Tulloch, J. H. Davis, and M. Bloom. 1979. The properties of gel state lipid in membranes of *Acholeplasma laidlawii* as observed by ^2H NMR. *FEBS Lett.* 100:57-61.

Smith, I. C. P. and H. C. Jarrell. 1983. Deuterium and phosphorous NMR of microbial membranes. *Acc. Chem. Res.* 16:266-272.

Smith, I. C. P. 1989. Application of solid state NMR to the lipids of model and biological membranes. *In* NMR: Principles and Applications to Biomedical Research. J. W. Pettegrew, editor. Springer-Verlag, New York. p 124-156.

Solomon, I. 1958. Multiple echoes in solids. *Phys. Rev.* 110:61-65.

Spiess, H. W. and H. Sillescu. 1981. Solid echoes in the slow-motion regime. *J. Mag. Res.* 42:381-389.

Speyer, J. B., R. T. Weber, S. K. Das Gupta, and R. G. Griffin. 1989. Anisotropic ^2H NMR spin-lattice relaxation in L_α-phase cerebroside bilayers. *J. Am. Chem. Soc.* 28:9569-9574.

Spiegel, S. and P. H. Fishman. 1987. Gangliosides as bimodal regulators of cell growth. *Proc. Natl. Acad. Sci. USA* 84:141-145.

Sprague, S. A. and L. A. Staehelin. 1984. Effects of reconstitution method on the structural organization of isolated chloroplast membrane lipids. *Biochim. Biophys. Acta* 777:306-322.

Stockton, G. W., K. G. Johnson, K. W. Butler, A. P. Tulloch, Y. Boulanger, I. C. P. Smith, J. H. Davis, and M. Bloom. 1977. Deuterium NMR study of lipid organisation in *Acholeplasma laidlawii* membranes. *Nature.* 269:267-268.

Strenk, L. M., P. W. Westerman, and J. W. Doane. 1985. A model of orientational ordering in phosphatidylcholine bilayers based on conformational analysis of the glycerol backbone region. *Biophys. J.* 48:765-773.

Smith, I. C. P., K. W. Butler, A. P. Tulloch, J. H. Davis, and M. Bloom. 1979. The properties of gel state lipid in membranes of *Acholeplasma laidlawii* as observed by ^2H NMR. *FEBS Lett.* 100:57-61.

Smith, I. C. P. and H. C. Jarrell. 1983. Deuterium and phosphorous NMR of microbial membranes. *Acc. Chem. Res.* 16:266-272.

Smith, I. C. P. 1989. Application of solid state NMR to the lipids of model and biological membranes. *In* NMR: Principles and Applications to Biomedical Research. J. W. Pettegrew, editor. Springer-Verlag, New York. p 124-156.

Solomon, I. 1958. Multiple echoes in solids. *Phys. Rev.* 110:61-65.

Spiess, H. W. and H. Sillescu. 1981. Solid echoes in the slow-motion regime. *J. Mag. Res.* 42:381-389.

Speyer, J. B., R. T. Weber, S. K. Das Gupta, and R. G. Griffin. 1989. Anisotropic ^2H NMR spin-lattice relaxation in L_α-phase cerebroside bilayers. *J. Am. Chem. Soc.* 28:9569-9574.

Spiegel, S. and P. H. Fishman. 1987. Gangliosides as bimodal regulators of cell growth. *Proc. Natl. Acad. Sci. USA* 84:141-145.

Sprague, S. A. and L. A. Staehelin. 1984. Effects of reconstitution method on the structural organization of isolated chloroplast membrane lipids. *Biochim. Biophys. Acta* 777:306-322.

Stockton, G. W., K. G. Johnson, K. W. Butler, A. P. Tulloch, Y. Boulanger, I. C. P. Smith, J. H. Davis, and M. Bloom. 1977. Deuterium NMR study of lipid organisation in *Acholeplasma laidlawii* membranes. *Nature.* 269:267-268.

Strenk, L. M., P. W. Westerman, and J. W. Doane. 1985. A model of orientational ordering in phosphatidylcholine bilayers based on conformational analysis of the glycerol backbone region. *Biophys. J.* 48:765-773.

Thørgersen, H., R. U. Lemieux, K. Bock, and B. Meyer. 1982. Further justification for the exo-anomeric effect. Conformational analysis based on nuclear magnetic resonance spectroscopy of oligosaccharides. *Can. J. Chem.* 60:44-56.

Torchia, D. A. and A. Szabo. 1982. Spin-lattice relaxation in solids. *J. Mag. Reson.* 49:101-121.

Tvaroška. I. and S. Pérez. 1986. Conformational-energy calculations for oligosaccharides: a comparison of methods and a strategy of calculation. *Carb. Res.* 149:389-410.

Tvaroška, I. and L. Váklavik. 1987. Stereochemistry of nonreducing disaccharides in solution. *Carb. Res.* 160:137-149.

Tvaroška, I. 1989. Computational methods for studying oligo-and polysaccharide conformations. *Pure Appl. Chem.* 61:1201-1216.

Ukleja. P., J. Pirs, and J. W. Doane. 1976. Theory for spin-lattice relaxation in nematic liquid crystals. *Phys. Rev. A* 14:414-423.

Van De Ven, M. J. M. and Y. K. Levine. 1984. Angle-resolved fluorescence depolarization of macroscopically ordered bilayers of unsaturated lipids. *Biochim. Biophys. Act.* 777:283-296.

Vilfan, M., M. Kogoj, and R. Blinc. 1987. Nuclear spin relaxation due to order director fluctuations in the smectic A phase. *J. Chem. Phys.* 86:1055-1060.

Vold, R. L., W. H. Dickerson, and R. R. Vold. 1981. Application of the Jeener-Broekaert pulse sequence to molecular dynamics studies in liquid crystals. *J. Mag. Res.* 43:213-233.

Vold, R. R., R. L. Vold. 1988. Nuclear spin relaxation and molecular dynamics in ordered systems: models for molecular reorientation in thermotropic liquid crystals. *J. Chem. Phys.* 88:1443-1457.

Wada, H., Z. Gombos, and N. Murata. 1990. Enhancement of chilling tolerance of a cyanobacterium by genetic manipulation of a fatty-acid desaturation. *Nature.* 347:200-203.

Webb, M. S. and B. R. Green. 1990. Effects of neutral and anionic lipids on digalactosyldiacylglycerol vesicle aggregation. *Biochim. Biophys. Acta.* 1030231-237.

Weiner, S. J., P. A. Kollman, D. T. Nguyen. and D. A. Case. 1986. An all atom force-field for simulations of proteins and nucleic acids. *J. Comp. Chem.* 7:230-252.

Wefing, S., S. Jurga, H. W. Speiss. 1984. Orientation dependent spin-lattice relaxation of deuteron spin alignment. *In* 22nd Ampere Congress Proceedings, Zurich Ampere Committee: Zurich. 375-376.

Wiener, N. 1930. Generlized harmonic analysis. *Acta Math.* 55:117-258.

Williams, J. P., E. Maissan, K. Mitchell, and M. U. Khan. 1990. The manipulation of the fatty acid composition of glycerolipids in cyanobacteria using exogenous fatty acids. *Plant Cell Physiol.* 31:495-503.

Winsborrow, B. G., I. C. P. Smith, and H. C. Jarrell. 1991. Dynamics of glycolipids in the liquid-crystalline state: a ^{2}H NMR study. *Biophys. J.* 59:729-741.

Winsborrow, B. G., J.-R. Brisson, I. C. P. Smith, and H. C. Jarrell. 1992. Influence of the membrane surface on glycolipid conformation and dynamics. An interpretation of NMR results using conformational energy calculations. *Biophys. J.* 63:428-437.

Wittebort, R. J., C. F. Schmidt, and R. G. Griffin. 1981. Solid-state carbon-13 nuclear magnetic resonance of the lecithin gel to liquid-crystalline phase transition. *Biochem.* 20:4223-4228.

Wittebort, R. J., E. T. Olejniczak, and R. G. Griffin. 1987. Analysis of deuterium nuclear magnetic resonance line shapes in anisotropic media. *J. Chem. Phys* 86:5411-5420.

Wong, B. S., D. M. Miller, and J. H. Yopp. 1977. Proton pulsed NMR study on the cell constituents of *Aphanothece halophytica*, a blue-green alga. *in* Biomolecular Structure and Function. P. Agris, R. Leopky, and B. Sykes, Eds. Academic Press, NY. 2398-245.

Woods, V. L., L. E. Wolff, and D. M. Keller. 1986. Resting platlets contain a substantial centrally located pool of glycoprotein IIb-IIa complex which may be accessible to some but not other extracellular proteins. *J. Biol. Chem.* 261:15242-15251.

Yan, Z.-Y., and C. A. Bush. 1990. Molecular dynamics simulations and the conformational mobility of blood group oligosaccharides. *Biopolymers.* 29:799-811.